Optimisation of Stacking Sequence of Fibre Reinforced Plastic Laminated Composite Structures Subjected to Buckling

Joko SEDYONO

This thesis is submitted in partial fulfilment of the requirements of the University for the Award of PhD

Supervised by:

Associate Professor Homayoun Hadavinia

Faculty of Science, Engineering and Computing

Kingston University London

May 2014

Dedicated to

First I dedicate my effort during completion of this thesis to my God, Allah swt because of His Help I was able to finish this project. Thereafter I dedicate my thesis to my mother, my wife, my children Yusuf, Ilyas, Inas, and Aqis for their kindness, support and pray for me while they are waiting with patience for completion of my project.

Abstract

The objective of the present work is to develop mathematical/finite element based optimization techniques for fibre reinforced polymer (FRP) laminated composite structures subjected to buckling. Many issues arise when a laminated FRP composite structure subjected to compressive load and ultimately fail under buckling. Issues such as understanding FRP composite materials, buckling and post-buckling behaviour of the structure, delamination and detection of the crack front need attention. Hence, in the present research works were carried out in each of these areas.

Various experimental studies were carried out to study material characterisation, the delamination fracture toughness in mode I, mode II and mixed-mode I/II using DCB, ENF and MMB tests and buckling of FRP composite plates. From these series of test GIC, GIIC and fracture envelope under different mode mixity ratio were determined. Also the buckling tests of the plates with optimum and non-optimum stacking sequence were performed to verify the optimisation results. The effect of damage on buckling load was studied by tests on buckling of plates with pre-existing centrally located delamination patch at the plate mid-plane and on plate with a hole at the centre of the plate to investigate the effect of cut-out and damage on buckling load. Finally, IR thermography and CT-Scan non-destructive tests (NDT) were used for plates with pre-existing centrally located delamination patch to study the direction and the extent of delamination crack propagation after the buckling tests.

In the case of plates with pre-existing centrally located delamination patch with diameter less than 32mm, the critical buckling load has not changed. But when the delamination patch diameter reached to 48mm (at around 60% of plate width), there was significant reduction in the critical buckling load. In the case for plate with cut-out a noticeable reduction on the critical buckling load was observed when the diameter of the hole was more than 25% of the plate width.

IR thermography and CT-Scan images analysis of the plates after buckling tests showed that in plates with pre-existing centrally located delamination patch with a diameter of D=16 mm, the plate failure occurs near the loading edge. In the case of plates with delamination patch of D=32mm, some plates failed near the loading edge and in some plates crack

propagated along the ±45° fibre direction around delamination patch. However, for plates with delamination patch with diameter of D=48mm, in all samples the delaminated area propagated along the fibre direction around the delaminated area and no failure observed near the loading edge.

Inherent to the use of FRP composite materials is the inclusion of ply angles and stacking sequence as design variables. These design variables are discrete in nature. The optimization of these models is typically difficult due to their combinatorial nature and potential existence of multiple local minima in the search space.

In this research bottom-up enumeration search optimisation approach was developed for optimum design of stacking sequence of laminated composite structure for maximum critical buckling load above the required target load using MATLAB software. The optimised results were verified by buckling experiments and FE simulations. The developed programme is flexible to use for other loading condition. For the case of uniaxial compressive loading with preselected target buckling load, the optimum number of layers and orientation for 0/90 biaxial fabrics and unidirectional plies were determined. The percentage of difference between analytical buckling load and FEA eigen solution with experiments are about -13.1% and -3.2%, respectively.

Depending on the properties and arrangement of the skin and stiffener, different buckling modes and failure loads can occur in a stiffened plate. For shape optimisation of blade-stiffened plate subjected to buckling, Sequential Quadratic Programming (SQP), Genetic Algorithms (GA) and Simulated Annealing (SA) techniques were used in MATLAB optimisation programme in conjunction with ANSYS finite element software. The developed techniques are tested for minimum weight of a blade-stiffened plated with predefined stacking sequence of stiffener and the plate where the geometry parameters were design variables. In this work, the size of the stiffener height and the distance between the stiffener for a required target buckling load and optimum weight were determined.

Acknowledgment

Thanks God that I have the opportunity to do a PhD research in a subject that is very important not only in the field of engineering but also in all fields of science, i.e. optimisation. I was lucky to have a chance to work on FRP composite materials used in the structures that weight is one of the main issues. This is a very challenging subject particularly in thin-walled laminated structures subjected to buckling.

I have dedicated the past four years on this project. During this period in my life, I have been fortunate to be supervised by my Director of Study Associate Professor Homayoun Hadavinia. I thank you not only for recommending and supervising this project, but also for your time, support and friendship during the course of this project. I would also like to thank my supervisory team Dr Demetrios Venetsanos, Associate Professor Denis Marchant, Dr Jiamei Deng and Mr John Garcia.

I am grateful to Directorate General of Higher Education Republic of Indonesia for full financial support of my project through my institution Human Resources and Development of Universitas Muhammadiyah Surakarta Indonesia.

Many thank to Helen Bordbar at London Clinical Hospital who helped on doing CT-scan and John Flynn from Defect Detection Technology for IR Thermography non-destructive testing.

I am also very grateful for the support given by technical staff Alex Vine, Dean Wells, Martin Theobald at School of Mechanical & Automotive Engineering and Sean Downey at School of Civil Engineering. Thanks to Jackie Deacon in administration office, Christopher Hebbs in ISAC office and IT and the library staff at Kingston University. I appreciate assistance from Simran Harrar, an undergraduate student at School of Aerospace Engineering on buckling tests of plate with hole.

Finally I am grateful to my friends for all the encouragement and support I have received from them throughout my time at Kingston University namely Othman Al-Khudairi, Marwan Effendy, Dr Tri Riyadi, Dr Sarjito, and Patna Partana.

Joko Sedyono (BSc, MEng)

May 2014

Table of Contents

Chapter 3 Experimental Studies

Chapter 4 Theory of Optimisation

Chapter 7 Conclusions and Further Work

List of Figures

List of Tables

Nomenclature

a : Length of plate

A : Area

A_{ij} : The extensional stiffness

b : Width of plate

B_{ij} : Coupling stiffness

d : Plate thickness (mm)

D_{ij} : Bending stiffness

E_{ij} : Young's modulus

$f(x)$: Objective function

fy : Yield stress

F : Feasible region

F_x : Buckling load

$g(x)$: Inequality constraint

G_{ij} : Shear modulus

$h(x)$: Equality constraint

k : Radius of gyration

k_σ : Buckling factor

$[K]$: Stiffness matrix

I : Moment of inertia

L_e : Effective length of strut

m : $\cos\theta$

n : $\sin\theta$

n_c : Continuous variable

n_d : Discrete variables

n_i : Non-dimensional load

N : Load

N_c : Critical buckling load

N_{crit} : Critical buckling load

N_x : Critical buckling load

P : In-plane load

P_{cr} : Critical buckling load

Q_{ij} : Reduced stiffness matrix

$\bar{Q}_{ij}$: Transformed reduced stiffness matrix

$\Re^m$: Design space

$[S]$: Initial stress matrix

U : Unfeasible region

U_I : Material invariant

w : Out-of-plane displacement

w_o : Initial deformation amplitude

x : Design variable (in term of optimisation)

x^L : Lower bound

x^U : Upper bound

X : The set of continuous variable (in term of enumeration)

Y : The set of discrete variables

z_k : Ply distance from mid plane

θ : Ply angle

λ : Amplitude parameter, also eigen vector

λ_{rel} : Relative slenderness

v_{ij} : Poisson's ratio

ρ : Reduction factor

σ : In-plane stress

σ_{cr} : Critical buckling stress

σ_{crit} : Critical buckling stress

σ_{yc} : Compressive yield stress

$\{\psi_i\}$: The i^{th} eigenvector of displacements

Chapter 1

Introduction

1.1. Background

Structural design should be safe from sudden failure. There are two major categories leading to the sudden failure of structural components: material failure and structural instability, which is often called buckling. In case of material failures, the yield stress for ductile materials and the ultimate stress for brittle materials should be considered. However slender or thin-walled structures under compressive loading are susceptible to buckling. Buckling refers to the loss of stability of a structure and is usually independent of material strength and the load at which buckling occurs depends on the stiffness of a structure rather than material strength. This loss of stability usually occurs within the elastic range of the material. Buckling failure is primarily characterized by a loss of structural stiffness.

The stability/instability of thin-walled structures is a central concern regarding structural engineering. In this field, the stability of a structure is often confined to the elastic part of the phenomena. However, there is also interest to postbuckling stage of the instability. As an example of structural instability, one can consider the columns in a building made with a steel frame. These columns have to not only withstand the vertical loads of e.g. snow, but also lateral loads caused by the wind.

The buckling may be of global nature, as described above, but may also be of localized type. Local buckling is regional located buckling, e.g. the local shear buckling of certain bays of the fuselage shown in Figure 1.1. Local buckling occurs due to local compressive stresses and these local instabilities could lead to global buckling because of the loss of resistance of the cross section in question.

Fig. 1.1. Local buckling B 737-300 YR-BAC (Romanian-spotters, 2009).

A structure or a member in an equilibrium state under compressive load may become unstable and the structure acquires a new equilibrium state or a new trend of behaviour. When considering classical buckling theory the critical stress level is defined as the stress at which the perfect structure becomes unstable. This point is called the bifurcation point or bifurcation load.

Usually two more types of elastic instabilities are classified. These are limit equilibrium instability (snap-through buckling) and dynamic or flutter instability.

Considering the load-displacement behaviour shown in Figure 1.2 of a plate subjected to compressive in-plane load P, causing an out of plane displacement *w* measured typically at one of the crest of a buckle. The Euler elastic critical buckling load for a linearised idealisation, P_{cr}, is when the plate will suddenly loose in-plane stiffness (A-C). This point is bifurcation point as the load path branches into two possible equilibrium paths. The other possible solution path, though unstable, is A-B. If geometric non-linearity, i.e. large displacement and large rotation, are considered in the analysis for the perfect plate under in-plane loading, path A-D in Figure 1.2 will be predicted where the stiffness is increasing as the load increases. The knowledge of plate behaviour after bifurcation that is called post-buckling region, is important, as the plate is capable of carrying load far beyond the critical load. However, in this region the stiffness is significantly reducing so the behaviour should be know precisely.

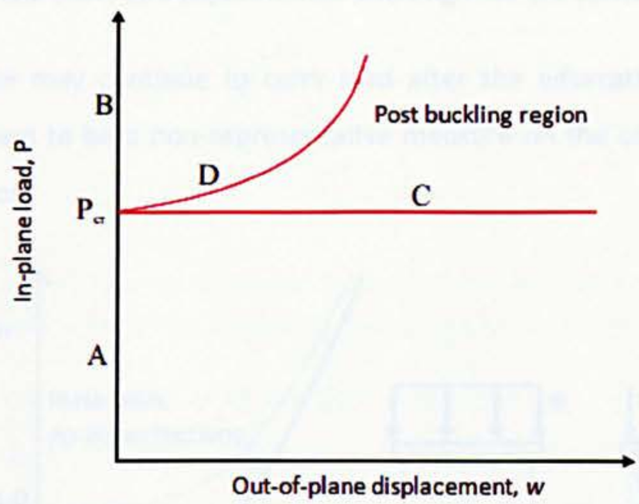

Fig. 1.2. Schematic description of typical load-displacement in a plate buckling.

As always concerning theoretical models for describing a physical structure, the assumptions made for the theory should be realistic. For example for solving the buckling of a plate, we may make assumptions such as an initially perfect flat plate and a perfectly isotropic homogenous material behaviour that are not precisely describing the real plate. These assumptions put limitations in the presented theory. We know that all materials to some extent are imperfect and they contain some flaws at different length scale. For example, a manufactured plate has an initial curvature, grains size is directionally oriented and probably residual stresses from uneven cooling or some machining exist in the plate. These facts makes the assumptions made in our analysis to some degree unrealistic and specifically in the buckling behaviour of structures the material and geometric imperfections have been proven experimentally to be detrimental.

Now when the assumptions are found to be an idealistic description of the real behaviour of the plates, the question arises how these initial imperfections affect the plate behaviour before, as well as after, the bifurcation point. Figure 1.4 shows the difference in behaviour of a plate when the plate imperfections are considered.

Considering Figure 1.3 two conclusions concerning how the imperfection influence the plate behaviour may be drawn. Firstly, buckling of a plate with inherent imperfections is gradual and it is very difficult to specify exactly critical load. Hence, there will be difficulties when theoretical and experimental buckling load are compared.

Secondly, the plate may continue to carry load after the bifurcation point. Thus, the critical load is shown to be a non-representative measure on the ultimate resistance of the plate in question.

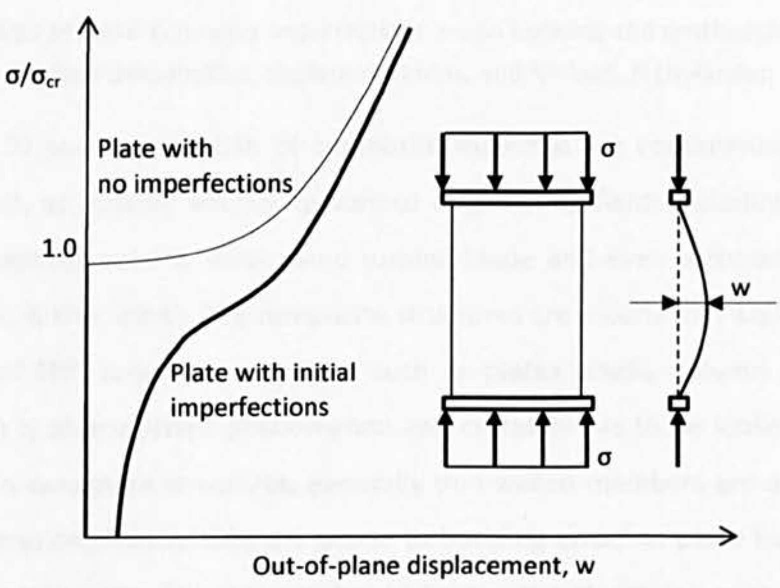

Fig. 1.3. The influence of initial plate imperfections with respect to a plate with no imperfections.

Nylander (1951) shows how an applied initial deformed shape with the amplitude w_0 (in the same shape as the deformed plate) affects the magnitude of lateral deformations under applied load. Furthermore, when the material is assumed ideal elastic, the model gives no information concerning the ultimate load. He concluded, the initial geometric imperfections primarily influence the plate stiffness and become more obvious with increased plate slenderness (see Figure 1.4).

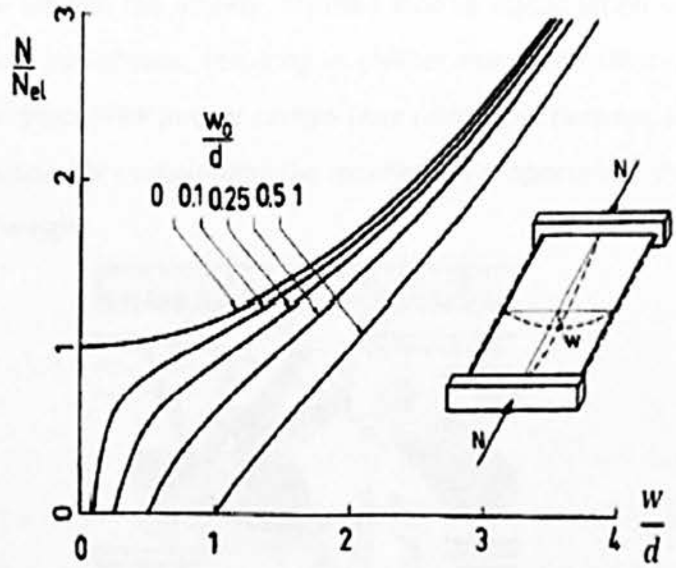

Fig. 1.4. The effect of initial geometry imperfections, w_o on buckling and postbuckling behaviour. w = out-of-plane deformation, d=plate thickness, and N= load, N (Nylander, 1951).

Over the last 20 years application of composite materials are continuously expanding, from areas such as military aircraft to various engineering fields including commercial aircraft, automobiles, robotic arms, wind turbine blade and even architecture (Kweon, Jung, Kim, Choi, & Kim, 2006). The composite structures are usually thin walled structures and buckling of FRP composite elements such as plates, shells, column etc. whether slender or thin is an important phenomenon and certainly has to be looked into at the design stage. In aerospace structures, generally thin walled members are used from the weight consideration. Hence, they are prone to buckling under in-plane loads. Cut-outs are generally made in the structures either to lighten the structures or to carry cables, etc. and these parts need special attention.

Pole-vaulting (see Figure 1.5), a competitive sport since 1984 is a track and field event in which a person uses a long, flexible pole, which today is usually made either of glass fibre or of carbon fibre as an aid to jump over a bar. The pole is under a large bending moment and elastic buckling occurs during the jump. In 1896 Olympics a 3.3m height achieved with bamboo pole. In 1960, there was a change in vaulting pole construction from bamboo to glass fibre reinforced polymer (GFRP) composites (Davis & Kukureka, 2012).

GFRP poles have a much higher failure stress than bamboo, so the poles were engineered to bend under the load of the athlete, thereby storing elastic strain energy that can be released as the pole straightens, resulting in greater energy efficiency. Modern vaulting poles can be made from GFRP and/or carbon fibre reinforced polymer (CFRP) composites. The addition of carbon fibres maintains the mechanical properties of the pole, but allows a reduction in the weight.

Fig.1.5. Pole-vaulting under bending load (E&T magazine, 2012).

For the FRP composite plates two survey articles by Leissa (1981) (1987) has extensively investigated the issue of buckling of laminated composite plates. In addition, Hui (1984) graphically presented the results for both the symmetric and anti-symmetric modes of buckling of anti-symmetric cross-ply plates with various aspect ratios. It should be emphasised that Reissner (1945), Whitney (1969) and Whitney and Pagano (1970) show that transverse shear effect is quite significant in laminated composite plates which will affect the behaviour of laminates under compressive loading. The reason is the high ratio of in-plane elastic modulus to transverse shear modulus.

Srivatsa and Murthy (1991) presented a parametric study of the compression buckling behaviour of stress loaded composite plate with a central circular cutout. Prabhakara and Datta (1997) studied the vibration and buckling behaviour of plates with centrally located cut-outs. Jain and Kumar (2003) analysed the post buckling response of square laminates with a central circular/elliptical cut-out.

Loatin and Morozov (2014) proposed a solution to the buckling of a rectangular sandwich plate with all the edges fully clamped (CCCC) and subjected to a uniaxial compressive loading. Their analysis of the out-of-plane deformation is based on the first order shear deformation theory (FSDT). The solution to the problem is reduced to the calculation of the eigenvector of corresponding homogeneous system of linear equations and determination of its least component.

Throughout operation, the composite laminate plates are generally subjected to compression loads that may cause buckling if overloaded. Consequently, their buckling behaviours are significant factors in safe and reliable design of these structures (Baba, 2007). The correct understanding of the structural behaviour of laminates, such as the deflections, buckling loads and modal characteristics, the through-thickness distributions of stresses and strains, the large deflection behaviour and, of extreme significance for obtaining strong, reliable multi-layered structures, the failure characteristics are necessary (Zhang & Yang, 2009). For predicting the buckling load and buckling mode form of a structure in the finite element program, the linear (eigenvalue) buckling analysis is an existing technique for estimation (Zor, Sen, & Toygar, 2005) but in general, the analysis of composite laminated plates is more complicated than the analysis of homogeneous isotropic ones (Shufrin, Rabinovitch, & Eisenberger, 2008).

1.2. Optimum Design of Laminate Sequence

One of the attractive advantages of the FRP composite materials is the ability to tailor them for any specific the structural usage, i.e., the material can be optimized by suitably selecting fibre orientation angle and layer thickness. In contrast to metallic materials, structural analysis of FRP laminated composite plates is more complicated due to anisotropy of each layer, and as a result, the design of laminated plates includes additional complexity.

Fukunaga et al. (1995) studied optimization of symmetrically laminated plates with simply supported or clamped edges to maximize buckling loads under combined loading. In their analysis they considered the coupling between bending and twisting. Optimal laminate configuration to maximize the buckling loads was obtained using a mathematical programming method where four lamination parameters were used as design variables.

Walker et al. (1996) used a finite element approach for the optimal stacking sequence design of symmetric laminated composite plates for maximum buckling load subjected to biaxial compression. The effect of optimization on the non-dimensionalised buckling load was investigated by plotting the buckling load against the design variable (Figure 1.6). The results show that the difference in the buckling loads of optimal and non-optimal plates could be quite substantial, emphasizing the importance of optimization for fibre composite structures.

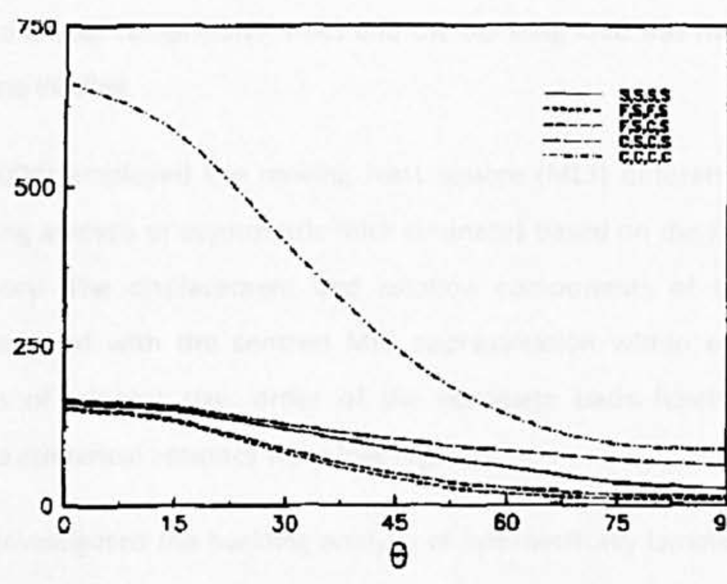

Fig. 1.6. Non-dimensionalised buckling load plotted against the ply angle for rectangular laminates with a/b = 0.5, number of layers: 4, and t/b = 0.01 (Walker, Adali, & Verijenko, 1996).

Walker (2001) studied optimal design of biaxially loaded laminated plates subject to a combination of free, simply supported and clamped edges for a maximum weighted combination of buckling load and resonance frequency. Walker (2002) also presented optimal designs of symmetrically laminated rectangular plates with different stiffener arrangements. The plate designs are optimised with the objective of maximising the buckling load with the ply fibre orientation as the design variable. During the optimisation procedure, the fitness of each laminate design is determined using the finite element method.

The plates were subject to a combination of simply supported, clamped and free boundary conditions and the design objective was the maximization of the biaxial buckling load.

Sciuva et al. (2003) performed optimization of laminated and sandwich plates with respect to buckling load and thickness was performed, using different sets of constraints such as the fundamental frequency, the maximum deflection under transverse uniform distributed load, the mass and the buckling load. The genetic and simulated annealing algorithms were employed together with two plate models. Adali et al. (2003) presented optimal design of composite laminates under buckling load uncertainty. The laminates were subjected to biaxial compressive loads and the buckling load was maximized under worst-case in plane loading.

Huang and Li (2004) employed the moving least square (MLS) differential quadrature method to buckling analysis of asymmetric thick laminates based on the first-order shear deformation theory. The displacement and rotation components of the plate were independently assumed with the centred MLS approximation within each domain of influence. Effects of support size, order of the complete basis functions and node irregularity on the numerical accuracy were investigated.

Xie et al. (2005) investigated the buckling analysis of symmetrically laminated composite plates with internal supports. Both the higher-order shear deformation theory and pb-2 Ritz displacement functions, corresponding to an arbitrary edge support were enclosed in the proposed method. The buckling behaviour of symmetrically laminated composite plates with line internal support and, circular internal supports were investigated under biaxial compression loading. Ni et al. (2005) presented a buckling analysis for a rectangular laminated composite plate with arbitrary edge supports subjected to biaxial compression loading. The higher-order shear deformation theory was employed and a special displacement function, which could express an arbitrary edge support, was introduced into the Rayleigh–Ritz method. Jones (2005) derived simple solutions to the most fundamental thermal buckling problems for uniformly heated unidirectional and symmetric cross-ply-laminated fibre-reinforced composite rectangular plates that were restrained in-plane at their edges in a single direction on two of the four edges, but were free to rotate on all edges.

Onkar et al. (2006) developed a generalized layerwise stochastic finite element formulation for the buckling analysis of both homogeneous and laminated plates with random material properties. A layerwise plate model was used to get accurate state of pre-buckled stresses in the plate. Gal et al. (2006) presented the buckling analysis of a laboratory-tested composite panel under axial compression by means of a simple shell finite element that is developed and presented. Buckling is achieved via incremental geometrically nonlinear analysis and monitoring of the tangent stiffness matrix at each increment.

Ungbhakorn and Singhatanadgid (2006) extended the Kantorovich method, a semi-analytical method, which requires iterative calculation by reducing the governing partial differential equations to a set of governing ordinary differential equations (ODE). They obtain the critical buckling load of symmetrically laminated composite rectangular plates with various combinations of the boundary conditions.

Lindgaard and Lund (2010) presented nonlinear buckling fibre angle optimization of laminated composite shell structures. The approach accounts for the geometrically nonlinear behaviour of the structure by utilizing response analysis up until the critical point. They obtained the sensitivity information by an estimated critical load factor at a precritical state. In the optimization formulation, the risk of "mode switching" is avoided by including the lowest buckling factors. The presented optimization formulation is compared to the traditional linear buckling formulation and two numerical examples, including a large laminated composite wind turbine main spar were studied.

Hemmatian *et al.* (2013) applied ant colony optimisation (ACO) for the multi-objective optimization of hybrid laminates for obtaining minimum weight and cost. The hybrid laminate is made of GFRP and CFRP plies using a modified variation of ACO so called the elitist ant system (EAS) in order to make the trade-off between the cost and weight as the objective functions. First natural frequency was considered as a constraint. The obtained results using the EAS method including the Pareto set, optimum stacking sequences, and the number of plies made of either glass or graphite fibres were compared with those using the genetic algorithm (GA) and any colony system (ACS) reported in literature.

In the current thesis optimal design of simply supported laminated composite plates subject to in-plane static loads for which the critical failure mode is buckling. The objective function is to maximize the buckling load capacity of laminated plates and the fibre orientation is considered as design variable.

1.3. Delaminations and Their Effect on Buckling Load

Delamination is separation of the plies due to out of plane stresses. Delaminations can be caused by low-velocity impact, fatigue load, air entrapments caused by manufacturing processes, or stress concentrations at free edges. The out-of-plane stresses, which naturally cause delamination, occur at many parts of structures as indicated in Figure 1.7, such as ply drops, skin-stiffener intersections, sandwich panel, free edges, near geometric discontinuities such as holes, cut-outs, flanges, stiffener terminations, bonded and bolted joints (The Composite Materials Handbook, 1997).

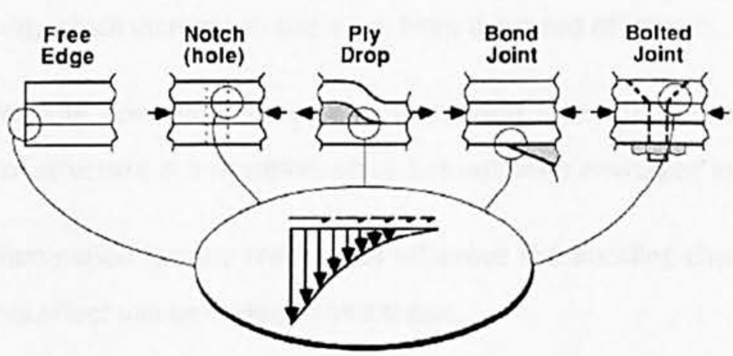

Fig. 1.7. Common structural elements which generate interlaminar stress concentrations (The Composite Materials Handbook, 1997).

Delaminations degrade the overall stiffness and strength of a laminated FRP structure. In particular, they may severely reduce the load-carrying capacity of the laminates under compressive loads. The level of reduction in load-bearing capacity depends on the shape, area, orientation and position of the delamination and the type of loading and boundary conditions.

With the increasing use of composite laminates, the compression behaviour of delaminated composite structures in particular has attracted increasing attention in recent years (Arani, Moslemian, & Arefmanesh, 2009). When a delaminated composite plate is subjected to uniaxial in-plane compression, local mode buckling of the delaminated region or mixed mode buckling (a combination of local and global mode buckling) may occur before global mode buckling. This results in the delaminated composite plate having a lower ability to resist compressive loads (Arani, Moslemian, & Arefmanesh, 2009).

Delaminations in FRP composite laminate can originate in the following conditions:

- At the manufacturing stage, e.g., adhesion failures and shrinkage cracks.
- During transportation and installation, when the applied loads to the structure becomes higher than design load or the character of load may be different, e.g. the structure experience impacts such as tool drop. Impact of foreign objects is the most important cause of delamination in FRP materials and even relatively light impacts can cause the delamination at the near-surface layers. The impact may create multiple delaminations, which increase in size away from the point of impact.
- Finally during the operation either due to loading other than the design load or application of structure in a situation which has not been envisaged in the design.

Presence of delamination for any reason will influence the buckling characteristic of the structure and this effect will be looked in this thesis.

1.4. Research Objectives

There are numerous studies on the buckling of laminated composite structures as FRP materials find widespread applications in many engineering fields such as aerospace, automotive, civil, and marine engineering because of their high specific strength and high specific stiffness, and their excellent damage tolerance and impact resistance. FRP laminates are generally thin structures and they are susceptible to buckling. The FRP laminates may be used as a plain plate or reinforced by stringers and stiffeners to enhance their buckling resistance.

The first objective of this research was to understand the structural behaviour of laminated FRP composites structure subjected to buckling with/without delamination and cut- out.

The second objective was the weight optimisation of laminated composite structures subjected to buckling. In order to find the optimum stacking sequence, i.e. fibre orientation angle and number of plies, enumeration search method has been used. The enumeration search method is one of the most robust optimisation techniques capable of finding the global optimum solution from a bottom-up strategy. Experimental works and FEA eigen buckling analysis have been carried out to verify the optimum solution.

Finally, in traditional design usually parametric analysis are used to obtain the best design. However, there is no guarantee that this design is the optimum one. On the other hand, in the shape optimisation design, the optimum solution is searched systematically.

In the present work, MATLAB optimisation tool box using Sequential Quadratic Programming (SQP), Genetic Algorithm (GA) and Simulation Annealing (SA) optimisation techniques in conjunction with ANSYS finite element software are used to find the maximum critical buckling load and minimum weight for a stiffened FRP composite plate for a set buckling load target by finding geometrical design variables.

1.5. Outlines of Thesis

After the introductory words in Chapter 1, Chapter 2 gives a brief overview about composites, stability and principle of buckling behaviour of fibre-reinforced composite thin-walled structures. As most of laminated FRP are thin structures, major stability issues regarding thin-walled structures have been highlighted. Finally, some non-destructive techniques for detecting delamination in FRP material are reviewed.

In Chapter 3 various experimental studies carried out in this project are presented. Four series of test, which were conducted for this project, are mechanical characterisation of unidirectional GFRP composite materials, the delamination fracture toughness in mode I, mode II and mixed-mode I/II using DCB, ENF and MMB tests, buckling of the plates with preselected stacking sequence to verify the optimisation results. In addition, some tests were carried out on buckling of plates with pre-existing centrally located delamination patch at the plate mid-plane to study the effect of delamination on critical buckling load of the plate. Thereafter specimens with cut out (hole) in middle part are employed for buckling load test and finally non-destructive tests were carried out on plates with pre-existing centrally located delamination patch to study the direction and the extent of delamination crack propagation and its effect on the critical buckling load. IR thermography and CT-Scan non-destructive testing have been used to study the delamination crack growth in the buckled plates.

In Chapter 4 background theories of optimisation are discussed and the advantages of the techniques which are used in buckling study in Chapters 5 and 6 are highlighted.

In Chapter 5 the Enumeration Search (ES) optimisation code is developed to obtain the minimum number of layers from a set of pre-selected fibre orientation for maximum critical buckling load. In the laminated FRP composite, the inclusion of ply angles as design variables is unavoidable. These design variables are discrete in nature because of manufacturing constraint. The optimization of laminated FRP composite for buckling strength is properly formulated with stacking sequence as design variables. The optimum solutions are compared with experimental results.

In Chapter 6 a shape optimisation methodology is developed and the method is applied to few case studies of buckling of laminated composite stiffened plate. In the optimisation technique, MATLAB and ANSYS software together with Sequential Quadratic Programming (SQP), Genetic Algorithm (GA) and simulated annealing (SA) optimisation techniques are used.

All the work presented in this thesis is summarised and concluded in Chapter 7. Furthermore, some proposals for future work are suggested.

1.6. References

Adali, S., Lene, F., Duvaut, G., & Chiaruttini, V. (2003). Optimization of laminated composites subject to uncertain buckling loads. *Compos Struct*, *62*, 261–9.

Arani, A. G., Moslemian, R., & Arefmanesh, A. (2009). Compressive behavior of a glass/epoxy composite laminates with single delamination. *Journal of Solid Mechanics, 1*(2), 84-90.

Baba, B. O. (2007). Buckling behavior of laminated composite plates. *J Reinf Plast Compos, 26*, 1637–55.

Davis, C. L., & Kukureka, S. N. (2012). Effect of materials and manufacturing on the bending stiffness of vaulting poles. *Physics Education, 47*(5), 524.

E&T magazine. (2012). *London 2012 olympic, pole vault technique-an annotated graphic.* Retrieved April 9th, 2014, from E&T: http://engtechmag.wordpress.com/2012/07/18/london-2012-olympics-pole-vault-technique-an-annotated-graphic/

Fukunaga, H., Sekine, H., Sato, M., & Iino, A. (1995). Buckling design of symmetrically laminated plates using lamination parameters. *Comput & Struct, 57(4)*, 643–9.

Gal, E., Levy, R., Abramovich, H., & Pavsner, P. (2006). Buckling analysis of composite panels. *Compos Struct, 73*, 179–85.

Hemmatian, H., Fereidoon, A., Sadollah, A., & Bahreininejad, A. (2013). Optimization of laminate stacking sequence for minimizing weight and cost using elitist ant system optimization. *Advances in Engineering Software*, 57, 8–18.

Huang, Y. Q., & Li, Q. S. (2004). Bending and buckling analysis of antisymmetric laminates using the moving least square differential quadrature method. *Comput Methods Appl Mech Eng, 193*, 3471–92.

Hui, D. (1984). Shear buckling of anti-symmetric cross-ply rectangular plates. *Fibre Sci. Technol., 21*, 327.

Jain, P., & Kumar, A. (2003). Post buckling response of square laminates with a central circular/elliptical cutout. *Comput. Struct., 65*, 119–125.

Jones, R. M. (2005). Thermal buckling of uniformly heated unidirectional and symmetric cross-ply laminated fiber-reinforced composite uniaxial inplane restrained simply supported rectangular plates. *Composites: Part A , 36*, 1355–67.

Kweon, J. H., Jung, J. W., Kim, T. H., Choi, J. H., & Kim, D. H. (2006). Failure of carbon composite-to-aluminum joints with combined mechanical fastening and adhesive bonding. *Compos Struct, 75*, 192–8.

Leissa, A. W. (1981). Advances in vibration, buckling and post buckling studies in composite plates, composite structures. Proceedings 1st International Conference on Composite Structures. *Applied Science Publishers.* London.

Leissa, A. W. (1987). A review of laminated composite plate buckling. *Appl. Mech. Rev., 40*, 5.

Lindgaard, E., & Lund, E. (2010). Nonlinear buckling optimization of composite structures. *Computer Methods in Applied Mechanics and Engineering*, Volume 199, Issues 37–40, 2319–2330.

Lopatin, A. V., & Morozov, E. V. (2014). Buckling of a uniformly compressed composite rectangular CCCC sandwich plate. *Composite Structures*, 332-340.

Ni, Q. Q., Xie, J., & Iwamoto, M. (2005). Buckling analysis of laminated composite plates with arbitrary edge supports. *Compos Struct, 69*, 209–17.

Nylander, H. (1951). *Initially deflected thin plate with initial deflections affine to additional deflection.* IABSE Publications.

Onkar, A. S., Upadhyay, C. S., & Yadav, D. (2006). Generalized buckling analysis of laminated plates with random material properties using stochastic finite elements. *Int J Mech Sci, 48*, 780–98.

Prabhakara, D. L., & Datta, P. K. (1997). Vibration, buckling and parametric instability of plates with centrally located cutouts subjected to in-plane edge loading (tension and compression). *Thin Walled Struct., 27*, 443–470.

Reissner, E. (1945). The effect of rotary inertia and shear on flexure motion of isotropic plates. *J. Appl. Mech., 12*, A69–77.

Romanian-spotters. (2009). *http://romanian-spotters.forumer.ro/t2215-aeroportul-bucuresti-aurel-vlaicu-baneasa-iunie-2009.*

Sciuva, D. M., Gherlone, M., & Lomario, D. (2003). Multiconstrained optimization of laminated and sandwich plates using evolutionary algorithms and higher-order plate theories. *Compos Struct, 59*, 149–54.

Shufrin, I., Rabinovitch, O., & Eisenberger, M. (2008). Buckling of laminated plates with general boundary conditions under combined compression, tension, and shear-A semi-analytical solution. *Thin-Wall Struct, 46*, 925–38.

Srivatsa, K. S., & Murthy, A. V. (1991). Stability of laminated composite plates with cut-outs. . *Comput. Struct., 43*, 213–219.

The Composite Materials Handbook. (1997)., MIL-17 Mil-HDBK-17-1F, U. S. Department of Defense.

Ungbhakorn, V., & Singhatanadgid, P. (2006). Buckling analysis of symmetrically laminated composite plates by the extended Kantorovich method. *Compos Struct, 73*, 120-128.

Walker, M. (2001). Multiobjective design of laminated plates for maximum stability using the finite element method. *Compos Struct, 54*, 389–93.

Walker, M. (2002). The effect of stiffeners on the optimal ply orientation and buckling load of rectangular laminated plates. *Comput Struct, 80*, 2229–39.

Walker, M., Adali, S., & Verijenko, V. E. (1996). Optimization of Symmetric Laminates for Maximum Buckling Load Including the Effects of Bending-Twisting Coupling. *Comp & Stru, 26(1)*, 313-319.

Whitney, J. M. (1969). The effect of transverse shear deformation on the bending of laminated plates. *J. Compos. Mater., 3*, 534–547.

Whitney, J. M., & Pagano, N. J. (1970). Shear deformation in heterogeneous anisotropic plates . *J. Appl. Mech., 37*, 1031–1036.

Xie, J. X., Ni, Q. Q., & Iwamoto, M. (2005). Buckling analysis of laminated composite plates with internal supports. *Compos Struct, 69*, 201–8.

Zhang, Y. X., & Yang, C. H. (2009). Recent developments in finite element analysis for laminated composite plates. *Compos Struct, 88*, 147–57.

Zor, M., Sen, F., & Toygar, M. E. (2005). An investigation of square delamination effects on the buckling behavior of laminated composite plates with a square hole by using three-dimensional FEM analysis. *J Reinf Plast Compos, 24*, 1119–30.

Chapter 2

Literature Review

2.1. Introduction

Fibre reinforced polymer (FRP) composites are advanced engineering materials with high specific strength and specific stiffness relative to other structural materials. Structural FRPs made from glass/carbon/Kevlar fibres with polyester, vinylester, and epoxy resins are lightweight, and environmentally resistant. FRPs not only have excellent properties such as lightweight, noncorrosive, nonmagnetic, and nonconductive, but also they exhibit excellent energy absorption characteristics which make them suitable for impact and crashworthiness applications, seismic response, and also for fatigue loading. These high performance characteristics make FRP composites a suitable choice for the requirements of aerospace applications. The first use of FRP composite materials dated back to the 1940s in the aerospace and naval applications and because of their superior performance, FRP composites are increasingly used in the aerospace industry since the 1960s and 1970s (Bakis, et al., 2002). Currently aircraft industry is one of the main application areas of FRP materials especially as in the aerospace industry weight is a sensitive parameter. The A350 XWB is the first Airbus with both fuselage and wing structures made primarily of carbon fibre-reinforced plastic (CFRP) (Figure 2.1).

Fig. 2.1. The first 21-metre long forward fuselage section for the A350 XWB made from CFRP (Airbus, 2014).

In this chapter buckling behaviour of composite plates, effect of delamination on buckling performance of FRP composite plates, common non-destructive testing methods used for evaluation of damage in FRP laminates, and optimisation methods of composite laminate will be reviewed.

2.2. Buckling Analysis of Composite Plate

The mechanics of laminated composite materials is generally studied at two levels: small scale micromechanics and large scale macromechanics. In the micromechanics the relationship between the properties of the constituent's materials and those of the lamina are defined by analysis of a representative volume element (RVE). However, for most engineering design an analysis based on the micromechanical level is unrealistic. At the macromechanical level, the properties of the individual layers are assumed to be known in advance and the aim is to establish the interaction of the individual layers of a laminate with one another and their effects on the overall response of the laminate. In other words macromechanics is based on continuum mechanics, which models each lamina as homogeneous and orthotropic and ignores the fibre/matrix interface. At present the use of macromechanical formulations in designing composite laminates is well established and the buckling analysis will be based on macromechanics approach.

The buckling behaviour of laminated composite thin plates has been a subject of interest for many years. Amongst the various aspects of mechanical behaviour of a structures made of composite materials, buckling is one of the main concern in the design of thin-walled structures. This is due to fact that laminated FRP composites are thin-walled and it made from relatively low stiffness polymer and high strength fibres. As a result FRP composite structures has the potential to undergo large deformation and they are vulnerable to global and local buckling before reaching the material strength failure under service loads(e.g Figure 2.2).

Source: EU (2005)

Fig. 2.2. Local buckling in airplane fuselage (Belesis & Labeas, 2010).

The buckling theory for structures began with the studies made by Leonhard Euler on the stability of flexible compressed columns (Euler, 1744). The column is assumed to have a uniform cross-section and either is ideally straight or has some defined initial curvature (Benham, Crawford, & Armstrong, 1996) (Ahanchian, 2008). If a structure (such as a strut) is subjected to an in-plane compression loading, there will be no out-of-plane displacements until the load is reached to the critical buckling load (P_{cr}) when failure starts to occur. This failure is termed buckling and is widespread in slender members. The slenderness ratio L_e/k relates the effective length of the strut to the radius of gyration k of the cross section where $k = \sqrt{\frac{I}{A}}$ and L_e is the effective length of the strut depending on the end conditions (Euler, 1744) (Benham, Crawford, & Armstrong, 1996). In general if

$\frac{L_e}{k} < 0.3\sqrt{\frac{\pi^2 E}{\sigma_{YC}}}$, the strut will be stocky and compressive theory will apply and if $\frac{L_e}{k} > 2\sqrt{\frac{\pi^2 E}{\sigma_{YC}}}$, the strut will be slender and buckling theory will apply. σ_{YC} is the compressive yield stress.

The analysis of plate buckling will be based on classical laminated plate theory (CLPT) (Barbero, 2011) (Kassapoglou, 2010). According to CLPT the components of reduced stiffness matrix for each ply are:

$$
\begin{aligned}
&Q_{11} = \frac{E_1}{1-\nu_{12}\nu_{21}}, \quad Q_{22} = \frac{E_2}{1-\nu_{12}\nu_{21}}, \\
&Q_{12} = \frac{\nu_{12}E_2}{1-\nu_{12}\nu_{21}} = \frac{\nu_{21}E_1}{1-\nu_{12}\nu_{21}}, \quad Q_{66} = G_{12}
\end{aligned}
\tag{2.1}
$$

where E_1 and E_2 are modulus of elasticity in fibre and transverse to fibre directions, and G_{12} is shear modulus in 12 plane and ν_{12}, ν_{21} are Poisson's ratios. The components of transformed reduced stiffness matrix in the global coordinate system are:

$$
\begin{aligned}
&\overline{Q}_{11} = m^4 Q_{11} + n^4 Q_{22} + 2m^2n^2 Q_{12} + 4m^2n^2 Q_{66} \\
&\overline{Q}_{22} = n^4 Q_{11} + m^4 Q_{22} + 2m^2n^2 Q_{12} + 4m^2n^2 Q_{66} \\
&\overline{Q}_{12} = m^2n^2 Q_{11} + m^2n^2 Q_{22} + \left(m^4 + n^4\right) Q_{12} - 4m^2n^2 Q_{66} \\
&\overline{Q}_{66} = m^2n^2 Q_{11} + m^2n^2 Q_{22} - 2m^2n^2 Q_{12} + \left(m^2 - n^2\right) Q_{66} \\
&\overline{Q}_{16} = m^3n Q_{11} - mn^3 Q_{22} + \left(mn^3 - m^3n\right) Q_{12} + 2\left(mn^3 - m^3n\right) Q_{66} \\
&\overline{Q}_{26} = mn^3 Q_{11} - m^3n Q_{22} + \left(m^3n - mn^3\right) Q_{12} + 2\left(m^3n - mn^3\right) Q_{66}
\end{aligned}
\tag{2.2}
$$

where m = cos θ and n = sin θ. The extensional (A), coupling (B), and bending (D) stiffness matrices are:

$$A_{ij} = \sum_{k=1}^{n} [\overline{Q}_{ij}]_k (z_k - z_{k-1}) \quad (2.3)$$

$$B_{ij} = \frac{1}{2} \sum_{k=1}^{n} [\overline{Q}_{ij}]_k (z_k^2 - z_{k-1}^2) \quad (2.4)$$

$$D_{ij} = \frac{1}{3} \sum_{k=1}^{n} [\overline{Q}_{ij}]_k (z_k^3 - z_{k-1}^3) \quad (2.5)$$

Note that for symmetric laminates B matrix is zero.

For large deflection of an especially orthotropic symmetric laminated plate where A_{16}=A_{26}=0, D_{16}=D_{26}=0 and B_{ij}=0, the first von Karman equation becomes:

$$\begin{aligned} D_{11}\frac{\partial^4 w}{\partial x^4} + 2(D_{12} + 2D_{66})\frac{\partial^4 w}{\partial x^2 \partial y^2} + D_{22}\frac{\partial^4 w}{\partial y^4} \\ = N_x \frac{\partial^2 w}{\partial x^2} + 2N_{xy}\frac{\partial^2 w}{\partial x \partial y} + N_y \frac{\partial^2 w}{\partial y^2} - p_x \frac{\partial w}{\partial x} - p_y \frac{\partial w}{\partial y} - p_z \end{aligned} \quad (2.6)$$

For a plate under biaxial loading N_{xy}= p_x= p_y= p_z=0, and Eq. (2.6) reduces to:

$$D_{11}\frac{\partial^4 w}{\partial x^4} + 2(D_{12} + 2D_{66})\frac{\partial^4 w}{\partial x^2 \partial y^2} + D_{22}\frac{\partial^4 w}{\partial y^4} = N_x \frac{\partial^2 w}{\partial x^2} + N_y \frac{\partial^2 w}{\partial y^2} \quad (2.7)$$

In the above *w* is the out-of-plane displacement of the plate.

The solution of *w* for a plate with simply supported edges (SSSS) is:

$$w = \sum\sum A_{mn} \sin\frac{m\pi x}{a} \sin\frac{n\pi y}{b} \quad (2.8)$$

Substituting *w* from Eq. (2.8) in Eq. (2.7) and if the plate aspect ratio defined as *R= a/b* then

$$\pi^2 A_{mn} \left\lfloor D_{11} m^4 + 2(D_{12} + 2D_{66}) m^2 n^2 R^2 + D_{22} n^4 R^4 \right\rfloor = -A_{mn} a^2 \left\lfloor N_x m^2 + N_y n^2 R^2 \right\rfloor \quad (2.9)$$

Let $k=N_y/N_x$ and N_x=-N_c then from Eq. (2.9) results

$$N_c = \frac{\pi^2\left[D_{11}m^4 + 2(D_{12}+2D_{66})m^2n^2R^2 + D_{22}n^4R^4\right]}{a^2(m^2+kn^2R^2)} \tag{2.10}$$

For a plate under uniaxial loading $N_y = 0$ and $k = 0$; therefore for SSSS boundary condition Eq. (2.10) simplifies to:

$$N_c = \frac{\pi^2\left[D_{11}m^4 + 2(D_{12}+2D_{66})m^2n^2R^2 + D_{22}n^4R^4\right]}{a^2m^2}. \tag{2.11}$$

For a plate with clamped-simply supported-clamped-simply supported (CSCS) boundary conditions subjected to uniaxial loading the solution to Eq. (2.7) becomes

$$N_c = \frac{\pi^2}{b^2}\sqrt{D_{11}D_{22}}(K) \tag{2.12}$$

where N_c is critical buckling load, b is the width of the specimen, and K is

$$K = \begin{cases} \dfrac{4}{\lambda^2} + \dfrac{2(D_{12}+2D_{66})}{\sqrt{D_{11}D_{22}}} + \dfrac{3}{4}\lambda^2; & 0 < \lambda < 1.662 \\ \dfrac{m^4+8m^2+1}{\lambda^2(m+1)} + \dfrac{2(D_{12}+2D_{66})}{\sqrt{D_{11}D_{22}}} + \dfrac{\lambda^2}{m^2+1}; & \lambda > 1.662 \end{cases} \tag{2.13}$$

where $\lambda = \frac{a}{b}\left(\frac{D_{22}}{D_{11}}\right)^{1/4}$ and m is an integer number which represents the number of half-wave in load wise direction and a is the length of the plate in the direction of loading.

Haftka *et al.* (1992) (1999) reported that the stacking-sequence design of a laminated plate for buckling using CLPT can be formulated as a linear problem using ply-orientation-identity design variables.

A simply supported laminated plate of composite materials under biaxial compression is shown in Figure 2.2. The loads per unit length in the x and y directions are $\lambda \cdot N_x$ and $\lambda \cdot N_y$, respectively, with λ being an amplitude parameter. The laminate is assumed to be symmetric and composed of 0, 90, and ±45 degree plies. All plies have the same thickness t. For most applications the laminate are balanced. The laminate is composed of N plies.

From Eq. (2.10) it can be deduce that the laminate buckles when the load amplitude reaches the critical value λ_{cr} given by

$$\lambda_{cr}(m,n) = \frac{\pi^2[D_{11}(m/a)^4 + 2(D_{12}+2D_{66})(m/a)^2(n/b)^2 + D_{22}(n/b)^4]}{(m/a)^2 N_x + (n/b)^2 N_y} \tag{2.14}$$

Where *m* and *n* are the number of half-waves in x and y directions, respectively, that minimise λ_{cr}. In the present study, the minimisation over *m* and *n* is performed by checking for all possible values of *m* and *n*.

The flexural stiffness D_{11}, D_{12}, D_{22}, and D_{66} can be expressed in terms of three integrals, V_0, V_1, and V_3, and five material invariants U_i, i =1, ...,5, which depend on the stacking sequence as

$$\begin{aligned} D_{11} &= U_1V_0 + U_2V_1 + U_3V_3 \\ D_{22} &= U_1V_0 - U_2V_1 + U_3V_3 \\ D_{12} &= U_4V_0 - U_3V_3 \\ D_{66} &= U_5V_0 - U_3V_3 \end{aligned} \tag{2.15}$$

where

$$\begin{aligned} V_0 &= \int_{-h/2}^{h/2} z^2 dz = \frac{1}{3}\sum_{k=1}^{N} p_k (z_k^3 - z_{k-1}^3) \\ V_1 &= \int_{-h/2}^{h/2} z^2 \cos 2\theta dz = \frac{1}{3}\sum_{k=1}^{N} p_k \cos 2\theta_k (z_k^3 - z_{k-1}^3) \\ V_3 &= \int_{-h/2}^{h/2} z^2 \cos 4\theta dz = \frac{1}{3}\sum_{k=1}^{N} p_k \cos 4\theta_k (z_k^3 - z_{k-1}^3) \end{aligned} \tag{2.16}$$

Note *h* is total thickness of the laminate, *z* the distance from the plane of symmetry (see Figure 2.3), θ the ply-orientation angle, and p_k a variable that is equal to one if the k^{th} ply is occupied and is equal to zero if the ply is empty. Constraints are applied during the optimisation to ensure that p_k can be zero only for the outermost plies.

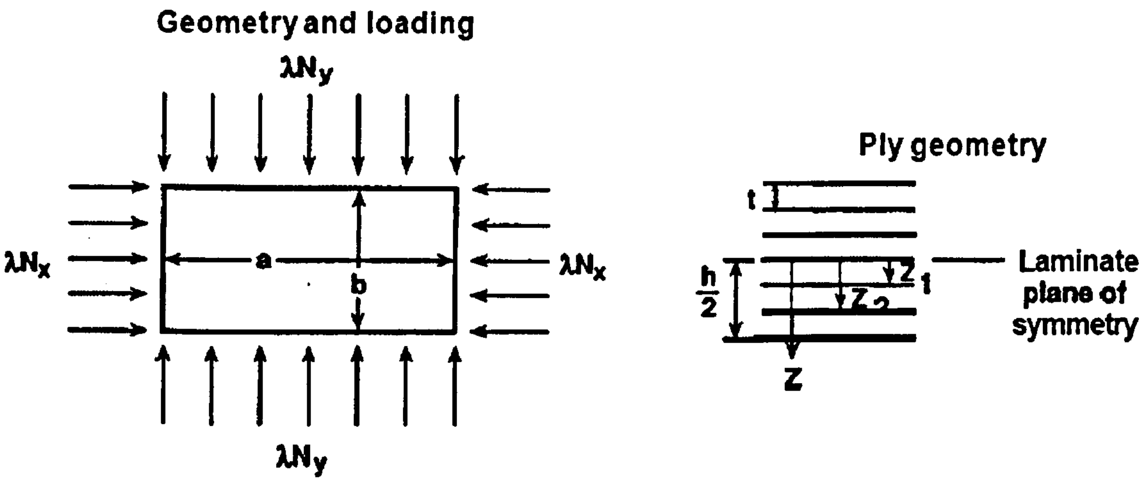

Fig. 2.3. Geometry of laminated plate and biaxial loading scheme (Haftka & Walsh, 1992).

The material invariants are:

$$
\begin{aligned}
U_1 &= \tfrac{1}{8}(3Q_{11} + 3Q_{22} + 2Q_{12} + 4Q_{66}) \\
U_2 &= \tfrac{1}{2}(Q_{11} - Q_{22}) \\
U_3 &= \tfrac{1}{8}(Q_{11} + Q_{22} - 2Q_{12} - 4Q_{66}) \\
U_4 &= \tfrac{1}{8}(Q_{11} + Q_{22} + 6Q_{12} - 4Q_{66} \\
U_5 &= \tfrac{1}{8}(Q_{11} + Q_{22} - 2Q_{12} + 4Q_{66}
\end{aligned}
\tag{2.17}
$$

It is more general to work in terms of non-dimensional loads n_x and n_y, flexural stiffness d_{ij}, integrals v_0, v_1, and v_3, and material constants u_i defined as

$$
\begin{aligned}
&n_x = 1.5\frac{N_x a^2}{\pi^2 E_1 t^3}, \quad n_y = 1.5\frac{N_y a^2}{\pi^2 E_1 t^3}, \quad d_{ij} = 1.5\frac{D_{ij}}{E_1 t^3} \quad i,j = 1,2,6 \\
&v_i = 1.5\frac{V_i}{t^3}, \quad i = 0,1,3, \\
&u_i = \frac{U_i}{E_1}, \quad i = 1,\ldots,5.
\end{aligned}
\tag{2.18}
$$

Then λ_{cr} becomes

$$
\lambda_{cr}(m,n) = \frac{d_{11}m^4 + 2(d_{12} + 2d_{66})m^2 n^2 (a/b)^2 + d_{22} n^4 (a/b)^4]}{m^2 n_x + n^2 (a/b)^2 n_y}
\tag{2.19}
$$

and the non-dimensional flexural stiffness terms are given as

$$
\begin{aligned}
d_{11} &= u_1 v_0 + u_2 v_1 + u_3 v_3 \\
d_{22} &= u_1 v_0 - u_2 v_1 + u_3 v_3 \\
d_{12} &= u_4 v_0 - u_3 v_3 \\
d_{66} &= u_5 v_0 - u_3 v_3
\end{aligned}
\tag{2.20}
$$

Beznea *et al.* (2011) studied the buckling of composite plates using classical bifurcation and finite element analysis. They derived the critical buckling equations for various edge conditions for perfect plates. The buckling phenomena mean collapse of the structure at the maximum point in a load versus out of plane displacement after bifurcation happens. The way the buckling happen depends on its geometrical and material properties and also on how the structure is loaded.

Beznea *et al.* (2011) narrates that according to the level of bending energy, the buckling of plates can occur in two ways: bifurcation buckling and limit point buckling. Bifurcation buckling is an instability point in which a sudden change in the shape of the structure occurs. Therefore it is a point in a load versus out of plane displacement where two equilibrium paths intersect. On the other hand, limit point buckling is an instability in which the load-out of plane displacement reaches a maximum and then exhibits negative stiffness while releasing strain energy. During limit point buckling there are no sudden changes in the equilibrium path; however, if load is continuously increased then the structure may jump or "snap" to another point on the out of plane displacement curve. For this reason, this type of instability is often called "snap-through" buckling, because the structure snaps to a new equilibrium location. The load-out of plane displacement curve also has a zero slope at the point of maximum load (or limit point).

Buckling analysis of a plate may be divided into three types (Beznea & Chirica, 2011):

- Classical buckling analysis;
- Difficult classical effects;
- Non classical phenomena.

The classical buckling analysis may be described by the curve 1-3 shown in Figure 2.4 where in-plane loading force (N) plotted against the out-of-plane displacement (w) for a representative point of the plate. By assuming that the loading is applied in the mid-plane

of the plate and under the condition of perfect symmetry, no out-of-plane displacement will occur. The loading may increase up to the yield point as illustrated by curve 1-2. However if instability occurs at $N=N_{cr}$ bifurcation will starts. This means that the loading versus out-of-plane displacement curve takes the path 4 and buckling will occur. Note that at N_{cr} a small perturbation will generate out-of-plane displacement.

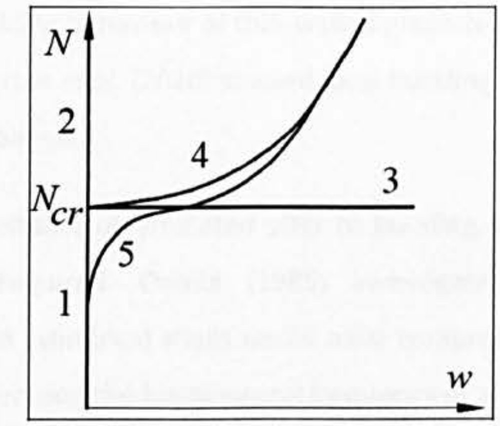

Fig. 2.4. Variation of out of plane displacement, w, versus in-plane load, N (Beznea & Chirica, 2011).

The classical linear analysis, which is a generalization of the Euler buckling, should indicate that w increases to infinite at $N=N_{cr}$ (curve 3). Actually, the nonlinear effects started to act and after an initial finite displacement, the in-plane loading N is increasing and subsequently the displacement is increasing. In this case the plate is able to carry load distant in excess of N_{cr} before it collapse as shown by curve 4. This is called a "postbuckling curve" because it shows the behaviour of the plate after the buckling load N_{cr} is reached.

The difficulty in the classical buckling analysis arises when vibrations, non-homogeneities, variable thicknesses, shear deformations, springs, and nonlinear relations between stresses and strains are present.

Non classical buckling analysis involves considerations of the effects such as imperfections, non-elastic material behaviour, dynamic effects of the loading, and the fact that the in-plane loading is not in the mid-plane of the plate. Finally, it may point out that no plate is initially perfect (perfectly flat or perfectly symmetry) and if initial deviation from flatness or symmetry exists, the buckling behaviour of the plate will follow

the path similar to the curve 1-5 shown in Figure 2.4. In this case, no clear buckling point is distinguishable. The deviations of the plate from the flatness and symmetry are usually called imperfections (for laminated FRP composites initial transversal imperfection or delamination) (Beznea & Chirica, 2011).

Local buckling of laminated composite plates has gained a lot of attention. Reddy *et al.* (1985) studied the local buckling behaviour of thin-walled graphite/epoxy I-section beams under axial compression. Tarjan *et al.* (2010) studied local buckling analysis of thin-walled open or closed section FRP beams.

In order to optimise the resistance of laminated plate to buckling, structural optimisation under buckling load is required. Onoda (1985) investigated optimum laminate configurations for laminated cylindrical shells under axial compression. Hanagud (1985) studied the problem of maximizing the fundamental frequency of a thin walled beam with coupled bending and torsional modes. Knight (1985) reported result of an experimental and analytical study of the postbuckling behaviour of selected curved stiffened graphite-epoxy panels loaded in axial compression. The postbuckling response and failure characteristic of the panels are presented. Arnold *et al.* (1985) studied buckling, postbuckling, and crippling of shallow curved composite plates with edge stiffeners. Bisagni and Lanzi (2002) studied postbuckling optimisation of composite stiffened panels using neural networks. Stevens *et al.* (1996) investigated buckling and postbuckling of composite structures. Bambach (2009) studied photogrammetry measurements of buckling modes and interactions in channels with edge-stiffened flanges.

Burg (2011) reported on isotropic plate buckling. The schematic load-displacement diagram when buckling occurs for isotropic plate is shown in Figure 2.6. In the reality, however, the load-displacement diagram of plate will follow the path shown in Figures 2.6 and 2.7. Using finite element analysis the entire buckling behaviour of the plate under loading can be analysed. The true behaviour of the plate will be realised if all the effects such as plasticity, initial imperfections and second order effects, are considered in the model.

Burg (2011) identified the critical Euler plate buckling stress (σ_{cr}) as the starting point for any method, since it is used to determine the relative plate slenderness. Euler plate buckling stress (σ_{cr}) is the stress level at which buckling occurs in a perfect plate. By overlooking imperfections, and assuming linear elastic material:

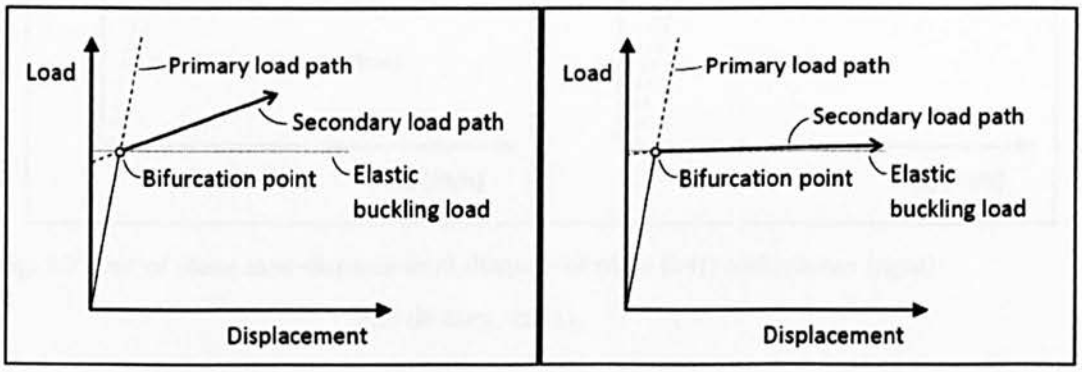

Fig. 2.5. The ideal load-in plane displacement diagram of a plate (left) and a column (right) for elastic buckling (van de Burg, 2011).

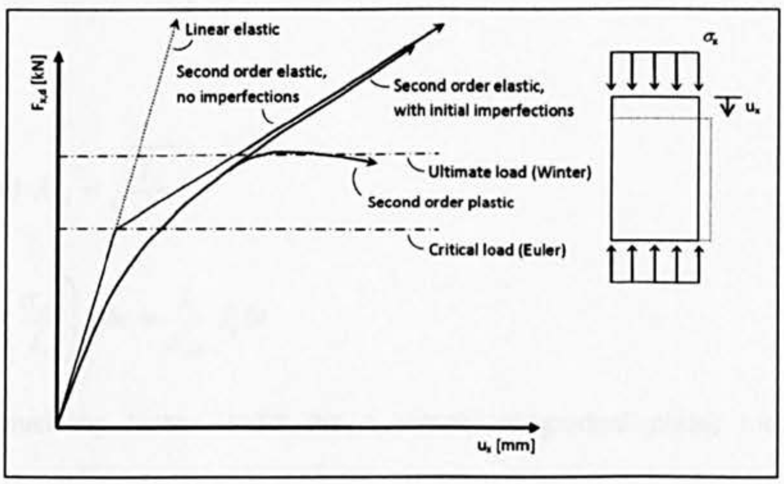

Fig. 2.6. The real load-in plane displacement diagram (van de Burg, 2011).

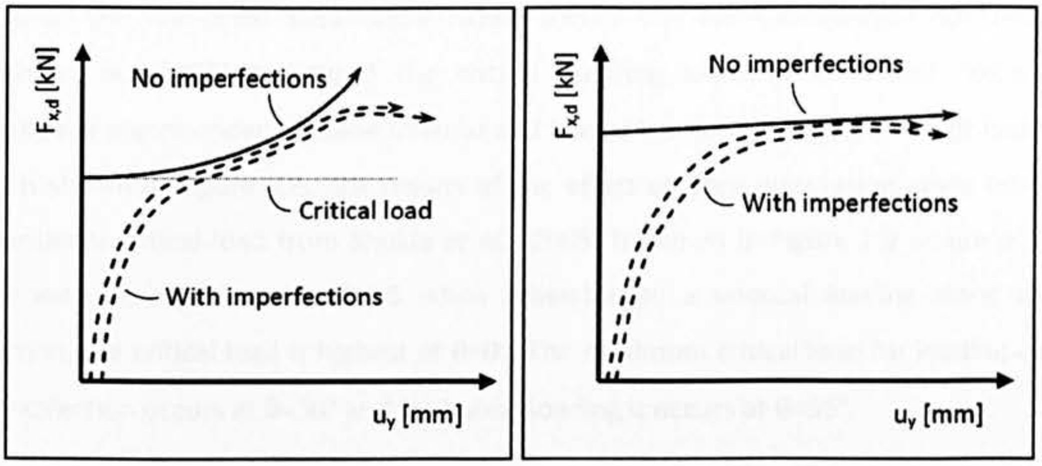

Fig. 2.7. Out of plane load-displacement diagram of plate (left) and column (right) (van de Burg, 2011).

$$\sigma_{cr} = \frac{k_\sigma \pi^2 E}{12(1-\upsilon^2)(b/t)^2}$$
$$\text{where } k_\sigma = \left(\frac{m}{\alpha} + \frac{\alpha}{m}\right)^2, \alpha = \frac{a}{b}, m = 1,2,3,... \tag{2.21}$$

$$N_{cr} = \sigma_{cr} bt \tag{2.22}$$

If $\sigma_{cr} = \rho f_y$ and $\lambda_{rel} = \sqrt{\frac{f_y}{\sigma_{cr}}}$,

$$N_{cr} = \rho f_y bt = \left(\frac{\sigma_{cr}}{f_y}\right) f_y bt = \frac{1}{\lambda_{rel}^2} f_y bt \tag{2.23}$$

where k_σ is buckling factor, valid for a simply supported plate, loaded by pure compression, ρ is reduction factor, f_y is yield stress, λ_{rel} is relative slenderness and $\frac{1}{\lambda_{rel}^2}$ is widely known as the Euler hyperbola.

Since no manufactured plate is without initial deformation and residual stresses, George Winter (Winter, 1947) conducted many experiments on cold formed steel sections and based on von Karman came up with:

$$\rho = \frac{b_{eff}}{b} = \sqrt{\frac{\sigma_{cr}}{f_y}}\left(1 - 0.22\sqrt{\frac{\sigma_{cr}}{f_y}}\right) \quad \text{or} \quad \rho = \frac{\lambda_{rel} - 0.22}{\lambda_{rel}^2} \quad \text{if} \quad \lambda_{rel} \geq 0.673 \tag{2.24}$$

Based on the first-order shear deformation theory and von-Karman-type nonlinearity, Shukla *et al.* (2005) estimated the critical buckling loads of laminated composite rectangular plates under in-plane uniaxial and biaxial loading. The estimation of buckling load is shown in Figure 2.8. The results of the effect of fibre orientation angle on non-dimensional critical load from Shukla *et al.* (2005) is shown in Figure 2.9 where a CSCS plate with an aspect ratio of 0.5 when subjected to a uniaxial loading along the *x* direction, the critical load is highest at θ=0°. The maximum critical load for loading along the *y* direction occurs at θ=30° and for biaxial loading it occurs at θ=55°.

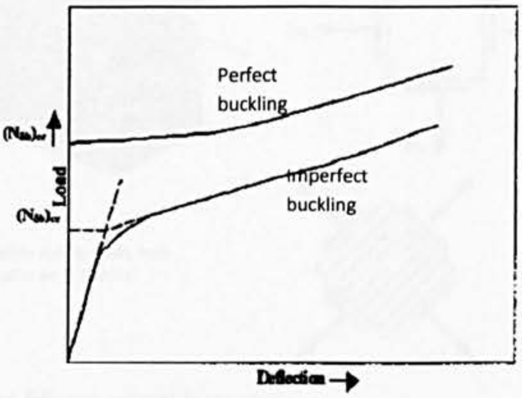

Fig. 2.8. The estimation of critical buckling load (Shukla, Nath, Kreuzer, & Sateesh Kumar, 2005).

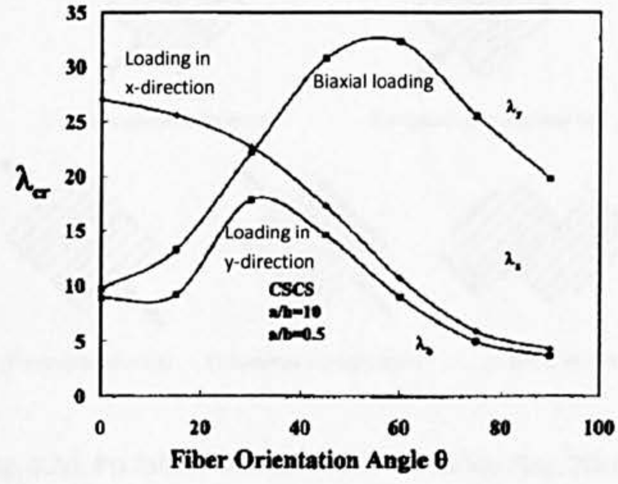

Fig. 2.9. The relationship of fibre orientation angle and non-dimensional critical load for four-layer asymmetric angle-ply CSCS square plate (Shukla, Nath, Kreuzer, & Sateesh Kumar, 2005).

The strain that a laminate can reach before micro-cracking occur depends strongly on the toughness and properties of the resin system. For brittle resin systems, such as most polyester, this point occurs a long way before laminate failure. Resin micro-cracks do not immediately reduce the ultimate properties of the laminate, since the ultimate strength of a laminate in tension is governed by the strength of the fibres. It should also be noted that when a composite is loaded in tension, for the full mechanical properties of the fibre component to be achieved, the resin must be able to deform to at least the same extent as the fibre. Figure 2.10 shows modes of failure in a lamina.

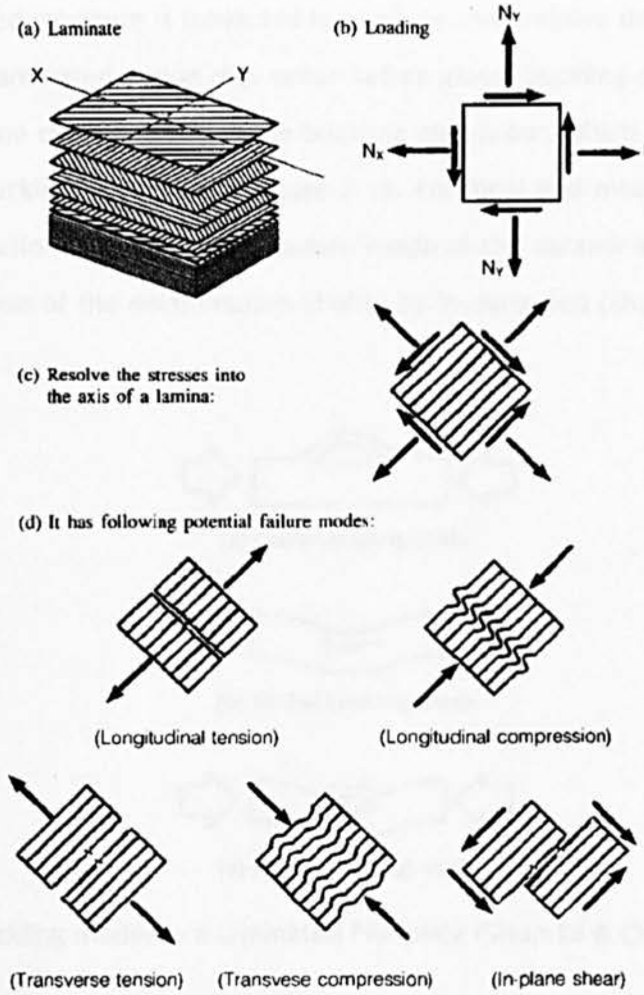

Fig. 2.10. Ply failure modes (Shun-Fa & Ching-Ping, 2000).

2.3. Buckling of Delaminated FRP Composite Plates

One of the most common failure modes for laminated composite structures is interlaminar delamination. Delamination can be caused by in-service accidents (e.g., low velocity impact), high stress concentrations from geometrical discontinuity or a manufacturing defect (e.g., imperfect curing process). Due to the presence of the delaminated area, buckling of laminated structures can reduce the designed structure strength when it is subjected to compressive loading. Hence the structural stability is one of the most likely modes of failure for thin-walled laminated FRP composite structures. Since buckling can lead to a catastrophic failure, it must be taken into account at the design stage of FRP composite structures.

When a delaminated structure is subjected to in-plane compressive dominated load, local buckling of the delaminated region may occur before global buckling of the laminate (see Figure 2.11). In some cases a mixed mode buckling may occur, which is a combination of local and global buckling as shown is Figure 2.11. For local and mixed buckling modes, growth of delamination is generally the failure mode of the delaminated composite and post buckling analysis of the delamination should be investigated (Shun-Fa & Ching-Ping, 2000).

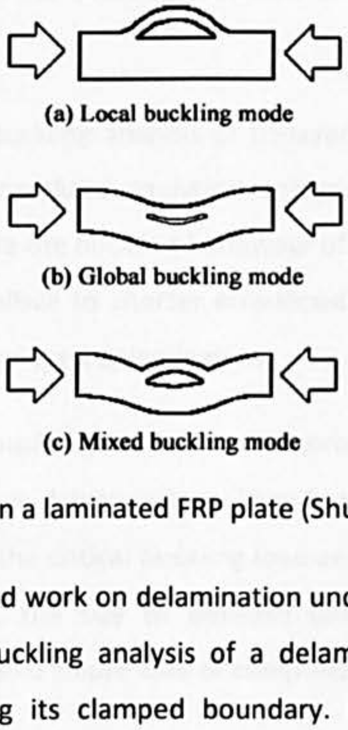

Fig. 2.11. Buckling modes in a laminated FRP plate (Shun-Fa & Ching-Ping, 2000).

Many researchers have conducted work on delamination under buckling load. Yin and Fei (1985) studied an elastic postbuckling analysis of a delaminated circular plate under axisymmetric compression along its clamped boundary. Chen and Bai (2002) have described postbuckling behaviour in face/core interface debonded composite sandwich plate. Aviles and Carlsson (2007) studied postbuckling and debond propagation in sandwich panels subjected to in-plane compression. They used nonlinear finite element analysis to predict initiation of debond and propagation in compression loaded foam cored sandwich panels containing a circular face/core debond. Cappello and Tumino (2006) studied the buckling and postbuckling behaviour of unidirectional and cross-ply laminated composite plates with multiple delaminations using numerical analysis. Wang and Dong (2007) used energy method to study hygrothermal effects on local buckling for triangular and lemniscate delamination shapes near the surface of cylindrical laminated shells. Parlapalli and Shu (2004) analysed the buckling behaviour of a two-layer beam with a single asymmetric delamination under clamped and simply supported boundary conditions. Kyoung *et al.* (1999) investigated buckling and postbuckling behaviours of composite cross-ply laminates with multiple delaminations.

Kim and Hong (1997) studied buckling and postbuckling behaviour of composite laminates with a delamination. A finite element analysis is generated for studying the buckling and postbuckling behaviours of a laminated composite with an embedded delamination. They reported there is a delamination size below that the buckling load and postbuckling behaviour are not affected, yet the buckling load decreases as the delamination size increases.

Parlapalli *et al.* (2005) studied buckling analysis of tri-layer beams having asymmetrical enveloped delaminations. A generalized analytical analysis using classical engineering solution is proposed to investigate the buckling behaviour of the beam. They reported the critical buckling load is not sensitive to shorter enveloped delaminations whereas it is strongly influenced by longer enveloped delamination.

Aslan and Sahin (2009) studied buckling behaviour and compressive failure of composite laminates containing multiple large delaminations. They found the longest size and near-surface delamination influences the critical buckling load and compressive failure load of composite laminates. However, the size of beneath delaminations does not affect buckling load value and compressive failure load of composite laminates.

Arman *et al.* (2006) investigated critical delamination diameter of laminated composite plates under buckling loads. They showed that the important decreases occur in the critical buckling load after a certain value of the delamination diameter. They also studied the effect of fibre orientations on buckling load.

Tafreshi (2004) studied delamination buckling and postbuckling in composite cylindrical shells under external pressure. She showed very small delamination area has no significant effect on the critical buckling load. Nevertheless, for large delamination area, especially when delamination is closer to the free surface of the laminate, the critical load of buckling is low. Tafreshi (2004) reported that the buckling load was highly influenced by the laminate stacking sequence. There are stacking sequences that favour delamination growth and others that exhibit high resistance against the crack extension. Finally, she stated a laminate can be tailored to delamination growth resistance.

Many researchers concluded any delamination in structures, particularly those near the surfaces, decrease the critical buckling load.

2.4. Non-Destructive Testing (NDT) of FRP Laminates

2.4.1. Introduction

Since the raw material is effectively processed at the same time as the manufacturing of composite components, there are many aspects, which require validation to ensure quality of the finished parts. Assuming the manufacturing process, component design and material selection have been adequately and correctly specified, visual and non-destructive testing form the first stage of quality control. Nevertheless, non-destructive test (NDT) can be used for identification of damages in FRP laminate. Brief descriptions of some of the NDE techniques which are used in this project are given below.

2.4.2. Infrared Thermography

Thermography is a science of measuring temperature changes on the surface of materials due to stress generated thermal fields or uneven distribution of heat from an excitation heat source. Thermography is a non-destructive investigation tool that allows remote sensing capabilities to detect imperfections in the materials. The technique is able to detect anomalies spatially since imperfections disrupt heat transfer. An excitation source is the heat source that introduces energy to cause heat energy transfer.

Whilst a uniform heat flux is supplied to a plate, any abnormal variations in the resulting temperature distribution in the structure are indications of flaws in the material. Thermal imaging is carried out by means of infra-red (IR) television photography. Figure 2.12 shows the region of IR radiation is between 0.79 µm and 1 mm (Harris, 1999). In materials of higher thermal conductivity such as CFRP detection is more difficult. A remote monitoring technique is used during transient heat transfer by rapid scanning of the induced thermal fields using TV/video-compatible infra-red imagers. This set up forms the basis of the pulse video thermography (PVT) technique.

IR thermography can be used for strain analysis. Johnson (2006) used quantitative infrared (IR) thermography measurements to describe the fatigue damage process in laminated GFRP composites. The temperature changes on the surface of laminated GFRP composite specimens caused by damage during fatigue loading are tracked and thermoelastic stress analysis (TSA) technique is used to relate the surface deformation to the IR emission (see Figure 2.13).

Johnson also used IR thermography for identifying stress concentration in a bonded single lap joint (Johnson, 2006). Figure 2.14 shows his testing setup along with a schematic of the TSA data acquisition. The IR camera captured images at rates of more than 400 frames per second. The applied load signal was used to integrate synchronized TSA images that correspond to peak values of loading.

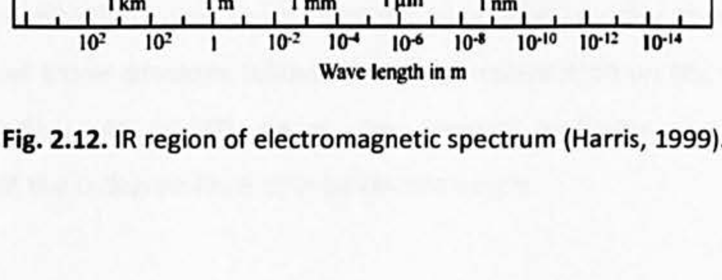

Fig. 2.12. IR region of electromagnetic spectrum (Harris, 1999).

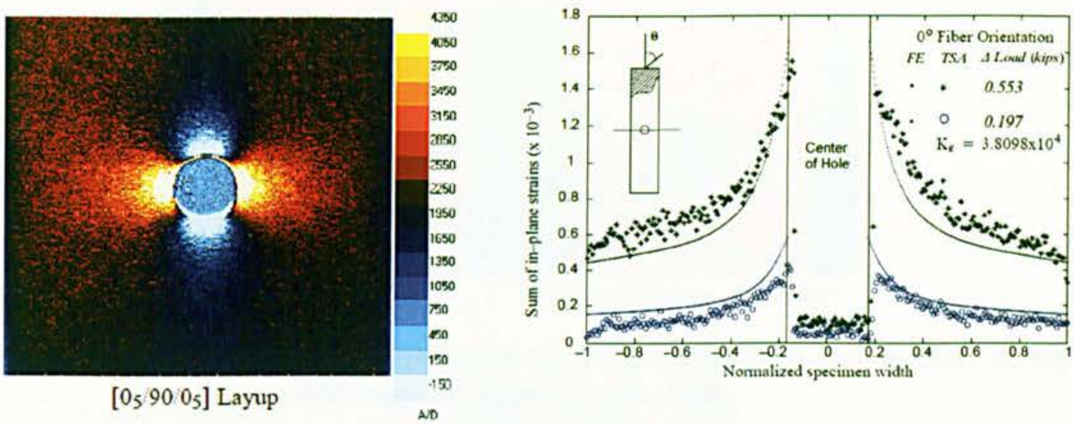

Fig. 2.13. TSA image of $[0_5/90/0_5]$ glass/epoxy of an open-hole plate (left) and its horizontal line interrogation for verification of thermomechanical calibration (right) (Johnson, 2006).

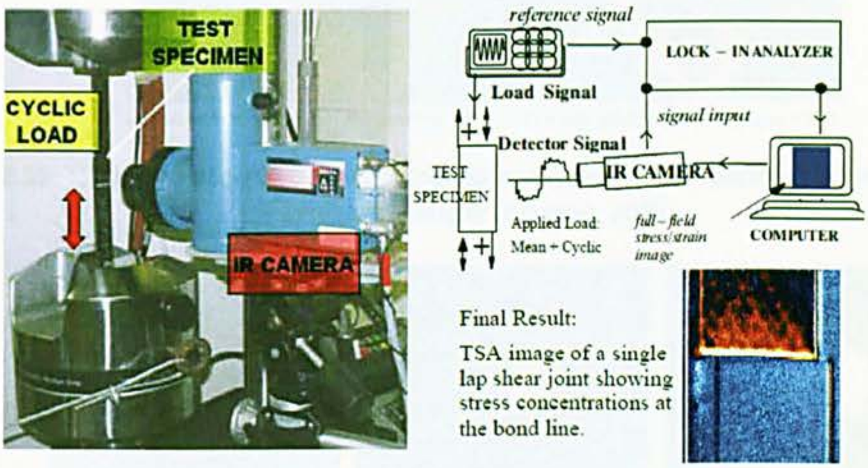

Fig. 2.14. Thermoelastic testing set–up (Johnson, 2006).

Johnson (2006) also explored the use of quantitative IR thermography measurement to describe the fatigue damage process in laminated GFRP composites. Figures 2.15 and 2.16 highlight different stages in the fatigue life of the notched quasi–isotropic specimen. The figures show TSA images between 300 to 90,505 cycles, the damage is due to matrix cracking and delaminations near the surface ply progresses quickly at various locations, and the growth of these damages follows the fibre's orientation on the surface layers to both straight edges. At 90,505 cycles the thermal emission shows some stress concentrations at the 0 degree fibre strip below the notch.

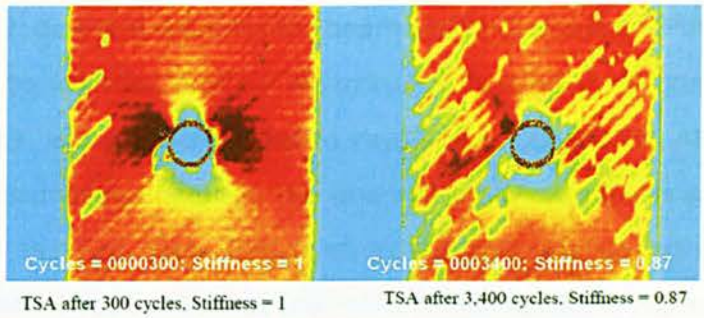

Fig. 2.15. TSA images of quasi-isotropic [-45/0/45/90]$_s$ S2-glass/epoxy open-hole specimen during initial stages of fatigue (Johnson, 2006).

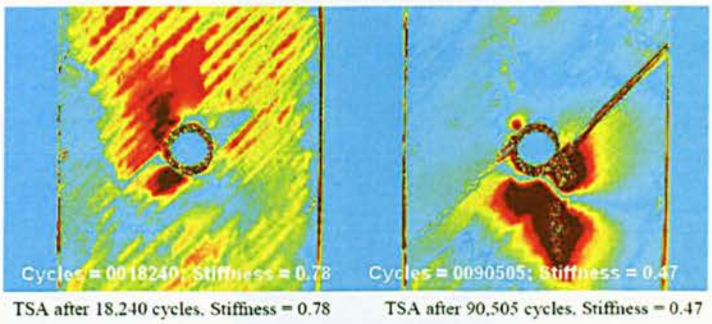

Fig. 2.16. TSA image of quasi-isotropic S2-glass/epoxy open-hole specimen during progressive stages of fatigue (Johnson, 2006).

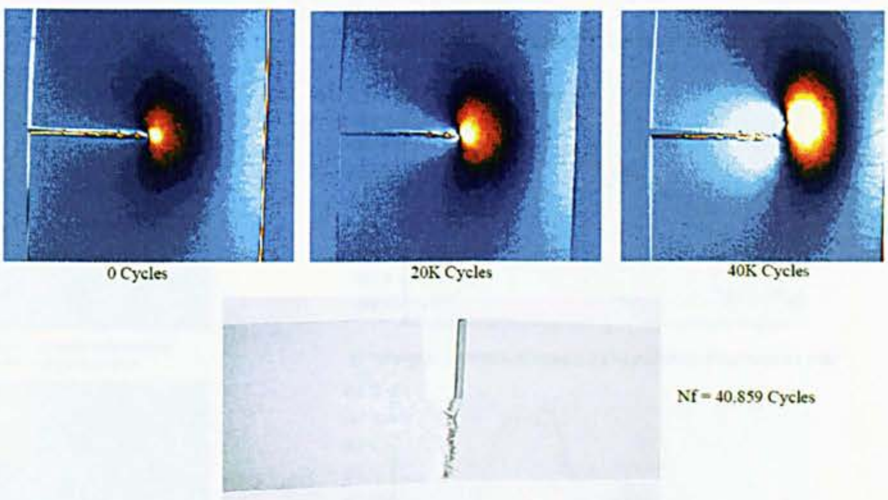

Fig. 2.17. IR-image of fatigue damage propagation ESE(T) specimen (Johnson, 2006).

Figure 2.17 shows the distribution of the in-phase TSA signal in the area around the crack tip of the pultruded thick-section eccentrically loaded single-edge-notched (Tension), ESE(T), specimen. The contours shown indicate the normal stresses and stress intensities in the material. The location of the crack tip and changes in the stress contours in the pultruded specimen can be tracked as the crack propagates until failure (Johnson, 2006).

Sultan *et al.* (2012) detected delamination depth and thickness in a GFRP plate. The plates were fabricated by inserting artificial delamination located at different thickness (see Figure 2.18 & 2.19) and at different depths (see Figure 2.20 & 2.21). Aluminium foil was used to insert delamination between the layers of the plate. Heat propagates from the front surface to the rear face. Delaminations become thermal barriers, delay heat diffusion and reflect the heat back to the surface. This results in higher temperature at delaminated areas than in non-delaminated regions.

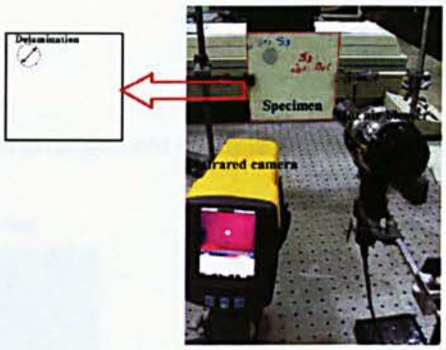

Fig. 2.18. Experimental arrangement for delamination thickness thermography Sultan *et al.* (2012).

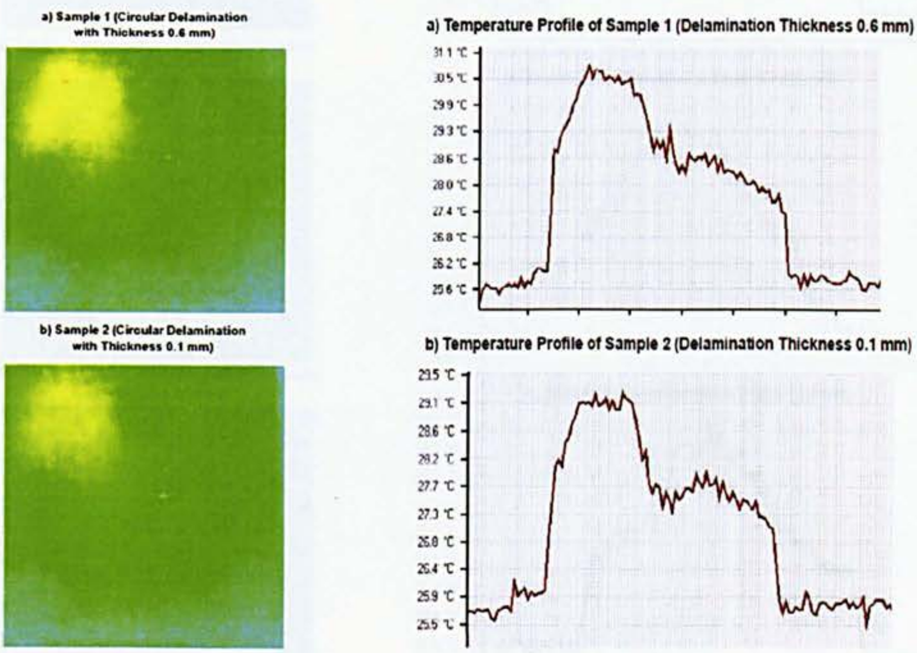

Fig. 2.19. Temperature thermography images (left) and surface temperature profiles (right) Sultan *et al.* (2012).

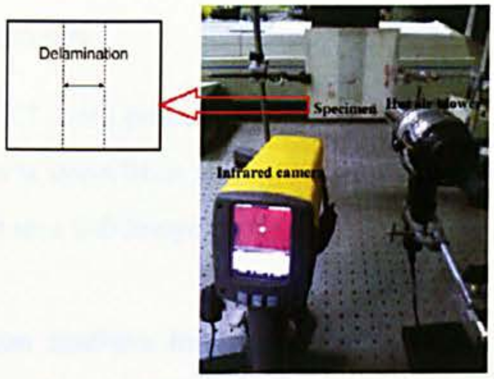

Fig. 2.20. Experimental arrangement for delamination depth thermography Sultan *et al.* (2012).

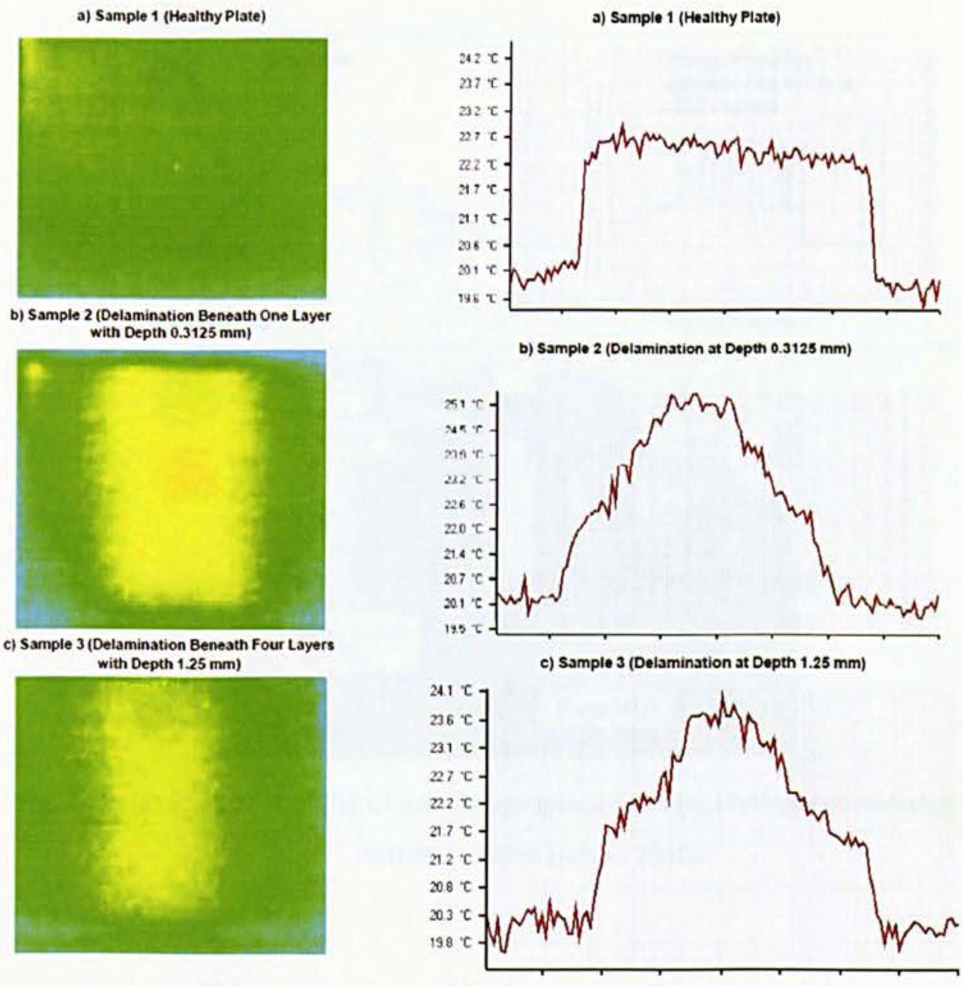

Fig. 2.21. Temperature thermography images (left) and surface temperature profiles (right) Sultan *et al.* (2012).

Boritu *et al.* (2011), Mieloszyk *et al.* (2012) and Sultan (2013) reported about delamination detection in FRP by thermography as well.

2.4.3. Computed Tomography

Computed tomography (CT scan) passes x-rays through a body of material, and collects them via a receiver. This is done from multiple angles around the body, and the results then interpreted to build up a 3-D image of the part.

The schematic of CT scan machine for material science and medical applications are shown in Figure 2.22 and 2.23, respectively.

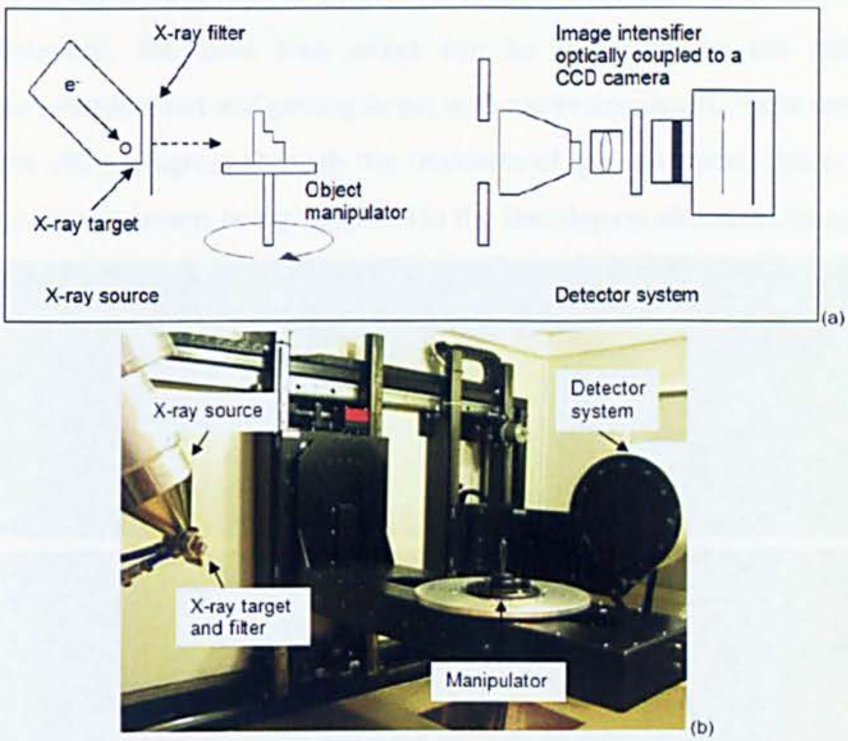

Fig. 2.22. (a) Schematic of the CT scan imaging setup and (b) Photograph showing the key instrumentation (Amos, 2010).

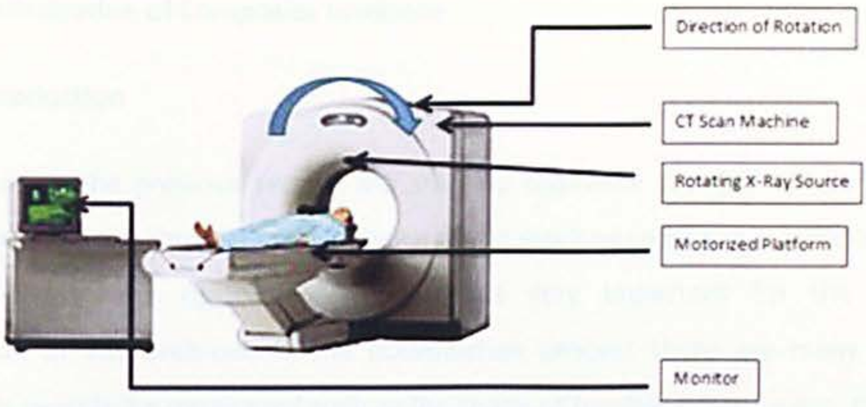

Fig. 2.23. CT scan machine for medical application (Weebly).

Figure 2.24 shows reconstructed CT slices taken from the impact damaged CFRP specimens. Damage propagation of shear cracks, fibre breakage, and delaminations have all been detected. The pine tree affect can be identified by the delaminations progressively spreading out and getting larger with increasing depth. These delaminations appear as the slices progress through the thickness of the specimen. This is due to the oblong shape delaminations being stretched in the fibre lay-up direction (Amos, 2010)

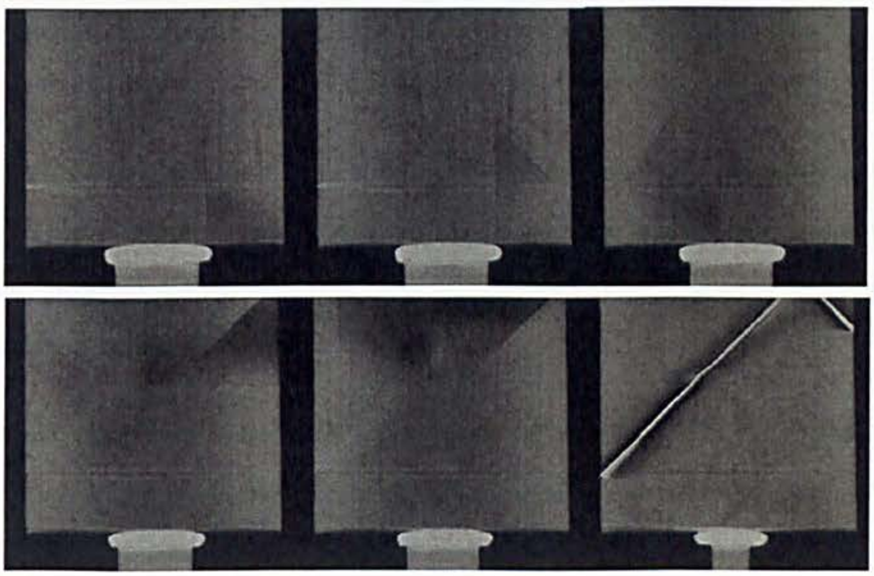

Fig. 2.24. Cross-sectional CT slices through the thickness of an impact damage CFRP (Amos, 2010).

In this research both IR-thermography and CT scan are used for the detection of delamination and damage in the buckled GFRP laminates.

2.5. Optimisation of Composite Laminate

2.5.1. Introduction

As discussed in the previous section the stacking sequence strongly affects the critical buckling load and the route to proper choice of the stacking sequence is optimisation. The proper choice of an optimisation strategy is very important for the successful optimisation of any problem. In the optimisation process there are many important parameters need to be considered such as the shape of feasible design space, the number of design variables, constrained or unconstrained problem, the number of constraints, the type of design variables (continuous, discrete or mixed), the type of objective function, linear or nonlinear functions, local and global optima, etc.

According to Gantovnik (2005) optimization algorithms can be categorised into two classes:

1. Deterministic methods

These methods work normally with continuous design variables and need a small number of function evaluations, but they may not find a global optimum point.

2. Nondeterministic methods

These methods work entirely using only function values and can work with discrete variables and (with infinite time) find a global optimum in the presence of several local optima. The common methods in this class are random search, genetic algorithms (GAs) and simulated annealing (SA).

In this work for optimisation of stacking sequence of laminated FRP plates, four methods (Enumeration, SQP, GA and SA) have been used and will be briefly discussed. More detail about these four methods of optimisation will be described in Chapter 4.

2.5.2. Enumeration (or Exhaustive) Search Method (ESM)

Enumeration search is one of the first attempts in optimum design of laminated composite materials, consisted of trying all possible combinations of design variables and simply selecting the best combination. Although cumbersome, this technique was successfully used to find the global optimum solution by finding the lightest laminated composite during the 1970s (Ghiasi, Pasini, & Lessard, 2009) (Waddoups, 1969) (Verette, 1970).

Denny (1998) investigated a number of probabilistic and exhaustive computational search techniques in the construction field. The search method and enumeration techniques developed in his thesis have led to the discovery of a number of new results.

2.5.3. Sequential Quadratic Programming (SQP)

SQP is one of the deterministic methods. Boggs (1996) introduced SQP in the basic theory of mathematical programming for optimisation. He discussed the method very comprehensively but he did not apply this method to laminated composite materials.

Epelman (Epelman) described and explained comprehensively continuous optimisation methods. He not only explored SQP method but also other methods such as unconstrained problems, line search methods, steepest descent algorithm, rate of convergence, newton's methods, constrained optimisation, linear constrained problem, barrier methods, duality theory of nonlinear programming, primal-dual interior point methods for linear programming and introduction to semi definite programming.

Fletcher (2007), Gill & Wong (2010) and Morales *et al.* (2010) in their papers explained SQP method from basic theory.

Relatively few researchers applied SQP to laminated composite design optimisation.

2.5.4. Genetic Algorithm (GA)

Genetic algorithm (GA) has become a powerful and robust tool for function optimization (Deb, 2001) (Goldberg, 1989). These algorithms are computational simple but powerful in their search for improvement in successive generations (Nagendra, Haftka, & Gurda, 1992). GA mimics some of the natural process observed in natural evolution. The basic techniques of GA are designed to simulate mechanism of population genetics and natural laws of survival. One of the big advantages of GA is that it does not require differentiability of either objective function or constraints (Nagendra, Haftka, & Gurda, 1992). The constraint handling capacity of GA is better than classical optimization techniques because of population based approach (Callahan & Weeks, 1992). Nagendra *et al.* (1992) studied the buckling optimization of laminate sequence with strain constraints. Callahan & Weeks (1992) studied the optimum design of composite laminates for maximizing laminate strength and stiffness with fixed number of plies. They employed tournament selection scheme in the selection process. Single point crossover is used with a crossover probability of Pc = 0.75 and mutation probability of 0.1 per cent. Kogiso *et al.* (1994) applied GA with memory for design of minimum thickness composite laminates subject to strength, buckling and ply contiguity *conditions.*

Muc and Gurba (2001) used GA for layout optimization of composite structures with finite element optimization of objective function. Sivakumar *et al.* (1999) used GA for optimizing the composite laminates with cut-outs undergoing large amplitude oscillations. They compared GA with many other algorithms and found GA to be better in almost every aspect.

It is observed that most researchers have used closed form solution to solve the bending, buckling or vibration problems. FEM has proved to be a good approximation for structures for which closed form solution is not possible. In the study presented here, optimization of composite laminates is carried out for maximizing the buckling load with and without cut-out using GA. The effects of various parameters such as aspect ratio, cut-out size, crossover and mutation probabilities on the buckling load are investigated.

Genetic algorithm is an evolutionary optimisation technique using "survival of the fittest" to improve a population of solutions. If the population size is suitably large, GA is not at the risk of being stuck in a local optimum. Nevertheless, finding a global solution is not necessarily guaranteed to be successful unless an infinite number of iterations are performed. GA has been the most popular method for optimising the stacking sequence of a laminated composite, despite the high computational cost (Venkataraman & Haftka, 1999).

Many researchers have done optimisation with GA method such as Soremekum et al. (2001) and Yoshikawa et al. (2008).

Table 2.1 Effect of loading on the optimum weight of the laminate by different failure criteria in the region of fibre breaks along line-B (based on TW), Naik *et al.* (2005).

Loading N_x (N/mm)	Stacking sequence			Laminate weight			Savings in weight (%)	
	FMB	MS	TW	FMB (kg)	MS (Kg)	TW (Kg)		
1000	$[0_6]_T$	$[0_6]_T$	$[0_7]_T$	114	114	133	14	14
2000	$[0_{11}]_T$	$[0_{11}]_T$	$[0_{14}]_T$	209	209	266	21	21
3000	$[0_{17}]_T$	$[0_{16}]_T$	$[0_{20}]_T$	323	304	380	15	20
4000	$[0_{22}]_T$	$[0_{21}]_T$	$[0_{27}]_T$	418	399	513	19	22
5000	$[0_{28}]_T$	$[0_{27}]_T$	$[0_{33}]_T$	532	513	627	15	18
6000	$[0_{33}]_T$	$[0_{32}]_T$	$[0_{40}]_T$	627	608	760	18	20
7000	$[0_{39}]_T$	$[0_{38}]_T$	$[0_{46}]_T$	741	722	874	15	17
8000	$[0_{44}]_T$	$[0_{43}]_T$	$[0_{53}]_T$	836	817	1007	17	19
9000	$[0_{50}]_T$	$[0_{48}]_T$	$[0_{59}]_T$	950	912	1121	15	19
10 000	$[0_{55}]_T$	$[0_{53}]_T$	$[0_{66}]_T$	1045	1007	1254	17	20
11 000	$[0_{61}]_T$	$[0_{59}]_T$	$[0_{73}]_T$	1159	1121	1387	16	19
12 000	$[0_{66}]_T$	$[0_{64}]_T$	$[0_{79}]_T$	1254	1216	1501	16	19

Ply thickness = 0.1 mm.

Naik *et al.* (2005) investigated design optimisation for weight minimization of composite laminates under a specified loading. Optimum weight designs are determined based on failure mechanism based (FMB), the maximum stress (MS) and Tsai-Wu (TW) failures criteria. The results shown in Table 2.1 suggest that there is no significant difference in weight saving of the laminate when the load increases.

2.5.5. Simulated Annealing (SA)

Simulated annealing mimics the annealing process in metallurgy, globalizes the greedy search by permitting unfavourable solutions to be accepted with a probability related to a parameter called "temperature". It is initially assigned a higher value, which corresponds to more probability of accepting a bad move and is gradually reduced by a user-defined cooling schedule. Holding the best solution is recommended in order to preserve the good solution (Erdal & Sonmez, 2005). SA is the most common method after genetic algorithms (GA) for stacking sequence optimisation of laminated composite materials (Lombardi, Haftka, & Cinquini, 1992) (Sargent, Ige, & Ball, 1995) (Sadagopan & Pitchumani, 1998) (Bakis & Arvin, 2006).

2.6. Summary

In this chapter, the importance of FRP composite materials in engineering structural applications and specifically their use in the aerospace industry where the weight of the structure is a sensitive parameter has been investigated.

In addition, the fundamental governing equations of classical laminated plate theory (CLPT) for analysis of laminates were discussed and the governing equation of buckling of laminated plates presented. Literature review of important past work related to FRP laminates buckling behaviour, delamination buckling, and non-destructive testing caused by buckling load are discussed.

2.7. References

Ahanchian, N. (2008). *Effects of stacking sequence and cut-out size on buckling behaviour of composite plates.* MSc Thesis, Faculty of Engineering Kingston University.

Airbus. (2014). *http://www.airbus.com/galleries/photo-gallery/dg/idp/20090-a350-xwb-extra-wide-fuselage/?share=1.*

Amos, M. (2010). *Advanced industrial X-ray computed tomography for defect detection and characterisation of composite structures.* Manchester: Doctor Thesis, University of Manchester.

Arman, Y., Zor, M., & Aksoy, S. (2006). Determination of critical delamination diameter of laminated composite plates under buckling loads. *Composites Science and Technology, 66*, 2945-2953.

Arnold, R. R., Yoo, S. Y., & Mayers, J. (1985). Buckling, postbuckling, and crippling of shallow curved composite plates with edge stiffeners. *AIAA.*

Aslan, Z., & Sahin, M. (2009). Buckling behavior and compressive failure of composite laminates containing multiple large delaminations. *Composite Structures, 89*, 382-390.

Aviles, F., & Carlsson, L. A. (2007). Post-buckling and debond propagation in sandwich panels subject to in-plane compression. *Engineering Fracture Mechanics, 74*, 794-896.

Bakis, C. E., & Arvin, A. C. (2006). Optimal design of press-fitted filament wound composite flywheel rotors. *Compos Struct, 72*(1), 47-57.

Bakis, C. E., Bank, L. C., Brown, V. L., Cosenza, E., Davalos, J. F., Lesko, J. J., & Machida, A. (2002). Fiber reinforced Polymer Composites for Construction–State-of-the-Art Review. *J. of Composite for Construction, 2*, 73.

Bambach, M. R. (2009). Photogrammetry measurements of buckling modes and interactions in channels with edge-stiffened flanges. *Thin-Walled Structures, 47*, 485-504.

Barbero, J. E. (2011). *Introduction to composite materials design* (2nd ed.). CRC Press Taylor & Francis Group.

Belesis, S. D., & Labeas, G. N. (2010). Development of an efficient engineering methodology for non-linear damage and post-buckling analysis of large-scale structures. *International Journal of Structural Integrity, 1*(2), 126-139.

Benham, P. P., Crawford, R. J., & Armstrong, C. G. (1996). *Mechanics of Engineering Materials.* England: Pearson Prentice Hall.

Beznea, E., & Chirica, I. (2011). *Buckling and Post-buckling Analysis of Composite Plates, Advances in Composites Materials-Ecodesign and Analysis.* www.intechopen.com.

Bisagni, C., & Lanzi, L. (2002). Post-buckling optimisation of composite stiffened panels using neural networks. *Composite Structures, 58,* 237-247.

Boggs, P. T., & Tolle, J. W. (1996). Sequential quadratic programming. *Acta Numerica,* 1-52.

Boritu, A., Anghel, V., Constantin, N., Gavan, M., & Pascu, A. (2011). Non-destructive inspection of composite structures using active IR-thermography methods. *U.P.B. Sci. Bull., Series D, 73*(1), 71-84.

Callahan, J. K., & Weeks, E. G. (1992). Optimum design of composite laminates using genetic algorithm. *Compos. Eng. , 2,* 149–160.

Cappello, F., & Tumino, D. (2006). Numerical analysis of composite plates with multiple delaminations subjected to uniaxial buckling load. *Composite Science and Technology, 66,* 264-272.

Chen, H., & Bai, R. (2002). Postbuckling behavior of face/core debonded composite sandwich plate considering matrix crack and contact effect. . *Composite Structure, 57* , 305-313.

Deb, K. (2001). *Multi-objective optimization using evolutionary algorithms.* John Wiley and Sons.

Denny, P. C. (1998). *Search and enumeration techniques for incidence structures. .* CDMTCS Research Report Series, Centre for Discrete Mathematics and Theoretical Computer Science.

Epelman, M. A. (n.d.). IOE 511/Math 652: Continuous optimization methods, Section 1. MIT.

Erdal, O., & Sonmez, F. O. (2005). Optimum design of composite laminates for maximum buckling load capacity using simulated annealing. *Compos Struct, 71*(1), 45-52.

Euler, L. (1744). Additamentum I de curvis elasticits, methodus inveniendi lineas curvas maximi minimiui proprietate gaudentes. *Opera Omnia I., 24,* 231-294.

Fletcher, R. (2007, May 9). The sequential quadratic programming method.

Gantovnik, V. B. (2005). *An improved genetic algorithm for the optimization of composite structures.* Virginia: Dissertation, Virginia Polytechnic Institute and State University.

Ghiasi, H., Pasini, D., & Lessard, L. (2009). Optimum stacking sequence design of composite materials Part I: Constant stiffness design. *Composite Structure, 90,* 1-11.

Gill, P. E., & Wong, E. (2010, August). Sequential quadratic programming methods. CA: UCSD Department of Mathematics.

Goldberg, D. D. (1989). *Genetic algorithm in search, optimization, and machine learning.*. Addison–Wesley.

Gurdal, Z., Haftka, R. T., & Hajela, P. (1999). *Design and Optimisation of Laminated Composite Materials.* New York: A Wiley-Interscience Publication, John Wiley & Sons.

Haftka, R. T., & Walsh, J. L. (1992). Stacking-Sequence Optimisation for Buckling of Laminated Plates by Integer Programming. *AIAA Journal, 30*(3), 814-819.

Hanagud, S., Smith Jr., C. V., & Chattopadhyay, A. (1985). Optimal design of a vibrating beam with coupled bending and torsion. *AIAA.*

Harris, B. (1999). *Engineering Composite Materials.* The Institute of Materials, London..

Johnson, S. M. (2006). *Infrared thermography and thermoelastic stress analysis of composite materials and structural systems.* Thesis, Georgia Institute of Technology.

Kassapoglou, C. (2010). *Design and analysis of composite structures with applications to aerospace structures.* West Sussex: John Wiley & Sons, Ltd.

Kim, H., & Hong, C. (1997). Buckling and postbuckling behavior of composite laminates with a delamination. *Composites Science and Technology, 57,* 557-564.

Knight Jr., N. F., & Starnes Jr., J. H. (1985). Postbuckling behaviour of selected curved stiffened graphite-epoxy panes loaded in axial compression. *AIAA.*

Kogiso, M., Watson, L. T., Gurdal, L., Hftka, R. T., & Nagendra, S. (1994). Design of composite laminates by a genetic algorithm with memory. *Mech. Compos. Mater. Struct., 1,* 95–117.

Kyoung, W., Kim, C., & Hong, C. (1999). Buckling and postbuckling behavior of composite cross-ply laminates with multiple delaminations. *Composite Structures, 43,* 257-274.

Lombardi, M., Haftka, R. T., & Cinquini, C. (1992). Optimization of composite plates for buckling using simulated annealing. *AIAA/ASME/ASCE/AHS/ASC 33rd structures, structural dynamics and materials conference, Part 5,* (pp. 2552-2563). Dallas, Texas.

Mieloszyk, M., Krawczuk, M., Malinowski, P., Wandowski, T., & Ostachowicz, W. (2012). Active thermography method for delamination detection and localisation in composite structures. *6th European Workshop on Structural Health Monitoring.*

Morales, J. L., Nocedal, J., & Wu, Y. (2010, July 2). A sequential quadratic programming algorithm with an additional equality constrained phase.

Muc, A., & Gurba, W. (2001). Genetic algorithms and finite element analysis in optimization of composite structures.. *Compos. Struct., 54,* 275–281.

Nagendra, S., Haftka, R. T., & Gurda, Z. (1992). Stacking sequence optimization of simply supported laminates with stability and strain constraints. *J AIAA, 30*, 2132–2137.

Naik, G. N., Murty, A. V., & Gopalakrishnan, S. (2005). A Failure Mechanism Based Failure Theory for Laminated Composites Including the Effect of Shear Stress. *Composite Structures, 69*, 219-227.

Onoda, J. (1985). On the laminate configurations which maximize the axial buckling loads of composite cylindrical shells. *AIAA*.

Parlapalli, M. S., & Shu, D. (2004). Buckling analysis of two-layer beam with an asymmetric delamination . *Engineering Structures, 26*, 651-658.

Parlapalli, M. S., Wenge, T., & Shu, D. (2005). Buckling analysis of tri-layer beams with enveloped delaminations. *Composites: Part B, 36*, 33-39.

Reddy, A. D., Rehfield, L. W., Bruttomesso, R. I., & Krebs, N. E. (1985). Local buckling and crippling of thin-walled composite structures under axial compression. *AIAA*.

Sadagopan, D., & Pitchumani, R. (1998). Application of genetic algorithms to the optimal tailoring of composite materials. *Compos Sci Technol, 58*, 571-589.

Sargent, P. M., Ige, D. O., & Ball, R. N. (1995). Design of laminate composite layups using genetic algorithms. *Eng Comput, 11*(2), 59-69.

Shukla, K. K., Nath, Y., Kreuzer, E., & Sateesh Kumar, K. V. (2005). Buckling of laminated composite rectangular plates. *Journal of Aerospace Engineering, 18*(4), 215-223.

Shun-Fa, H., & Ching-Ping, M. (2000). Failure of Delaminated Carbon/Epoxy Composite Plates under Compression. *Journal of Composite Materials, 35*(18), 1634-1653.

Sivakumar, K., Iyengar, N. G., & Deb, K. (1999). Optimum design of laminated composite plates undergoing large amplitude oscillations. : . *Appl. Compos. Mater., 6*, 87–98.

Soremekum, G., Gurdal, Z., Haftka, R. T., & Watson, L. T. (2001). Composite laminate design optimization by genetic algorithm with generalized elitist selection. *Computers and Structurres, 79*, 131-143.

Stevens, K. A., Ricci, R., & Davies, G. A. (1996). Buckling and postbuckling of composite structures. *Composite, 26*, 189-199.

Sultan, R. A., Guirguis, S. W., Younes, M. M., & El-Soaly, E. E. (2013). Delamination detection by thermography. *International Journal of Engineering Research and Applications (IJERA), 3*(1), 279-288.

Sultan, R., Guirguis, S., Younes, M., & El-Soaly, E. (2012). Active infrared thermography technique for the non-destructive testing of composite material. *Int. J. Mech. Eng. & Rob. Res., 1*(3), 131-142.

Tafreshi, A. (2004). Delamination buckling and postbuckling in composite cylindrical shells under external pressure. *Thin-Walled Structures, 42*, 1379-1404.

Tarjan, G., Sapkas, A., & Kollar, L. P. (2010). Local web buckling of composite (FRP) beams. *Journal of Reinforced Plastic and Composites, 29*(10), 1450-1462.

van de Burg, M. J. (2011). *Plate buckling in design codes the difference between NEN 6771 and NEN-EN 1993-1-5.* The Netherlands: Master Thesis, Delft University of Technology.

Venkataraman, S., & Haftka, R. T. (1999). Optimization of composite panels - a review. *14th Annual technical conference of the American society of composites.* Dayton, OH.

Verette, R. M. (1970). *Stiffness, Strength and Stability Optimisation of Laminated Composites.* Northrop Aircraft Co., Hawthorne, California: Report NOR-70-138.

Waddoups, M. E. (1969). *Structural Airframe application of Advanced Composite Materials-analytical Methods.* . Air Force Materials Laboratory, Wright-Patterson Air Force Base, Ohio.: Report AFML-TR-69-101, Vol. VI.

Wang, X., & Dong, K. (2007). Local buckling for triangular and lemniscate delaminations near the surface of laminated cylindrical shells under hygrothermal effects. *Composite Structures, 79*, 67-75.

Weebly. (n.d.). *Ct scan diagram*. Retrieved Feb 2014, from http://computertomography.weebly.com/ct-scan-diagram.html

Winter, G. (1947). Strength of thin steel compression flanges. *ASCE, 112*.

Yin, W. L., & Fei, Z. (1985). Delamination buckling and growth in a clamped circular plate. *AIAA*.

Yoshikawa, M., Yamauchi, H., & Terai, H. (2008). Hybrid architecture of genetic algorithm and simulated annealing. *Engineering Letters, 16*(3), 3-11.

Chapter 3

Experimental Studies

3.1. Introduction

When a laminated composite structure is subjected to in-plane compression, there is danger of delamination, i.e. separation of layers from each other. This will affect the stiffness and strength of the laminate. Hence characterisation of the onset of delamination growth and its subsequent development during buckling and postbuckling is important.

In the first part of this chapter the experimental works carried out on mechanical characterisation of the GFRP material, and characterisation of the mode I, mode II and mixed-mode I/II delamination fracture toughness of a unidirectional glass/epoxy fibre reinforced polymer (GFRP) composite material and analysis of the data obtained from the tests will be reported. The double cantilever beam (DCB), 3 point end notched flexure (3ENF) and mixed-mode bending (MMB) tests were chosen to characterise the mode I, mode II and mixed-mode I/II delamination fracture toughness values, respectively.

Next the experimental results of buckling/postbuckling tests of laminated GFRP plates with various stacking sequences will be presented. Also the buckling behaviour of damaged laminated GFRP plates caused by either inserting a pre-existing centrally located delamination patch at the mid-plane or by drilling a hole at the centre of the GFRP plate prior to buckling and postbuckling testing will be demonstrated. From these tests conclusions are drawn relating the effect of delamination on the buckling load and response, and the results are validated by comparing to reported works.

Finally, non-destructive testing (NDT) are employed to examine the damage evolution during delamination growth and failure of the buckled GFRP laminates using CT-scan and IR-thermography.

3.2. Tensile Test

The ASTM standard D3039 'Standard Test Method for Tensile Properties of Polymer Matrix Composites' (ASTM Specification D3039/D3039M, 2006) has been used for tensile testing of GFRP materials. The standard requires tabs to be bonded to the ends of the specimens for mounting in the grips of testing machine. Without tabs due to stress concentration at the grips failure is likely to occur near the grip points causing a risk for the results to be reported with a lower overall tensile strength and greater variability.

The tests carried out on specimens with a layup of 0, ±45 and 90 degrees with respect to the loading direction to calculate the material properties such as Young's modulus, shear modulus, Poisson's ratio, shear strength and ultimate tensile strength and strain in fibre and normal to fibre directions. The tests are carried out with measuring applied load and strain gauges were used for measuring strain therefore stress-strain behaviour of GFRP has been obtained.

3.2.1. Manufacturing of Tensile Test Specimens

All specimens in this thesis are fabricated from GFRP prepregs with E722 epoxy matrix supplied by Tencate Advanced Composites LTD, UK. The manufacturing steps of tensile test specimens are:

a. Cut out 6 layers of GFRP prepregs at 0°, 7 layers at ±45°, and 16 layers at 90° fibre orientation with 110x260 mm dimensions according to the ASTM D3039 standard (2006) for 0° and 90° and ASTM D3518 (2007) for ±45° (see Figure 3.1)

b. Put peel ply PTFE plastic over two aluminium plates and use none flammable tape to bonded them. The complete vacuum bagging scheme is shown in Figure 3.2.

c. Place prepregs on one of the aluminium plate

d. Use roller to get out all air bubbles

e. Cover the laminate with the second aluminium plate

f. Put nylon release film then lightweight breather/absorption fabric over both aluminium plates and use none flammable tape for sticking the fabric.

g. A vacuum valve placed through a hole into vacuum bag to extract air by vacuum pump. The bag was sealed air tight using sealing tape.

h. Vacuum bag was placed in the oven and connected to the vacuum pipe all through the curing process. The oven was initially heated to 90 °C for ramping up the aluminium plates and the material to the necessary cure temperature, after 30 minutes this was increased to 125 °C and the curing was sustained for a further 60 minute (see Figure 3.3 and 3.4). Finally the bag was taken out of the oven after curing cycle.

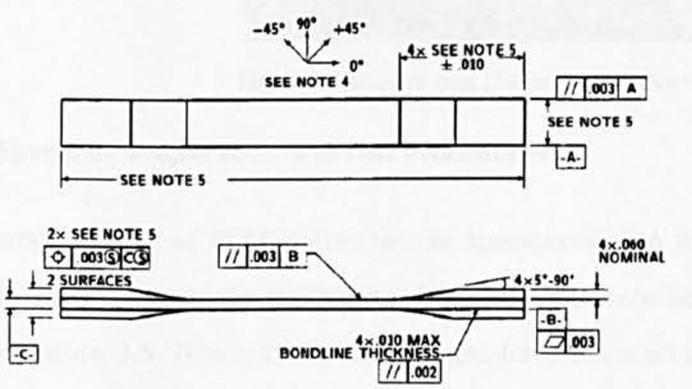

Fig. 3.1. Schematic of tensile test specimen (ASTM Specification D3039/D3039M, 2006).

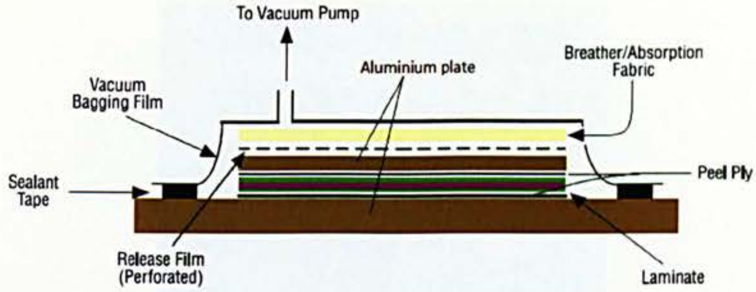

Fig. 3.2. Vacuum bagging scheme, modified from (Gurit).

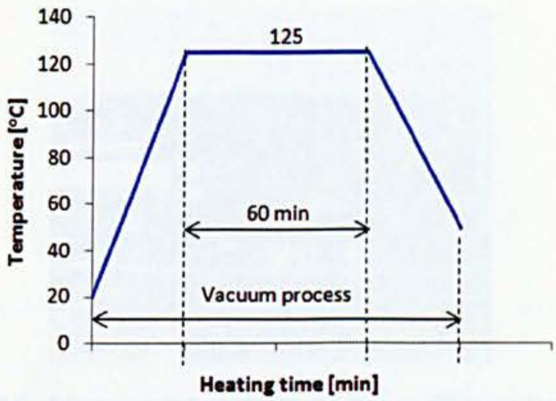

Fig. 3.3. Curing cycle of GFRP laminate.

Fig. 3.4. Vacuum bag placed in the oven.

3.2.2. Specimen Preparation and Test Procedures

After manufacturing of GFRP plates tensile specimens with the size of 250×25mm have been cut from the plate by machining. The end tabs were bonded to the specimens as shown in Figure 3.5. Finally two strain gauges have been attached to the centre part of the specimens, one in the direction of loading and the other normal to the direction of loading (see Figure 3.6). Figure 3.7 shows tensile specimen during testing.

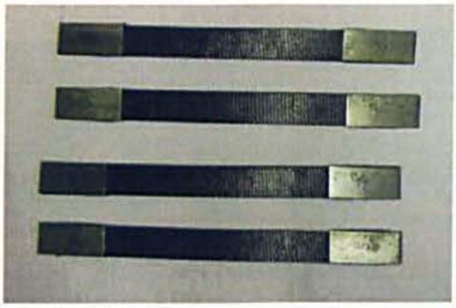

Fig. 3.5. Tensile specimens prior to attaching strain gauges.

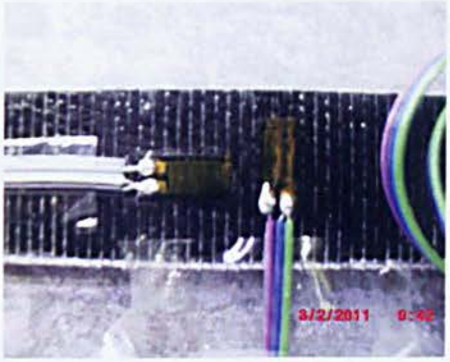

Fig. 3.6. Arrangement of strain gauges on 90° specimen.

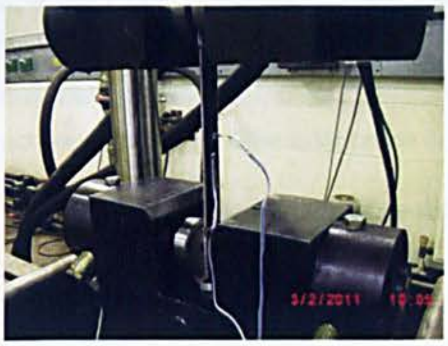

Fig. 3.7. Tensile testing of GFRP laminate.

3.2.3. Material Test Results

The results of tensile tests are summarized in Table 3.1. Typical fracture path in different tests are shown in Figures 3.8 -3.10.

Table 3.1. Material characteristic results from tensile test.

E_{11} [GPa]	E_{22} [GPa]	G_{12} [GPa]	ν_{12}	X_t [MPa]	Y_t [MPa]	S [MPa]
37±2	13±1	5±1	0.23±0.01	624±21	71±8	48±1

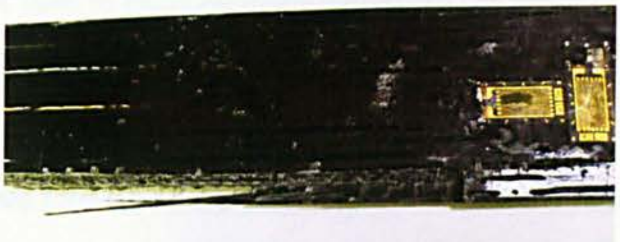

Fig. 3.8. Fracture path in 0° fibre orientation in tensile test.

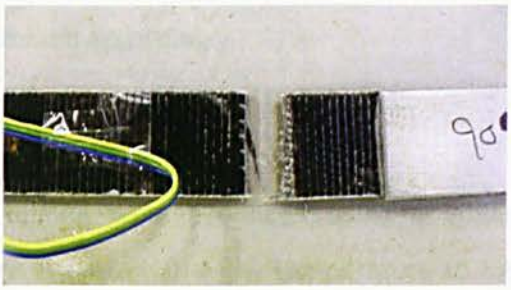

Fig. 3.9. Fracture path in 90° fibre orientation in tensile test.

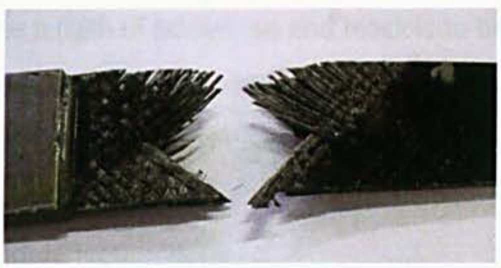

Fig. 3.10. Fracture path in ±45° fibre orientation in tensile test.

As can be seen from Table 3.1 the Young's modulus in fibre direction is about three times the Young's modulus in normal to fibre direction. Also the strength in fibre direction is almost 8.6 times of the strength in the transverse direction.

The fracture path in 0° and 90° is normal to principal stress direction as expected. On the other hand, at 45° specimens the fracture occurred in the direction of maximum shear stress along the fibres (see Figure 3.8-3.10).

3.3. Mode I Delamination Test-Double Cantilever Beam Test (DCB)

For characterising the pure mode I fracture behaviour of a laminated GFRP composite a Double Cantilever Beam (DCB) test can be used. The ASTM D5528-01 test standards

(2007) for this test is used to experimentally determine the mode I interlaminar fracture toughness (G_{IC}) and resistance curve for unidirectional fibre configurations.

Linear elastic fracture mechanics (LEFM) is valid when the size of damage zone (or fracture process zone) forming at the delamination crack front relative to the smallest dimension of the specimen geometry (in this case the thickness) sufficiently small. In that case a valid strain energy release rate (G) is inferred from the test and delamination fracture toughness determined accordingly.

3.3.1. Specimen Preparation

All specimens used in testing were produced using a unidirectional GFRP prepreg composite material, which is stored at a low temperature to increase its working shelf-life. The DCB specimens size are 125mm long, 25mm width and an initial crack starter insert from the loading line length of 50mm, an end block is to be bonded at both sides of a specimen to allow to grip the specimen in the testing machine (see Figure 3.11). The recommended rate of loading is at a constant cross-head displacement rate of 2mm/min, the crack propagation is monitored with a travelling microscope together with recording the corresponding load and deflection data.

The DCB specimens were produced from a plate using a template, which was sized for all the required specimens to be cut from it after setting with a buffer space added to allow for material loss during cutting process and to allow for matrix seepage loss at the edges. Each laminate layer was cut using this template from the unidirectional prepreg and laid up using the roller to firmly consolidate the layers and remove any potential trapped air between the layers. These were then placed on an aluminium sheet protected by a cover of PTFE film to aid in separation after curing. After half of the plies were laid up (9 layers) a thin PTFE sheet with a thickness of 20 μm and a length of 55 mm has been placed at one end of the plate to act as a pre-crack and another 9 layers were laid up. This allows accurate control of the initial crack length for fracture testing (see Figure 3.11). However, no additional precracking has been done and inserted PTFE crack from cured specimens is assumed as initial sharp crack. The dimension of DCB specimens follows ASTM D5528

(2007). When the necessary numbers of lamina layers were laid down the material was sandwiched by placing another aluminium sheet coated with a PTFE film over it.

As previously discussed in section 2.2.3.3, the standard vacuum bagging methods were used. This involved wrapping the aluminium sheets in an absorbent bleeder film which is in turn wrapped in a porous breather cloth. A vacuum valve is placed on top of the aluminium plate and the whole assembly is wrapped in a polymer vacuum bag and an airtight sealed with a tacky polymer sealant placed around the edges.

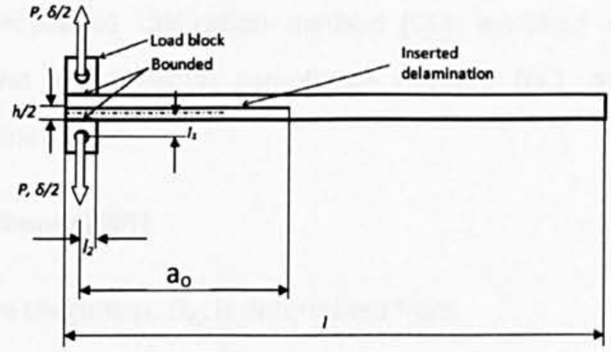

Fig. 3.11. Dimension of DCB specimen with width *b*.

Once this assembly is fully bagged a vacuum air extraction line is attached to the valve to extract the air from the bag and to pressure the laminate during the curing cycle. At this stage it is important to check that the bag has been sealed properly and no air leaking occurs. Once the proper functioning of the seal is confirmed, the assembly is then placed in a pre-heated vacuum oven where a vacuum hose is attached to the valve to produce a vacuum pressure throughout the curing process.

The oven was initially heated to 90 °C for ramping up the aluminium plates and the material to the necessary cure temperature, after 30 minutes this was increased to 125 °C and the curing was sustained for a further one hour. The oven was allowed to cool and the assembly removed, once this assembly had adequately cooled down the laminate was removed and left to fully cool down.

The DCB specimen were cut from the laminate and after manufacturing of composite DCB beams completed, the aluminium loading blocks were bonded to the specimens using an epoxy adhesive ESP110 which is cured at 150 °C for 45 minutes.

3.3.2. Data Reduction for DCB Specimens

There are six recommended methods for 'data reduction' to determine the mode I interlaminar fracture toughness (G_{Ic}) (ASTM Specification D5528, 2007); these are simple beam theory method (SBT), modified beam theory method (MBT), corrected beam theory method (CBT), compliance calibration method (CC), modified compliance calibration method (MCC) and experimental compliance method (EC). In the following these methods are explained.

a. Simple Beam Theory (SBT)

The mode I fracture toughness, G_{Ic}, is determined from

$$G_I = \frac{3P\delta}{2ba} \tag{3.1}$$

where a is crack length.

b. Modified Beam Theory (MBT)

$$G_I = \frac{3P\delta}{2b(a+|\Delta|)} \tag{3.2}$$

$$C = \delta / P \tag{3.3}$$

An example for finding the correction crack length, Δ, in equation (3.2) is shown in Figure 3.12 where Δ is found from the intercept of plot of a-$C^{1/3}$ curve with x-axis.

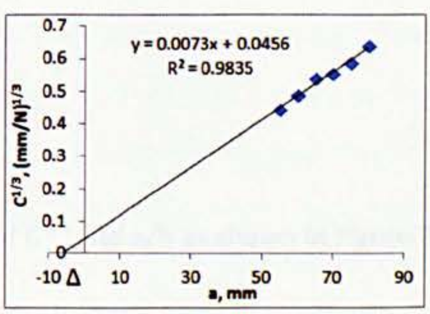

Fig. 3.12. Plot of crack length, a, versus $C^{1/3}$ to find Δ.

c. Corrected Beam Theory (CBT)

$$G_I = \frac{3P\delta}{2b(a+\Delta)} \cdot \frac{F}{N} \tag{3.4}$$

Where correction factors F and N can be found from

$$F = 1 - \frac{3}{10}\left(\frac{\delta}{a}\right)^2 - \frac{2}{3}\left(\frac{\delta l_1}{a^2}\right) \tag{3.5}$$

$$N = 1 - \left(\frac{l_2}{a}\right)^3 - \frac{9}{8}\left[1 - \left(\frac{l_2}{a}\right)^2\right]\frac{\delta l_1}{a^2} - \frac{9}{35}\left(\frac{\delta}{a}\right)^2 \tag{3.6}$$

d. Compliance Calibration Method (CC)

$$G_I = \frac{nP\delta}{2ba} \tag{3.7}$$

Where $n = \frac{\Delta y}{\Delta x}$ (3.8)

n is found from log *C*-log *a* relationships as be described in Figure 3.13.

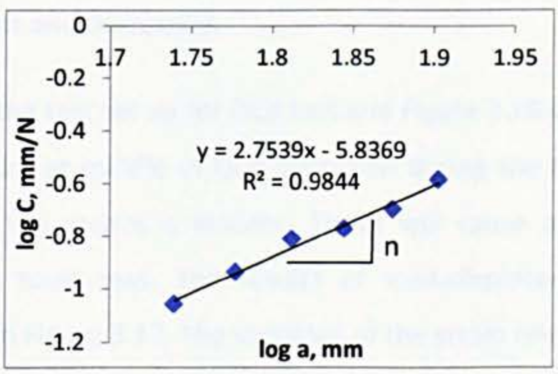

Fig. 3.13. Plot of Log *C* versus log *a*.

e. Modified Compliance Calibration Method (MCC)

$$G_I = \frac{3P^2C^{2/3}}{2A_1bh} \tag{3.9}$$

Where $A_1 = \frac{\Delta y}{\Delta x}$ (3.10)

A_1 is determined from plot of $C^{1/3}$ and a/h as shown in Figure 3.14.

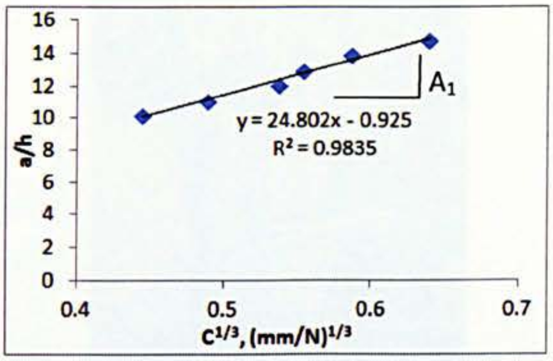

Fig. 3.14. Relationship between $C^{1/3}$ and a/h.

f. Experimental Compliance Method (EC)

$$G_I = \frac{P^2}{2b}\frac{dC}{da} \tag{3.11}$$

From plot of experimental *C* versus *a*, *C*(*a*) will be obtained and *dC*/*da* is calculated at any required crack length.

3.3.3. DCB Test Results and Discussion

Figure 3.15 illustrates the test set up for DCB test and Figure 3.16 shows the crack path in the interlaminar fracture at middle of DCB specimen during the test. The fibre bridging and microcracking in the matrix is evident. These will cause an R-curve for mode I delamination fracture toughness. The results of load-displacement from four tests specimens are shown in Figure 3.17. The variation of the strain release rate, G_I, calculated by various methods described in section 3.2.2 is presented in Figure 3.18. Figure 3.19 shows the average initiation fracture toughness, G_{Ic}, from four specimens. The crack initiation is chosen at the intersection of the load–displacement curve with a line corresponding to a compliance 5% higher than the initial one. The results show that the maximum G_{Ic} is measured from SBT method i.e. 557±72 J/m^2. This is because in SBT method the beam is assumed as a built-in cantilever beam rather than a beam on elastic foundation. But from the other methods a mode I delamination fracture toughness of an average of 460±15 J/m^2 based on CBT is obtained. The details of all specimens are summarised in Table 3.2.

Fig. 3.15. Mode I test set up for DCB specimen.

Fig. 3.16. Crack path in DCB test showing fibre bridging and microcracking.

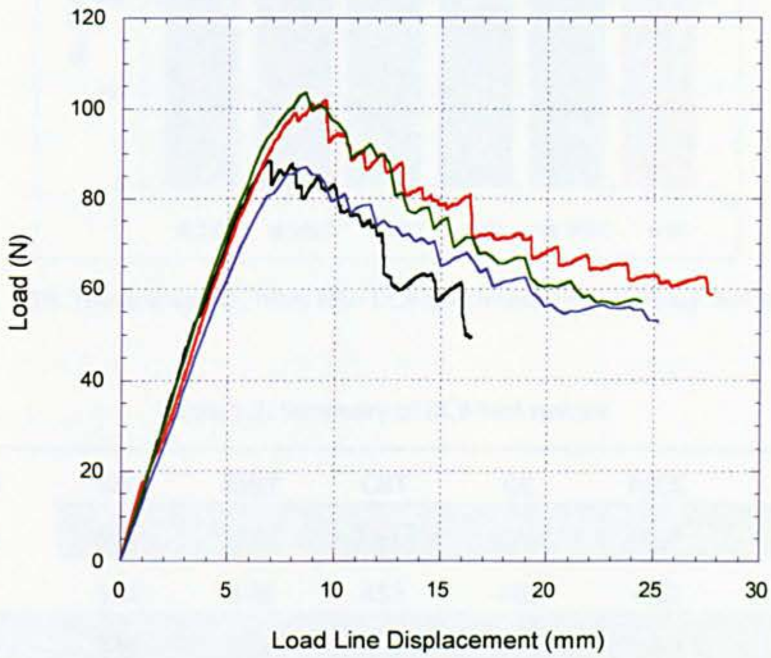

Fig. 3.17. Load–displacement in DCB specimens.

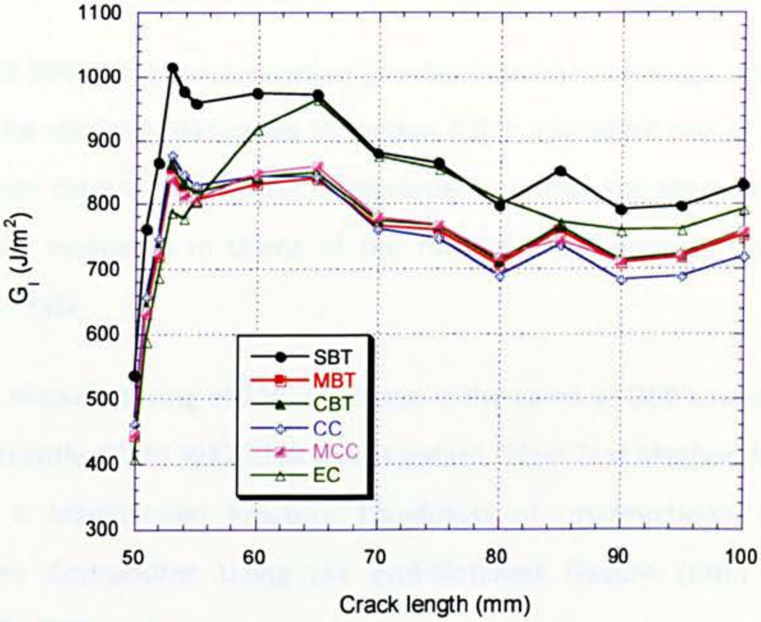

Fig. 3.18. Sample of resistance curve for DCB specimen.

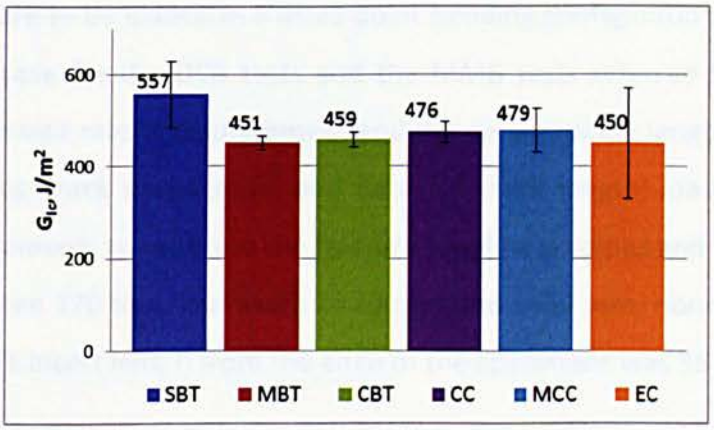

Fig. 3.19. The average G_{Ic} from four DCB specimens from various methods.

Table 3.2. Summary of DCB test results.

DCB	SBT	MBT	CBT	CC	MCC	EC
G_{IC}	**J/m^2**	**J/m^2**	**J/m^2**	**J/m^2**	**J/m^2**	**J/m^2**
S1	502	446	453	461	460	407
S2	**546**	**445**	**452**	**473**	**539**	**614**
S3	535	442	449	462	445	407
S4	**645**	**472**	**480**	**507**	**473**	**373**
Average	557±72	451±15	459±16	476±23	479±47	450±121

3.4. End Notch Flexure (ENF) Test

The purpose of ENF test is to determine interlaminar fracture toughness in mode II, G_{IIc}, according to the methods described in section 3.3.2. The 3ENF test is liable to produce unstable fracture propagation under displacement control and therefore the stability of this need to be evaluated in terms of the rate of strain energy release rate against fracture growth rate.

Generally, the manufacturing of ENF specimen is the same as DCB's nevertheless without load block. Currently ASTM WK22949 test standard "New Test Method for Determination of the mode II Interlaminar Fracture Toughness of Unidirectional Fiber Reinforced Polymer Matrix Composites Using the End-Notched Flexure (ENF) Test" has been approved for the ENF testing.

The specimens are to be loaded in a three point bending configuration as shown in Figure 3.20, as is the case for the DCB tests and the MMB tests referred to later the load is applied at a constant rate of displacement and the delamination length along pre-crack is monitored during crack propagation and data for crack length, load and displacement captured at increments to calculate the fracture toughness values and R-curve. The length of specimens were 170 mm, the width b=20 mm and L=50 mm, nominal thickness 2h=5 mm and the PTFE insert length from the edge of the specimens was 55 mm.

3.4.1. Preparation and Procedure of Test

Preparation of ENF specimen is almost the same as DCB except no loading block is necessary for this test (see Figure 3.20).

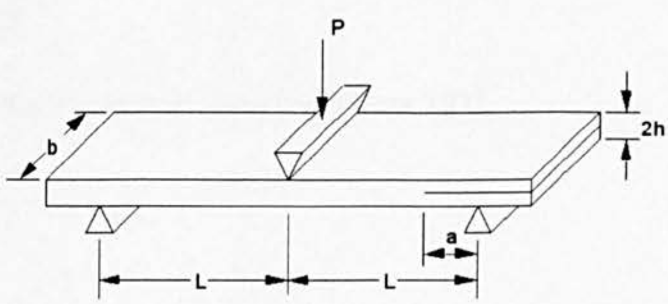

Fig. 3.20. Schematic diagram of End Notched Flexure (ENF) test according to ASTM WK22949 (2010) (www.composites.northwestern.edu).

3.4.2. Calculation of Fracture Toughness in Mode II ENF Tests

i. Direct Beam Method (DBT)

$$C = \frac{\delta}{P} \tag{3.12}$$

$$P = \frac{\delta}{C} \tag{3.13}$$

$$C = \frac{2L^3 + 3a^3}{8E_x bh^3} \tag{3.14}$$

$$\frac{dC}{da} = \frac{9a^2}{8E_x bh^3} \tag{3.15}$$

$$E_x = \frac{2L^3 + 3a^3}{8Cbh^3} \tag{3.16}$$

$$E_x = \frac{2L^3 + 3a^3}{8Cbh^3} = \frac{2L^3 + 3a^3}{8bh^3} \cdot \frac{1}{C} = \frac{2L^3 + 3a^3}{8bh^3} \cdot \frac{P}{\delta} = \frac{P(2L^3 + 3a^3)}{8bh^3\delta} \tag{3.17}$$

$$G_{II} = \frac{9a^2P^2}{16E_x b^2h^3} \tag{3.18}$$

$$G_{II} = \frac{9a^2P^2}{16b^2h^3} \cdot \frac{1}{E_x} = \frac{9a^2P^2}{16b^2h^3} \cdot \frac{8bh^3\delta}{P(2L^3 + 3a^3)} = \frac{9a^2P\delta}{2b(2L^3 + 3a^3)} \tag{3.19}$$

In the above b is the width of the specimen.

ii. Compliance Calibration Method (CCM)

$$C = ma^3 + C_0 \tag{3.20}$$

$$\frac{dC}{da} = 3ma^2 \tag{3.21}$$

$$G_{II} = \frac{P^2}{2b}\frac{dC}{da} = \frac{3ma^2P^2}{2b} \tag{3.22}$$

m is the slope of plot of C versus a^3 curve (see Figure 3.21).

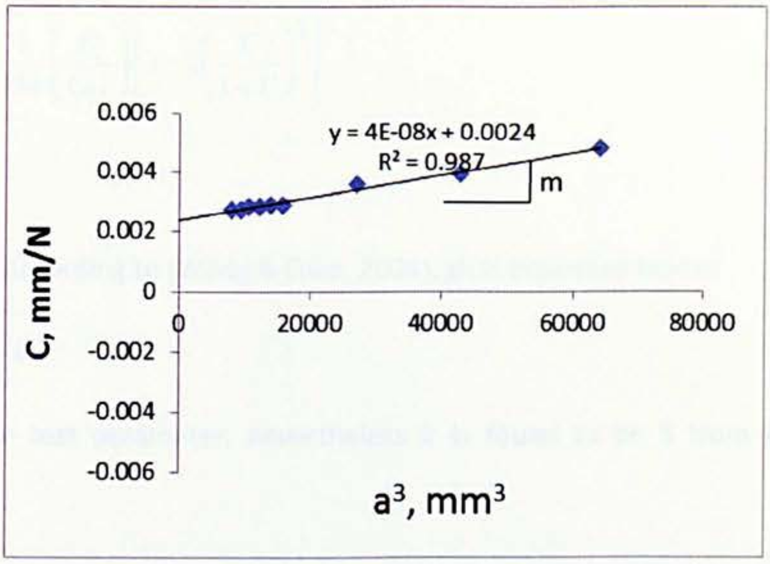

Fig. 3.21. Compliance versus cube of crack length.

iii. **Corrected Beam Theory (CBT)** (Wang & Williams, 1992)

$$\Delta_I = \chi = h\sqrt{\frac{E_1}{11G_{13}}\left[3-2\left(\frac{\Gamma}{1+\Gamma}\right)^2\right]} \tag{3.23}$$

$$\Gamma = 1.18\frac{\sqrt{E_1E_3}}{G_{13}} \tag{3.24}$$

$$\Delta_{II} = \chi h = 0.42\Delta_I \tag{3.25}$$

$$G_{II} = \frac{9(a+\Delta_{II})^2P^2}{16b^2h^3E_1} \tag{3.26}$$

$$G_{II} = \frac{9(a+\Delta_{II})^2P\delta}{2B[2L^3+3(a+\Delta_{II})^3]} \tag{3.27}$$

Usually experimental results deviate from elementary beam theory equation because of the deformation at the crack tip (ASTM Specification D6671/6671M, 2006). William (1989) modified equations according to the loading-line compliance-crack length relation by introducing the additional crack length χh as follows (Wang & Williams, 1992).

$$C = \frac{\delta}{P} = \frac{2L^3+3(a+\chi h)^3}{12E_1I} \tag{3.28}$$

$$\chi h = \Delta_{II} = h\sqrt{\frac{1}{13k}\left(\frac{E_1}{G_{12}}\right)\left\{3-2\left(\frac{\Gamma}{1+\Gamma}\right)^2\right\}} \tag{3.29}$$

$$\Gamma = \frac{\sqrt{E_1 E_2}}{kG_{12}} \tag{3.30}$$

where k = 4.8. According to (Wang & Qiao, 2004), χh is described below:

$$\chi h = \sqrt{\frac{E_1}{12\alpha G12}}h \tag{3.31}$$

where α is the test parameter, nevertheless it is found to be 5 from finite element analysis.

iv. **Corrected beam theory with effective crack length (CBTE)** (de Moura & de Morais, 2008)

$$C = \frac{2L^3 + 3a_e^{\,3}}{8E_1bh^3} + \frac{3L}{10G_{13}bh} \tag{3.32}$$

If the elastic properties are known, a_e can be easily obtained from the measured compliance C_m by

$$a_e = \sqrt[3]{\frac{8E_{1b}bh^3C_c}{3} - \frac{2L^3}{3}} \tag{3.33}$$

$$C_c = C_m - \frac{3L}{10G_{13}bh} \tag{3.34}$$

$$G_{II} = \frac{9P^2 a_e^{\,2}}{16b^2 E_{1b}h^3} \tag{3.35}$$

E_{1b} = longitudinal flexural modulus to be found from a separate bending test (see Figure 3.22).

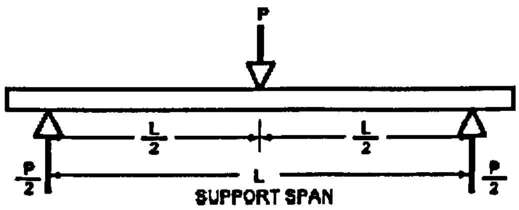

Fig. 3.22. Scheme of flexural loading three point bending (ASTM Specification D7264, 2007).

$$\delta = \frac{PL^3}{48EI} \quad , L = 100 \text{ mm} \tag{3.36}$$

$$E_{1b} = \frac{PL^3}{48\delta I} \tag{3.37}$$

v. **Compliance-Based Beam Method (CBBM)** (de Moura, Dourado, Morais, & Pereira, 2010)

$$C = \frac{3a_0^3 + 2L^3}{8bh^3 E_1} + \frac{3L}{10G_{13}bh} \tag{3.38}$$

$$C_{0c} = C_0 - \frac{3L}{10G_{13}bh} \tag{3.39}$$

$$C_c = C - \frac{3L}{10G_{13}bh} \tag{3.40}$$

$$a_e = \left[\frac{C_c}{C_{0c}} a_0^3 + \left(\frac{C_c}{C_{0c}} - 1\right)\frac{2L^3}{3}\right]^{1/3} \tag{3.41}$$

$$G_{II} = \frac{9P^2 a_e^2}{16b^2 E_f h^3} \tag{3.42}$$

$$E_f = \frac{3a_0^3 + 2L^3}{8bh^3 C_{0c}}\left(C_0 - \frac{3L}{10bhG_{13}}\right)^{-1} \tag{3.43}$$

3.4.3. ENF Result and Discussion

Figure 3.23 shows the ENF test set-up and Figure 3.24 illustrates load versus displacement measured from three ENF tests. Figure 3.25 shows variation of mode II energy release rate versus delamination crack length in one of the specimen calculated by various methods. The crack growth in ENF test at the start of propagation was unstable. Table 3.3

shows the average initiation fracture toughness, G_{IIc}, from three specimens. The measured value from compliance calibration test is the highest at 903±31 J/m^2. The average mode II delamination fracture toughness from other methods is about 706±47 J/m^2. The details of all specimens are summarised in Figure 3.26 and Table 3.3.

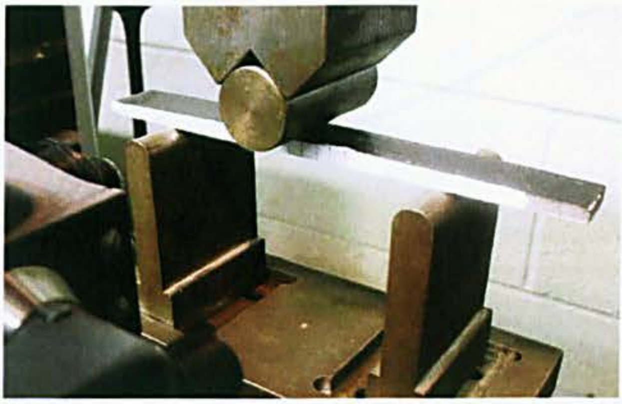

Fig. 3.23. ENF test set up.

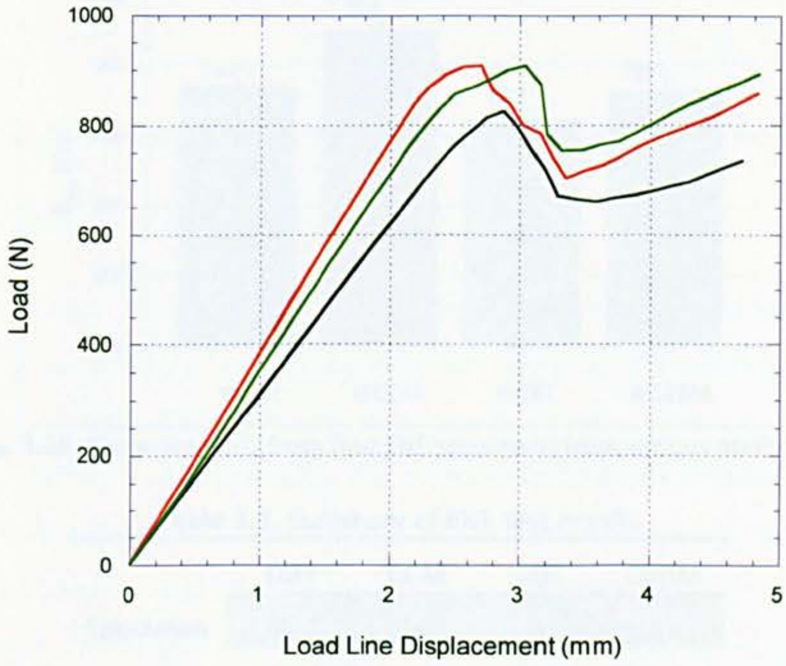

Fig. 3.24. Load–displacement curve of mode II.

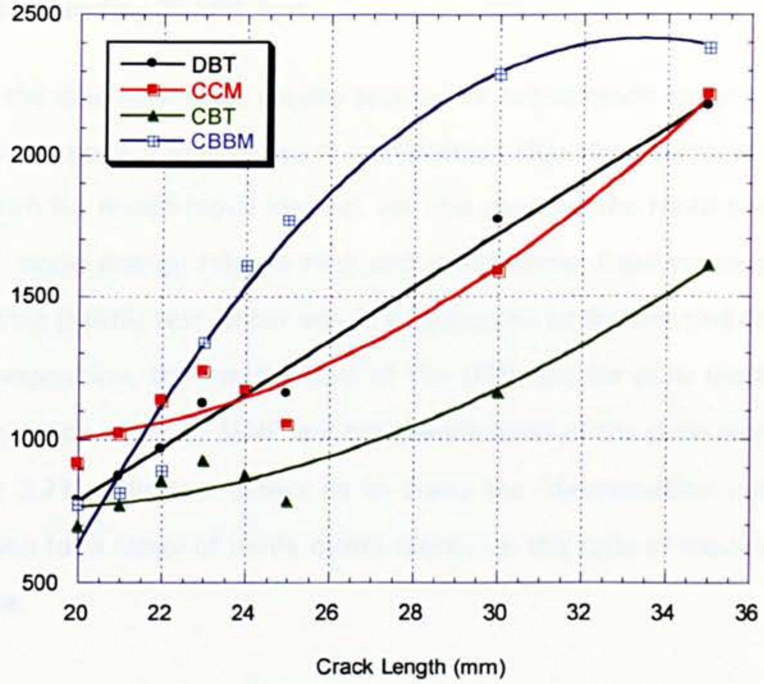

Fig. 3.25. Energy release rate in mode II versus delamination length curve.

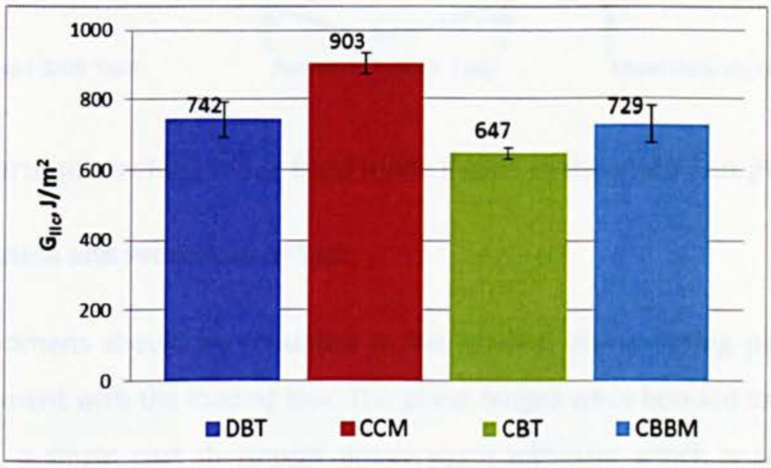

Fig. 3.26. The average G_{Ic} from four ENF specimens from various methods.

Table 3.3. Summary of ENF test results

Specimen	DBT J/m²	CCM J/m²	CBT J/m²	CBBM J/m²
S1	754	867	570	742
S2	686	928	676	672
S3	787	914	696	773
Average	742±51	903±31	647±63	729±51

3.5. Mixed Mode Bending (MMB) Test

In real structures the delamination is usually occurs in a mixed mode loading rather than pure mode I or pure mode II loading, so it is important that the delamination fracture toughness be known for mixed-mode loading. For this purpose the MMB test is used to determine mixed mode energy release rate and interlaminar fracture toughness. The mixed-mode bending (MMB) test which was first proposed by Reeder and Crews (1990) combines, by superposition, the mechanisms of the DCB test for pure mode I fracture toughness determination with the 3ENF test for identification of the pure mode II facture toughness (Figure 3.27). This test allows us to study the 'delamination initiation' and fracture propagation for a range of mode mixity ratios, i.e. the ratio of mode I to mode II of the loading state.

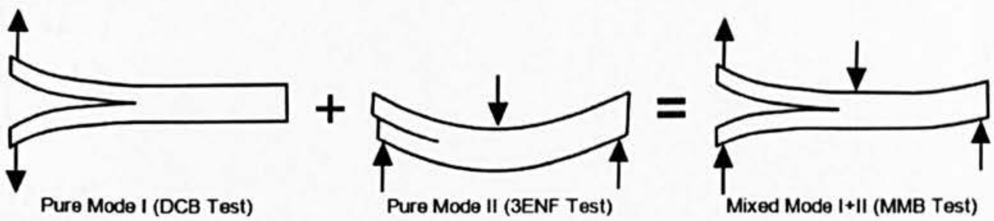

Fig. 3.27. Superposition of the mode I and mode II tests in the MMB Test (Reeder, 2003).

3.5.1. Preparation and Procedure of Test

The MMB specimens should be mounted in the loading clamps using piano hinges to allow the alignment with the loading line. The piano hinges were bonded to the specimen tip by ESP110, a single part thermoset epoxy paste adhesive which is cured in an air circulated oven at 150°C for 45 minute. The procedure of the test followed ASTM D6671 (2006) (see Figure 3.27). With the MMB test fixture shown in Figure 3.27 the mixed-mode I/II interlaminar fracture toughness across the range from pure mode I to pure mode II can be measured. The desired ratio of mode I to mode II is achieved by varying the length of the lever arm c (as illustrated in Figure 3.28), however the specimen span (2L=110 mm) remains constant throughout. The nominal widths of the specimens were 20mm and thickness 2h≈5 mm.

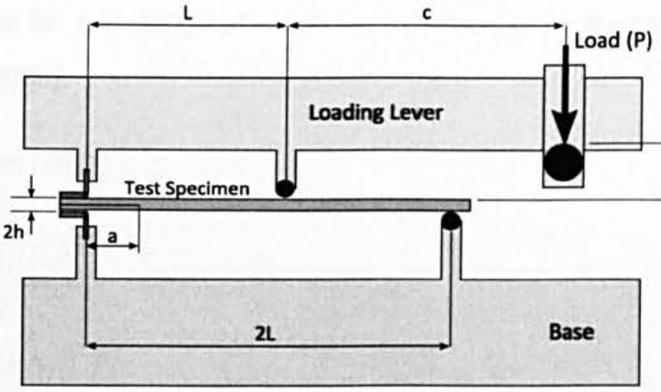

Fig. 3.28. Scheme of MMB fracture toughness test (Blanco, Turon, & Costa, 2006).

3.5.2. Formulation of Fracture Toughness in MMB Test

Beam Theory

$$P_I = \left(\frac{3c-L}{4L}\right)P \qquad P_{II} = \left(\frac{c+L}{L}\right)P \tag{3.44}$$

$$G_I = \frac{12a^2P_I^2}{b^2h^3E_1} \qquad G_{II} = \frac{9a^2P_{II}^2}{16b^2h^3E_1} \tag{3.45}$$

$$\frac{G_I}{G_{II}} = \frac{4}{3}\left(\frac{3c-L}{c+L}\right)^2, \quad c \geq \frac{L}{3} \tag{3.46}$$

From Eq. (3.46) and definition of mode mixity $\psi = G_{II}/G_T$ the length of lever arm c can be found from (Reeder & Crews, 1990):

$$c = \frac{L\left(\frac{1}{2}\sqrt{3\left(\frac{1-\psi}{\psi}\right)}+1\right)}{3-\frac{1}{2}\sqrt{3\left(\frac{1-\psi}{\psi}\right)}} \tag{3.47}$$

Other relationship for calculation of mode mixity ratio can be found in ASTM D6671 and in Blanco et al. (2006).

Wang and William (1992)

$$G_I^{ww} = \frac{12\left(a+h\left|\Delta_I\right|\right)^2 P_I^2}{b^2 h^3 E_1}$$
$$G_{II}^{ww} = \frac{9\left(a+0.42h\left|\Delta_I\right|\right)^2 P_{II}^2}{16 b^2 h^3 E_1} \tag{3.48}$$

$$\Delta_I = \chi = \sqrt{\frac{E_1}{11G_{12}}\left[3-2\left(\frac{\Gamma}{1+\Gamma}\right)\right]^2} \tag{3.49}$$

$$\Gamma = 1.18\frac{\sqrt{E_1E_2}}{G_{12}} \tag{3.50}$$

$$\frac{G_I^{ww}}{G_{II}^{ww}} = \frac{4}{3}\left(\frac{3c-L}{c+L}\right)^2\left(\frac{a+h\Delta_I}{a+0.42\Delta_I h}\right)^2 \tag{3.51}$$

Reeder and Crews (1990)

$$K = \frac{2bE_2}{h} \tag{3.52}$$

$$\lambda = \left(\frac{3K}{bh^3E_1}\right)^{1/4} \tag{3.53}$$

$$G_I = \frac{12P_I^2}{b^2h^3E_1}\left[a^2+\frac{2a}{\lambda}+\frac{1}{\lambda^2}\right] \quad \text{,withoutsheardeformatio}$$
$$G_I = \frac{9P^2(3c-L)^2}{4b^2h^3L^2E_1}\left[a^2+\frac{2a}{\lambda}+\frac{1}{\lambda^2}+\frac{h^2E_1}{10G_{12}}\right] \tag{3.54}$$
$$G_{II} = \frac{9P^2(c+L)^2}{16b^2h^3L^2E_1}\left[a^2+\frac{0.2h^2E_1}{10G_{12}}\right]$$

ASTM D6671 (2006)

$$G_I = \frac{12P^2(a+\chi h)^2(3c-L)}{16b^2E_{1f}h^3L^2}$$

$$G_{II} = \frac{9P^2(a+0.42\chi h)^2(c+L)^2}{16b^2E_{1f}h^3L^2}$$

$$E_{1f} = \frac{8(a_0+\chi h)^3(3c-L)^2+\left[6+(a_0+0.42\chi h)^3+4L^3\right](c+L)^2}{16L^2bh^3\left(\frac{1}{m}-C_{sys}\right)}$$

$$C_{sys} = \frac{1}{m_{cal}} - C_{cal}$$
$$C_{cal} = \frac{2L(c+L)}{E_{cal}b_{cal}t^3} \quad . \tag{3.55}$$

Note that I of the calibration beam should be at least 450 mm^4.

Compliance-Based Beam Method (CBBM) (de Moura, Oliveira, Morais, & Dourado, 2011)

$$G_I = \frac{12a_{eq}^2P_I^2}{B^2h^3E_{fl}},$$
$$a_{eqI} = \frac{1}{6\alpha}A - \frac{2\beta}{A}, \quad \alpha = \frac{8}{Bh^3E_{fl}}, \quad \beta = \frac{12}{5BhG_{12}}, \quad \gamma = -C_I,$$
$$A = \left[\left(-108\gamma + 12\sqrt{3\left(\frac{4\beta^3+27\gamma^2\alpha}{\alpha}\right)}\right)\alpha^2\right]^{1/3} \tag{3.56}$$
$$E_{fl} = \left(C_{0I} - \frac{12(a_0+h|\Delta_I|)}{5BhG_{12}}\right)^{-1}\frac{8(a_0+h|\Delta_I|)^3}{Bh^3}, \quad C_{0I} = \frac{8a_0^3}{E_1Bh^3}+\frac{12a_0}{5BhG_{12}}$$

$$G_{II} = \frac{9P_{II}^2 a_{eq}^2}{16B^2 E_{fII} h^3}, \quad a_{eqII} = \left[\frac{C_{IIcorr}}{C_{0IIcorr}} a_0^3 + \frac{2}{3}\left(\frac{C_{IIcorr}}{C_{0IIcorr}} - 1 \right) L^3 \right]^{1/3},$$

$$E_{fII} = \frac{3a_o^3 + 2L^3}{12I}\left(C_{oII} - \frac{3L}{5G_{LR}A} \right)^{-1}, \tag{3.57}$$

$$C_{IIcorr} = C_{II} - \frac{3L}{5G_{12}A}, \quad C_{II} = \frac{3a^3 + 2L^3}{12E_1 I} + \frac{3L}{5G_{12}A},$$

$$C_{0IIcorr} = C_{0II} - \frac{3L}{5G_{12}A}, \quad C_{0II} = \frac{3a_0^3 + 2L^3}{12E_1 I} + \frac{3L}{5G_{12}A}$$

3.5.3. MMB Test Results and Discussion

The size of MMB specimens were 150x20mm. The geometry of each specimen in turn was measured at three different locations and the average for width and thickness used in later calculations. As recommended in the ASTM D6671-06 standard a side of each MMB specimen is coated by a white correction fluid to allow the visual inspection of the crack during crack propagation. The initial pre-crack position at the end of the PTFE insert on the side of the specimen is marked, from this point marks at increments of 1mm up to a distance of 5mm are drawn, and then the mark are placed at 5mm increments up to a distance of 25mm.

Three specimens were tested using a lever length c=42mm which gives a higher mode II ratio of G_{II}/G_T=0.78; subsequently the test were carried out using a lever length of c=97mm which gives a lower mode II ratio of G_{II}/G_T=0.44.

The five different formulation discussed in section 3.4.2 are used to calculate the fractions of G_I, G_{II} and the total delamination fracture toughness was calculated from G_T= G_I+G_{II}. The MMB test setup and the results are shown in Figure 3.29-3.33 and Table 3.4 below.

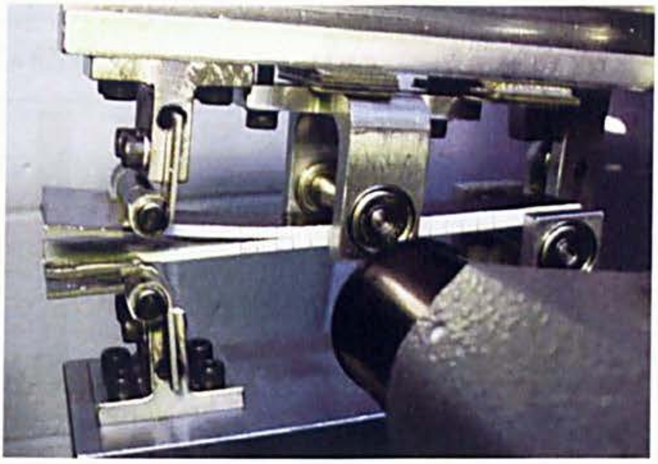

Fig. 3.29. Test set up of mixed mode bending (MMB).

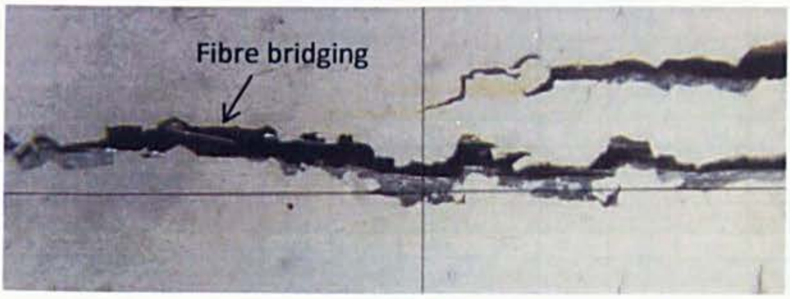

Fig. 3.30. Crack bifurcation and fibre bridging in MMB test.

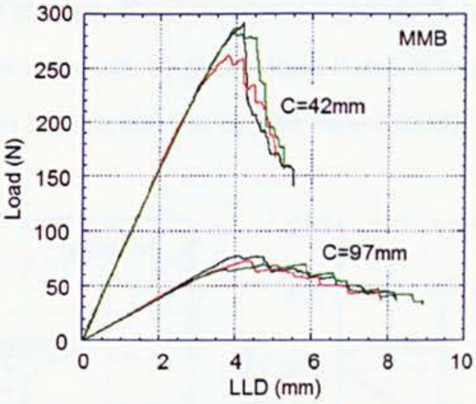

Fig. 3.31. Load versus load line displacement (LLD) in MMB tests at C=42mm and C=97 mm.

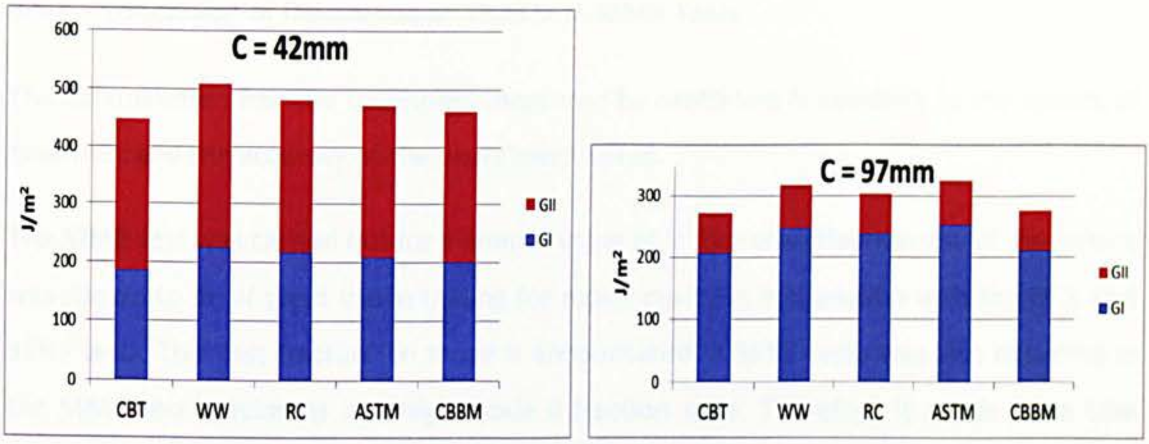

Fig. 3.32. Summary of MMB test result.

Table 3.4. Summary of MMB test result.

MMB	Corrected Beam Theory			Wang-Williams			Reader-Crew			ASTM			CBBM		
	GI	GII	GT	GI	GII	GT	GI	GII	GT	GI	GII	GT	GI	GII	GT
C=97 mm	221	69	290	266	75	340	256	70	326	269	75	344	198	69	267
	142	44	186	171	48	219	164	45	209	184	51	235	155	44	199
	257	80	338	306	86	392	295	81	376	311	88	399	282	80	362
Average	207±58	64±18	271±76	248±68	70±19	317±87	239±65	65±18	304±84	254±64	72±18	326±82	212±64	64±18	276±82
C=42 mm	214	299	513	260	325	585	250	303	553	225	282	507	232	299	532
	176	246	422	214	268	482	206	250	455	189	237	425	191	246	438
	168	235	403	205	256	461	197	238	435	212	266	478	182	235	417
Average	186±23	260±32	446±55	226±28	283±35	509±62	217±27	264±33	481±59	209±18	262±23	470±41	202±25	260±32	462±57

There are two types of envelope that could be plotted for the energy release rate (G) under Mode I and Mode II loading. The first one is a plot of G_I against G_{II} which shows the transition from pure Mode I through to pure Mode II and the second one is a plot of the total energy release rate G_T against the GII/G_T (see Figure 3.33).

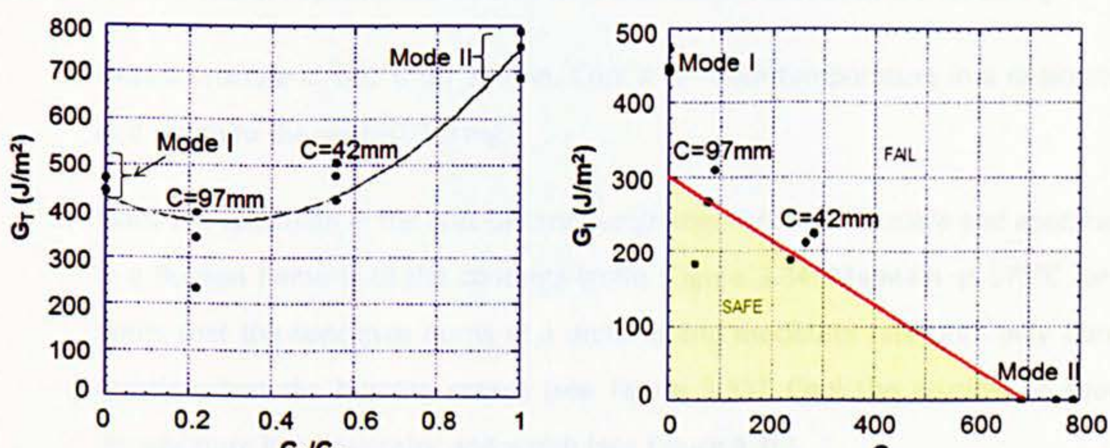

Fig. 3.33. Fracture envelope of delamination under different mode-mixity.

3.5.4. Conclusion of Delamination Studies in MMB Tests

The delamination fracture toughness measured by MMB test is sensitive to the quality of specimen and the accuracy of the experiment setup.

The MMB test was carried out for a limited value of 'c' but the effectiveness of the fixture was shown to be of great use in testing for mode mixity in conjunction with the DCB and 3ENF tests. The 'fast fracture' in mode II encountered in 3ENF tests was also occurred in the MMB test specimens in a high mode II fraction ratio. Therefore it needs extra care when carrying out the tests to obtain consistent data across the range of mixed-mode ratios.

The fracture toughness and the failure envelope produced were impacted by unstable crack propagation. Also in these tests a single crack front is assumed to exist rather than the observed bifurcations that were encountered (see Figure 3.30). Therefore the results derived from various theories have been impacted by these mechanisms.

3.6. Burn Out Test

The purpose of burn out test is to determine the fibre volume fraction in GFRP material.

3.6.1. Procedure of Burn Out Test

The procedure of burn out test is based on the ASTM D2584 (2002) as the following.

a. Heat a crucible at 600°C for 10 min. Cool it to room temperature in a desiccator and weigh to the nearest 1.0 mg.

b. Place the specimen in the crucible and weigh then heat the crucible and specimen in a Bunsen flame until the contents ignite (Figure 3.34. Maintain at 575°C for 3 hours that the specimen burns at a uniform and moderate rate until only fibres remain when the burning ceases (see Figure 3.35). Cool the crucible to room temperature in a desiccator and weigh (see Figure 3.36).

Fig. 3.34. Burn out test- Heating process.

Fig. 3.35. Specimen after burn out test (matrix has gone).

Fig. 3.36. Heated specimens are inside a desiccator.

Calculation of volume fraction of fibre, v_f, has been done by:

$$v_f = (m_f / \rho_f) / V_s \times 100\% \tag{3.58}$$

where m_f = mass of fibre (g), ρ_f = density of fibre (For E-glass i430.90.10 is 2.6 g/mm^3), V_s = volume of specimen (mm^3).

The volume fraction of fibre was found to be 61±2 %. This is consistent with the reported fibre volume fraction in the literature. When manufacturing laminates using vacuum bagging method, during curing seepage of resin occurs from the edges of specimen which results in a higher fibre volume fraction (Mazumdar, 2002) (Groover, 2007).

3.7. Buckling Test of Laminated Composite Plate

The purposes of buckling tests are to determine buckling and postbuckling behaviour of selected stacking sequence for GFRP laminates both with and without inserted delamination patch at mid-plane and for GFRP plates damaged by a hole at the centre of the plate. The details of specimen's sequences and dimensions are summarised in Table 3.6. The critical buckling loads extracted from these series of experiments are used for validation of FEA analysis and also for validation of optimisation results.

3.7.1. Manufacturing of the Specimen

Manufacturing of the laminated composite plates is based on vacuum bagging process as explained earlier for the manufacturing of tensile specimens and the dimensions are according to ASTM D7137 (2005).

Two set of damaged plates were also manufactured. In the first set at the centre of the plate and at the mid-plane a circular PTFE patch inserted with various diameters as shown in Figure 3.38. In another set of experiments a hole with various diameters is drilled at the centre of laminated plate.

3.7.2. Buckling Test Fixture

The buckling fixture is designed to be mounted in a universal test machine as reported by Ahanchian (2008). The fixture assembly is illustrated in Figure 3.37. The two loaded edges of the specimen are clamped by two top slide plates and two base slide plates and the vertical unloaded edges of the specimen are simply supported by knife edges of side plates. Figure 3.38 shows the real fixture which is made from steel.

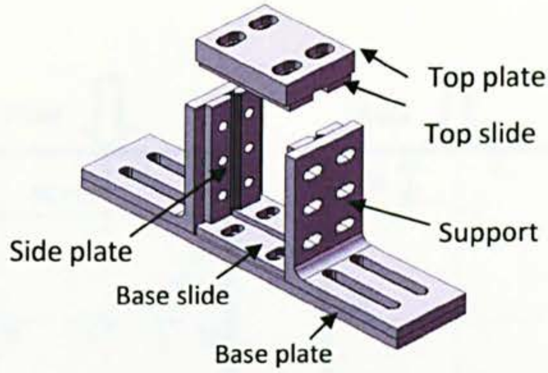

Fig. 3.37. The top and base parts of buckling fixture assembly (Ahanchian, 2008).

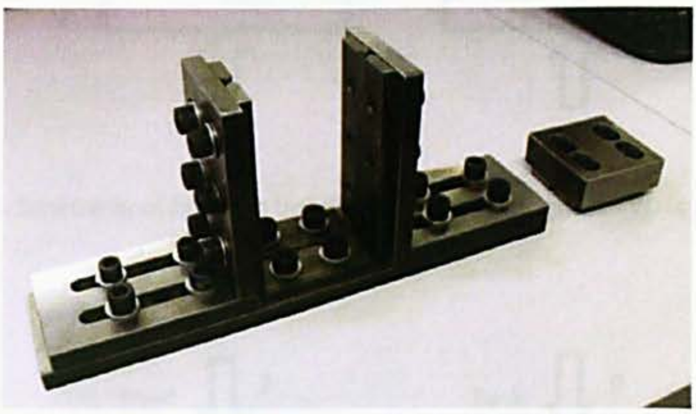

Fig. 3.38. Buckling test fixture support.

3.7.3. Buckling Test Setup

The experimental buckling tests are performed by 50kN Zwick/Roell universal testing machine on the laminated plates at Roehampton Vale Structural Laboratory. The test specimens are held in the test fixture during loading. The test support fixture is placed between the base of the machine and the upper moving head. The machine is stopped when the load dropped at failure. The out of plane displacement at selected points of the plate are monitored using four LVDTs (Linear Variable Differential Transformer) (see Figure 3.39). The experimental set up for the buckling tests of plates with a pre-existing centrally located delamination patch is shown in Figure 3.40. Then, the experimental set up for the buckling tests of plates with a pre-existing centrally hole (cut out) is shown in Figure 3.41. Figure 3.42 shows general set up for buckling test. In all the buckling tests the boundary conditions was clamped-simply supported-clamped-simply supported (CSCS).

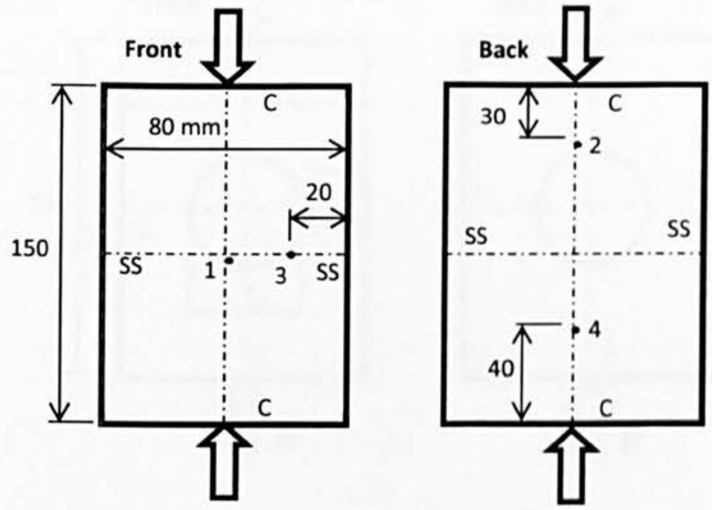

Fig. 3.39. Schematic of buckling test set up with points where LVDTs are attached.

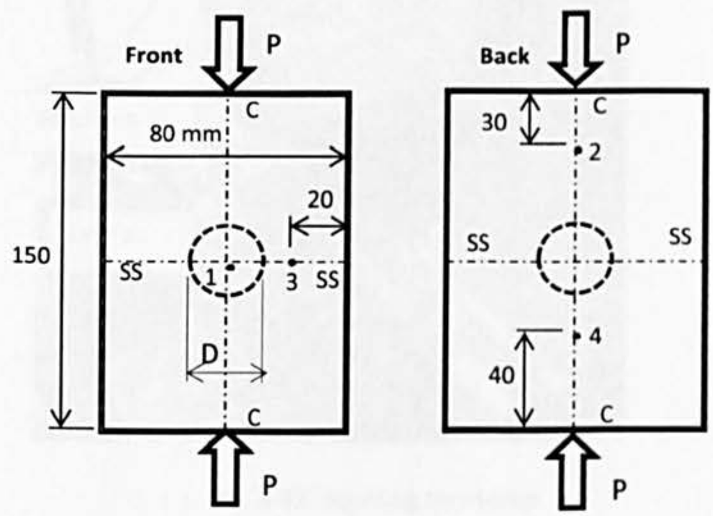

Fig. 3.40. Schematic of buckling test set up with points where LVDTs are attached in plates with a pre-existing centrally located delamination patch with D = 16, 32 & 48 mm at the mid-plane.

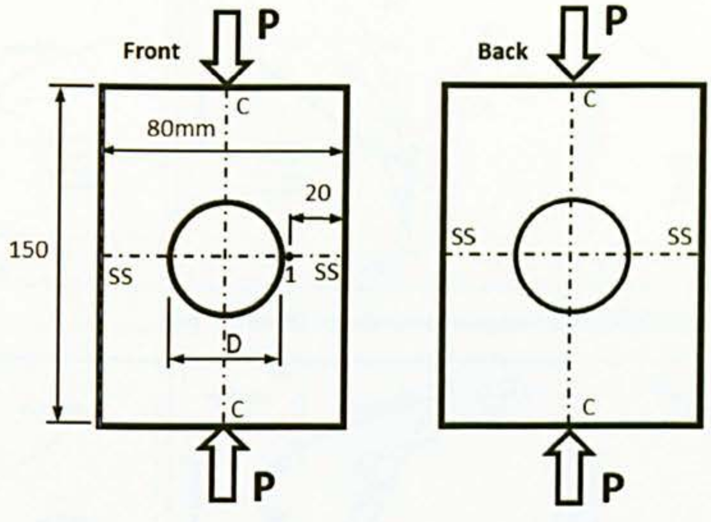

Fig. 3.41. Schematic of buckling test set up with points where LVDT is attached in plates without/with centrally located a hole (cut out) with D =0, 8 & 20mm.

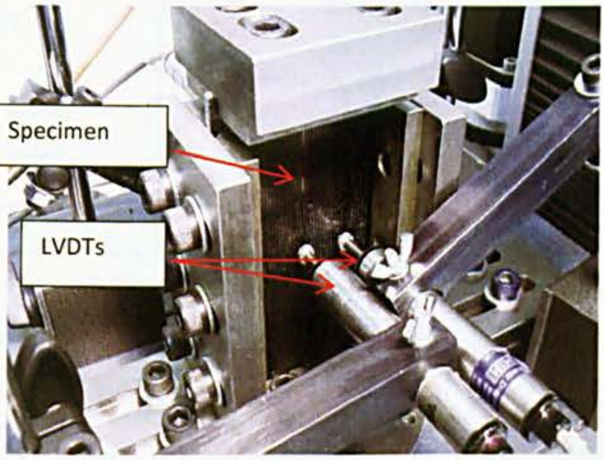

Fig. 3.42. Buckling test setup.

3.7.4. Results and Discussion

The results of load-out of plane displacement for different buckling tests are shown in Figures 3.43-3.47 and Table 3.6 and 3.7.

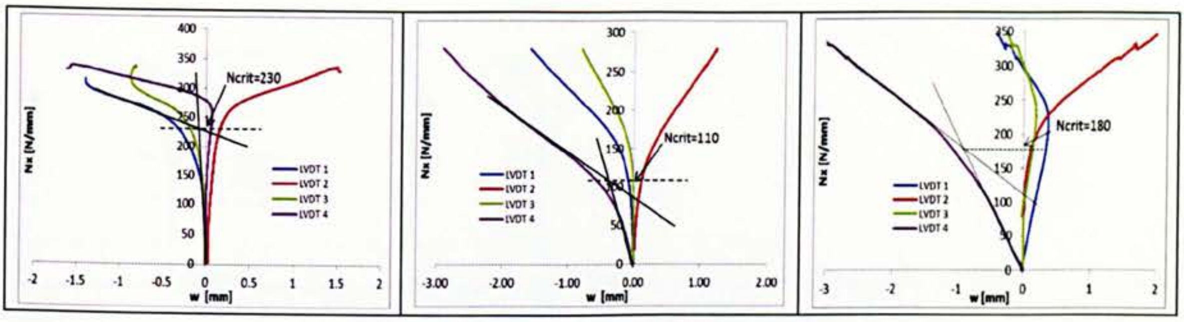

(a) Three B1 specimens, sequence $[0/90/0/0]_s$

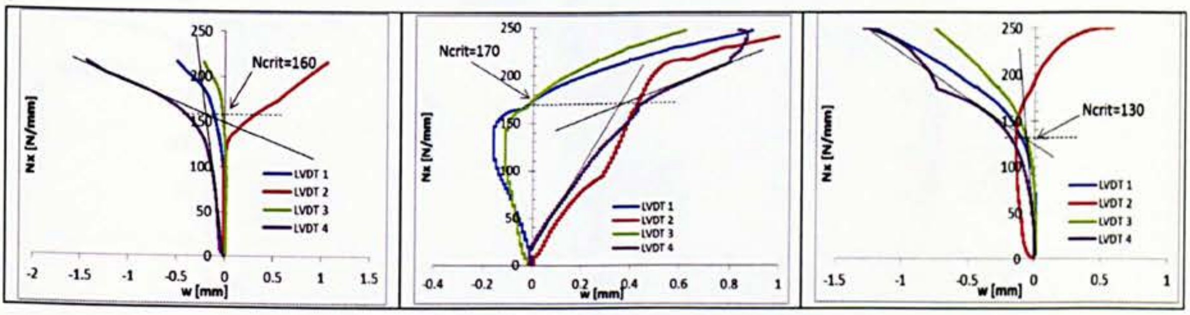

(b) Three B2 specimens, sequence $[90/0/45/-45]_s$

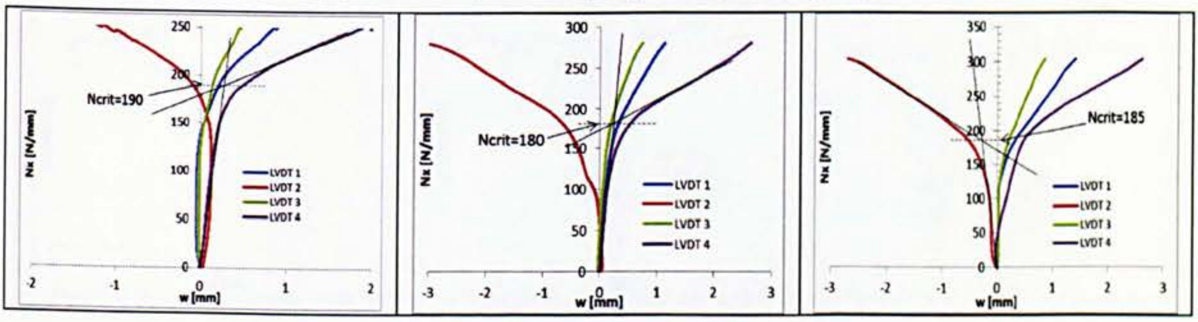

(c) Three B3 specimens, sequence $[0/0/90/90]_s$

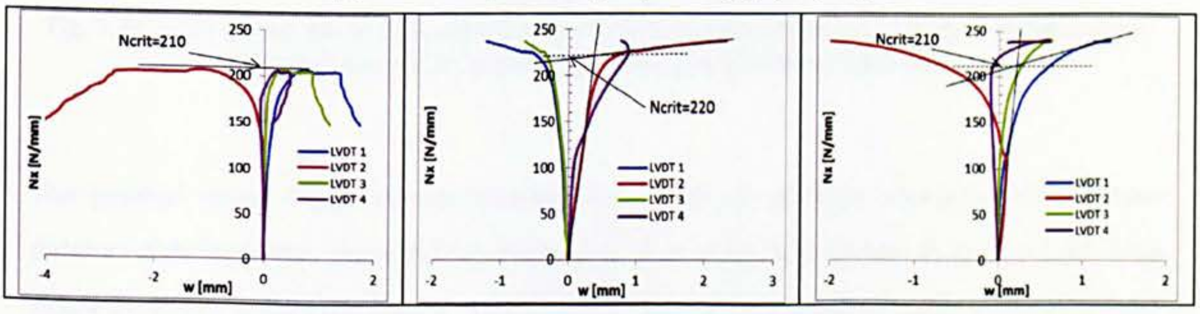

(d) B4 specimens, sequence $[(45/-45)_2]_s$

Fig. 3.43. Load (in N/mm) versus out of plane displacement (in mm) for undamaged for laminated plate (a) B1, (b) B2, (c) B3 and (d) B4 specimens.

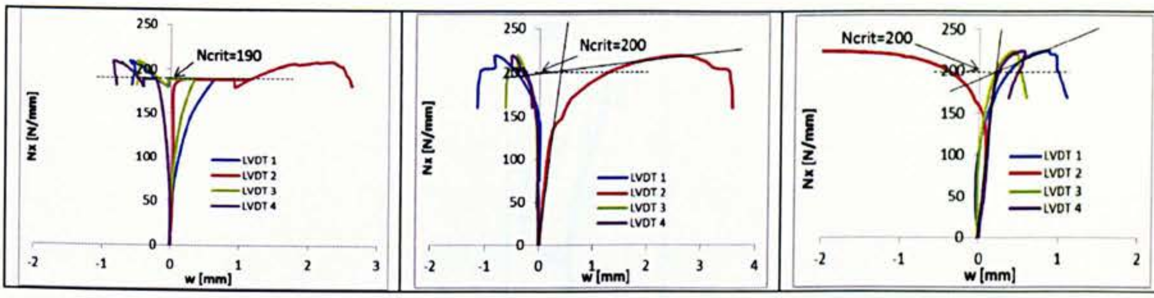

(a) D16 specimens, sequence $[(45/-45)_2]_s$

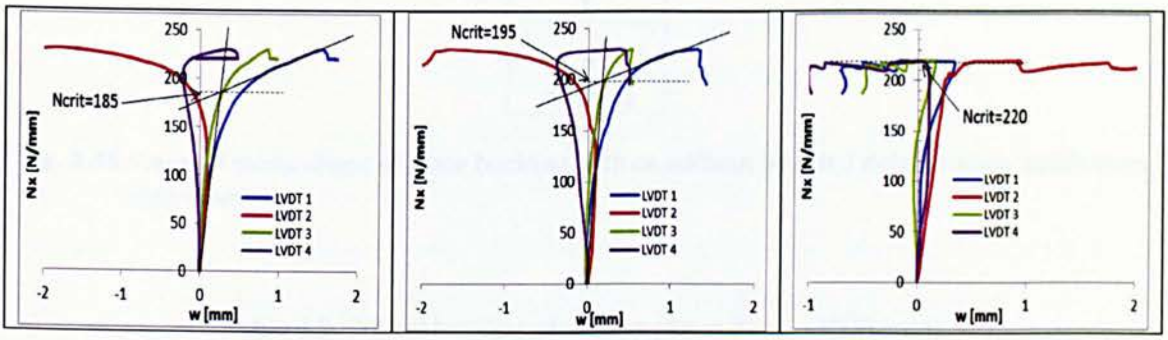

(b) D32 specimens, sequence $[(45/-45)_2]_s$

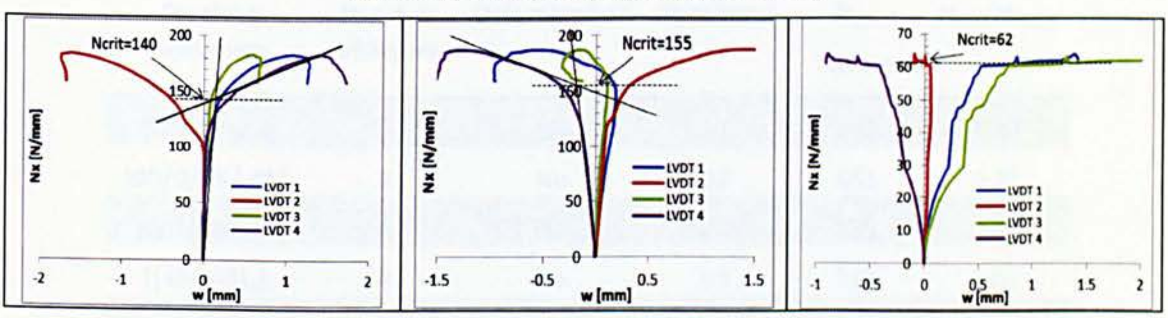

(c) D48 specimens, sequence $[(45/-45)_2]_s$

Fig. 3.44. Load versus out of plane displacement for laminated plate with inserted delamination with diameter of (a) 16mm, (b) 32mm and (c) 48mm specimens.

The general mode shape in the buckling tests with or without inserted delamination patches obtained from the readings from LVDTs positions are shown in Figure 3.45. This figure generally shows the mode shape of buckling is antisymmetric and it is similar to the first eigen mode finite element simulation results which has two half waves.

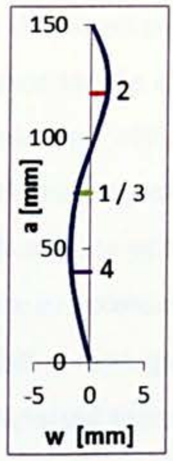

Fig. 3.45. General mode shape of plate buckling with or without inserted delamination patch from side view.

Table 3.5. Critical buckling of various plates (N_{target}=200N/mm).

Stacking sequence	Number of layers	Delamination	Specimen	N_{crit} N/mm	N_{crit}/N_{target}
$[0/90/0/0]_s$	8	No	B1	173	0.87
$[90/0/45/-45]_s$	8	No	B2	153	0.77
$[0/0/90/90]_s$	8	No	B3	185	0.93
$[(45/-45)_2]_s$	8	No	B4	213	1.07
$[(45/-45)_2]_s$	8	Yes	D16	197	0.99
$[(45/-45)_2]_s$	8	Yes	D32	200	1
$[(45/-45)_2]_s$	8	Yes	D48	119	0.6

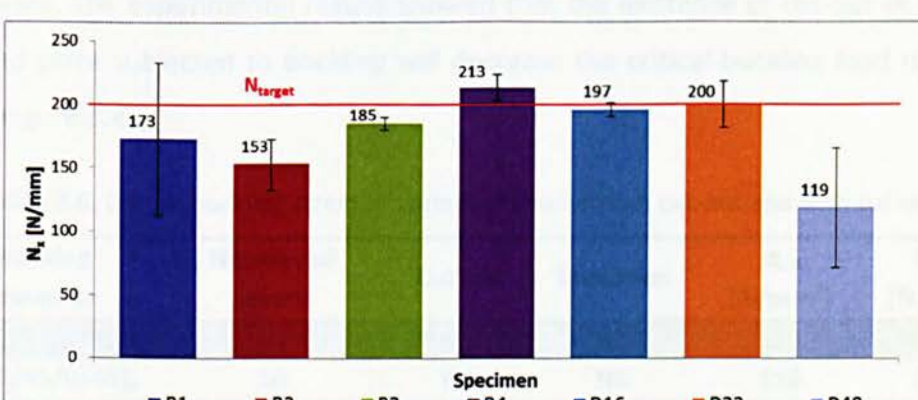

Fig. 3.46. Critical buckling value.

Figure 3.43, 3.46 and Table 3.5 show that specimen B4 with stacking sequence of $[(45/-45)_2]_s$ is the optimum laminate sequence for the case of undamaged plates. However in the case of plates with inserted delamination with diameter less than 32 mm the critical buckling load has not changed. But in the case of D48 specimen with the diameter of delamination at 48 mm (at around 60% of plate width) there is significant reduction in the critical buckling load. These results are in accordance with the results reported by Kim and Hong (1997) who studied buckling and postbuckling behaviour of composite laminates with a delamination. They reported there is a delamination size below that the buckling load and postbuckling behaviour are not affected, yet the buckling load decreases as the delamination size increases. Also Parlapalli *et al.* (2005) studied buckling analysis of tri-layer beams having asymmetrical enveloped delaminations reported the critical buckling load is not sensitive to shorter enveloped delaminations whereas it is strongly influenced by longer enveloped delamination. Finally Aslan and Sahin (2009) studied buckling behaviour and compressive failure of composite laminates containing multiple large delaminations and found the longest size and near-surface delamination influences the critical buckling load of composite laminates.

In further study of these plates by NDT tests using IR thermography and CT-Scan, it was found that the delamination for 16 mm and 32 mm diameter insertion has not grown but in the case of 48 mm diameter insert the delamination has propagated and this resulted in significant reduction in the critical buckling load.

Finally the effect of cut-out on the buckling resistance capacity of laminated plate was investigated. The experimental results showed that the existence of cut-out or hole in a laminated plate subjected to buckling will decrease the critical buckling load (see Table 3.6 and Figure 3.47).

Table 3.6. Critical buckling stress of various plates without cut-out and with cut-out.

Stacking sequence	Number of layers	Cut out	Specimen	σ_{crit} [N/mm²]	N_{crit} [N/mm]
$[45/0/45/0/45]_s$	10	No	H0	120	323
$[45/0/45/0/45]_s$	10	Yes	H8	116	348
$[45/0/45/0/45]_s$	10	Yes	H20	112	365

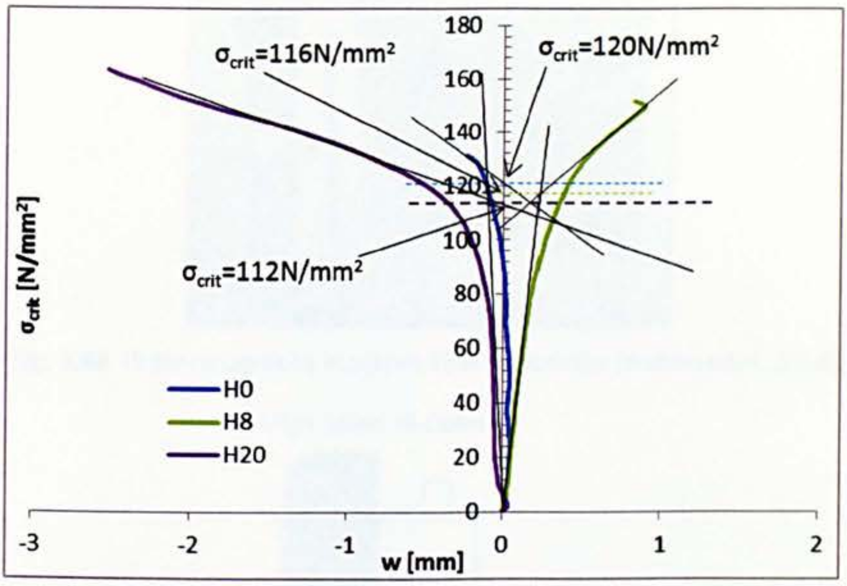

Fig. 3.47. Buckling stress σ_{crit} [N/mm^2] versus out of plane displacement for laminated plate with no hole and with hole (cut out) with diameter 8mm (H8) and 20mm (H20) (Simran, 2014).

3.8. Non-destructive Testing of Buckled Plates

The state of inserted delamination at the mid-plane of laminated plates after uniaxial buckling tests was studied by IR thermography and CT-Scan to investigate the state of the delamination crack front.

3.8.1. IR Thermography

For IR Thermography studies ThermoSpector DCG Systems is used in Germany. Figure 3.48 illustrates ThermoSpector machine for the test and Figure 3.49 shows IR thermography set up.

Fig. 3.48. IR thermography machine ThermoSpector (Heibenstein, 2014).

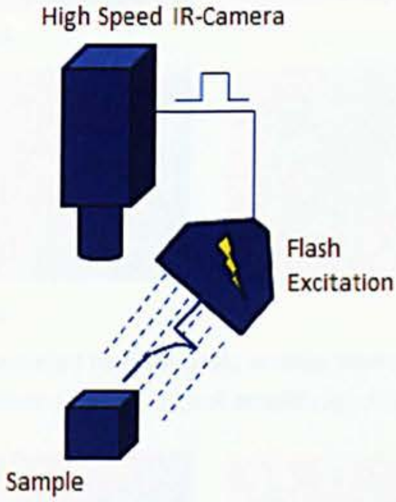

Fig. 3.49. IR thermography set up scheme (Heibenstein, 2014).

3.8.1.1. The IR thermography Results and Discussion

The results of IR thermography tests on $[(45/-45)_2]_s$ plates with pre-existing delamination patch are shown in Figure 3.50-3.55.

In none of the IR images the inserted PTFE film is visible. The IR images shows that for inserted delamination with a diameter of 16 mm the plate buckling and failure occurs near the loading edge and no crack growth observed around the pre-existing delamination patch. In the case of plates with inserted delamination of D=32mm some of them buckled and failed near the loading edge and in some of the plates crack propagated along the 45° fibre direction (see Figure 3.53). However in the case of PTFE insert with diameter of D=48mm, in all samples the delaminated area grows along the fibre direction around the delaminated area and no failure observed near the loading edge (see Figures 54-55).

The depth of inserted delamination affects the image of the IR thermography as reported by Sultan *et al.* (2013).

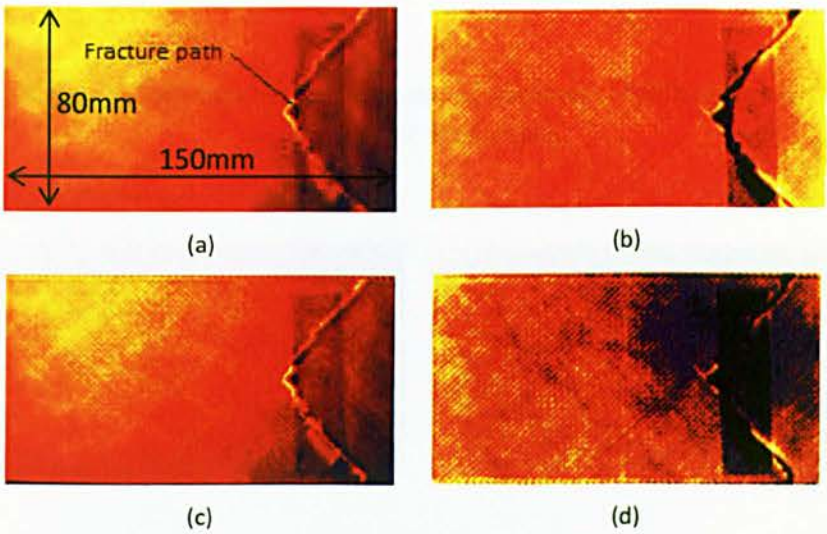

Fig. 3.50. Results of flash induced heating basic arrangement of D16a specimen (a) front amplitude, (b) front phase, (c) back amplitude, and (d) back phase.

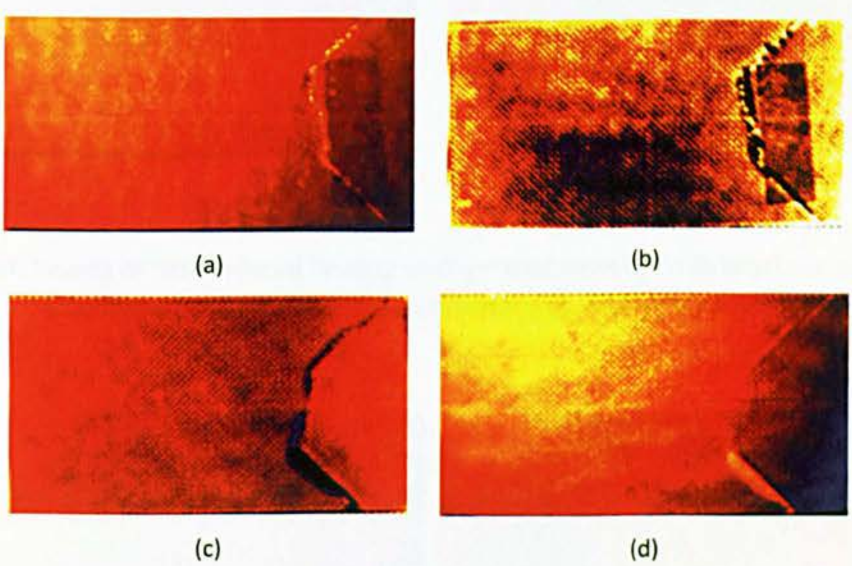

Fig. 3.51. Results of flash induced heating basic arrangement of D16b specimen (a) front amplitude, (b) front phase, (c) back amplitude, and (d) back phase.

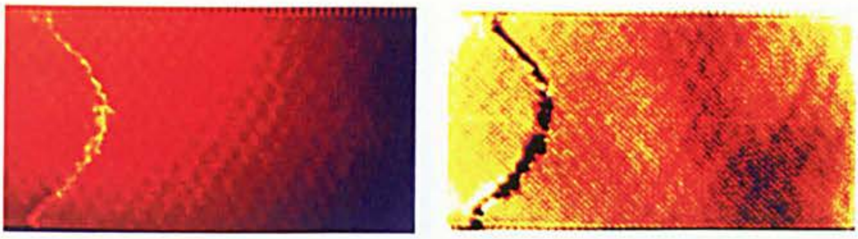

(a) (b)

Fig. 3.52. Results of flash induced heating basic arrangement of D32a specimen (a) front amplitude, (b) front phase.

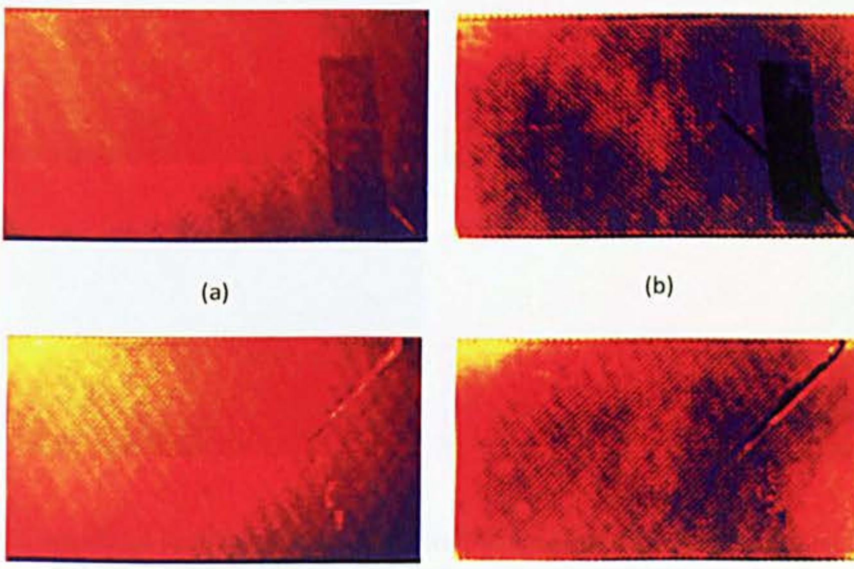

(a) (b)

(c) (d)

Fig. 3.53. Results of flash induced heating basic arrangement of D32b specimen (a) front amplitude, (b) front phase, (c) back amplitude, and (d) back phase.

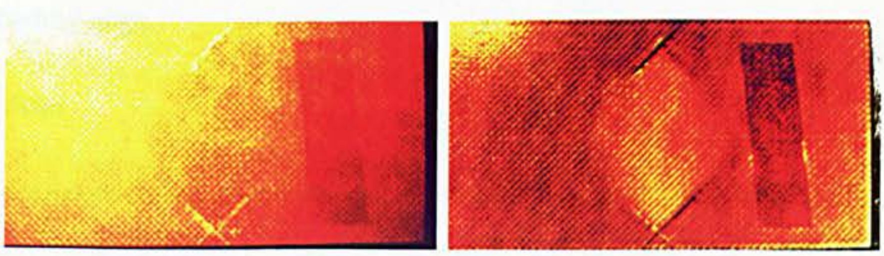

(a) (b)

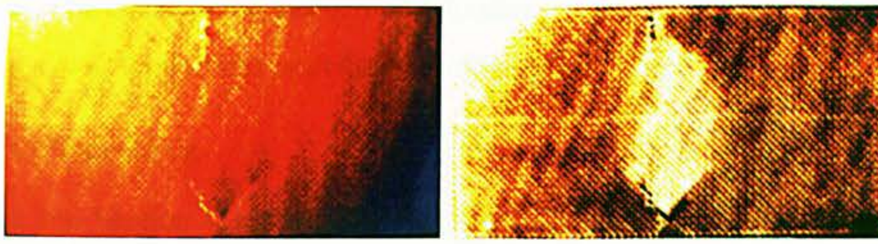

(c) (d)

Fig. 3.54. Results of flash induced heating basic arrangement of D48a specimen (a) front amplitude, (b) front phase, (c) back amplitude, and (d) back phase.

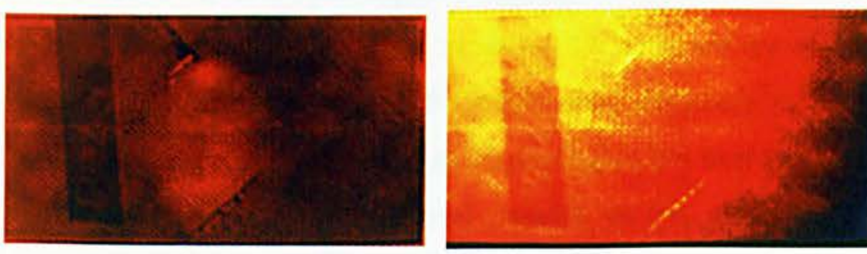

(a) (b)

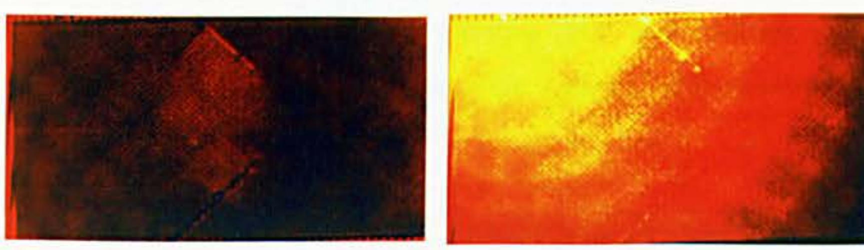

(c) (d)

Fig. 3.55. Results of flash induced heating basic arrangement of D48b specimen (a) front amplitude, (b) front phase, (c) back amplitude, and (d) back phase.

From the results of thermography it can be seen that different appearance emerges when 48 mm diameter delamination present. The fracture path is almost square around the delaminated area along the fibre direction whilst in the other specimens failure occurs near the loading edge.

3.8.2. CT Scan

The crack propagation in buckled delaminated plates under uniaxial loading also studied with CT-Scan. CT scan testing is a type of NDT which can be used to detect typical flaws within composite structures, such as cracks and interlaminar debonding. Therefore, this technique may be employed to evaluate the progressive delamination growth throughout the buckling experimental tests with different delamination sizes.

3.8.2.1. CT Scan Set Up

Courtesy to The London Clinic Hospital, a Siemens SOMATOM Definition AS 128 slice Computed Tomography (CT) scanner was used to obtain high definition images of the laminated GFRP composite plates. The laminated plates were placed flat on the CT table and scanned with the x-ray beam passing perpendicular to the plane of the delaminated insertion. Images were acquired using the standard CT x-ray energy of 120kV at the highest possible resolution utilizing all 128 0.6mm wide detectors. Image processing under a B 70f very sharp (bony) algorithm was found to give the best visualisation of the GFRP plates. Image data was reconstructed parallel to the plane of the inserted delamination with the highest possible resolution of 0.8mm image thickness and 0.5mm distance between the centres of images. Window level and contrast were manually adjusted to best visualise any damages in the plates. Figure 3.56 shows the set up scheme of the test.

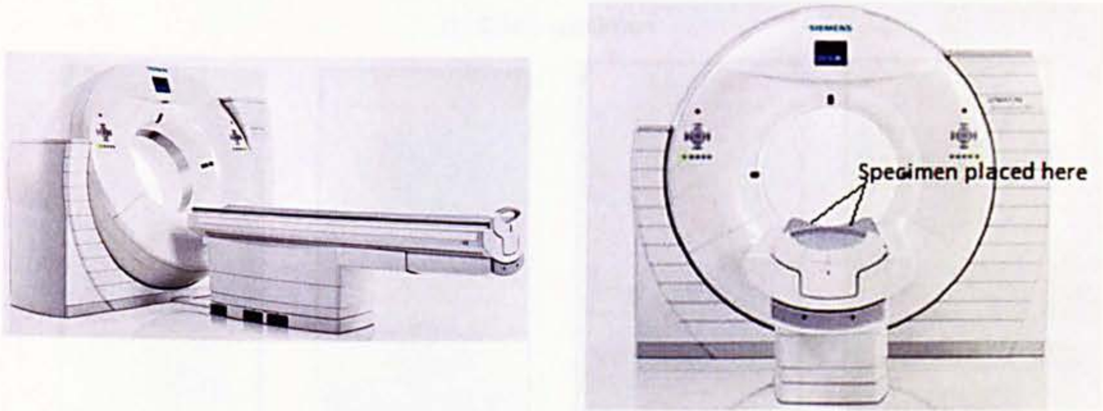

Fig. 3.56. Siemens SOMATON Definition AS+ and set up of specimen scheme (Siemens, 2014).

3.8.2.2. CT Scan Results and Discussion

The CT scan results of plates with pre-existing centrally located delamination patch are shown in Figure 3.57-3.59.

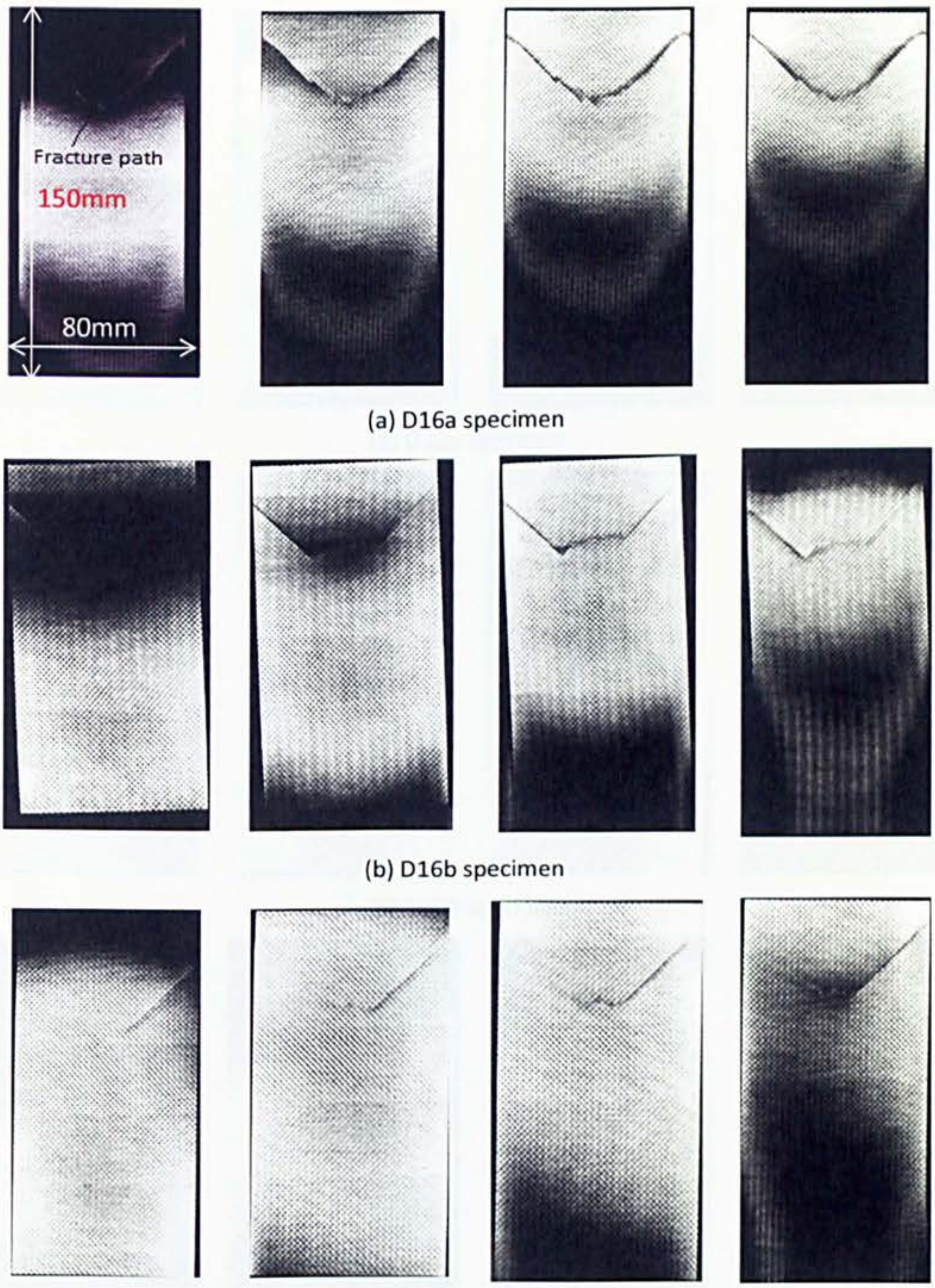

(a) D16a specimen

(b) D16b specimen

(c) D16c specimen

Fig. 3.57. Cross-sectional CT slices at various depth though the thickness of buckled GFRP plate with initial delamination diameter of 16 mm at the centre of the plate.

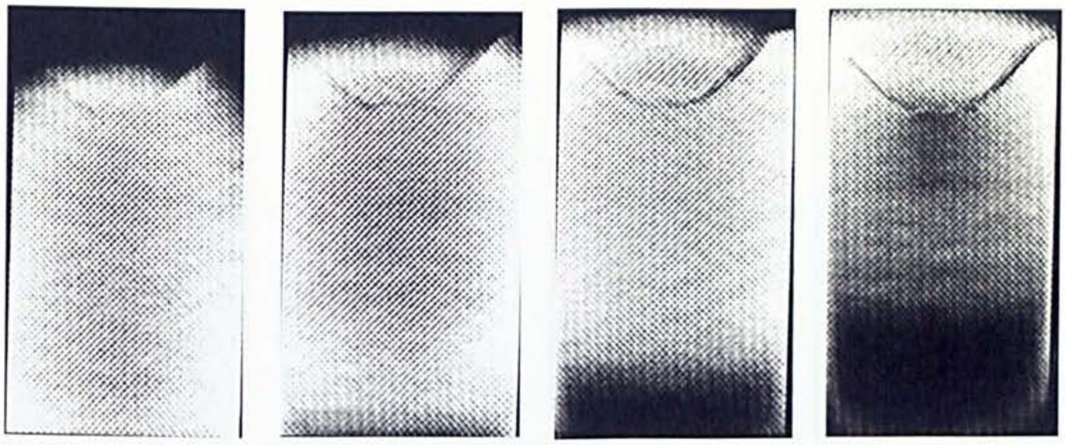

(a) D32a specimen

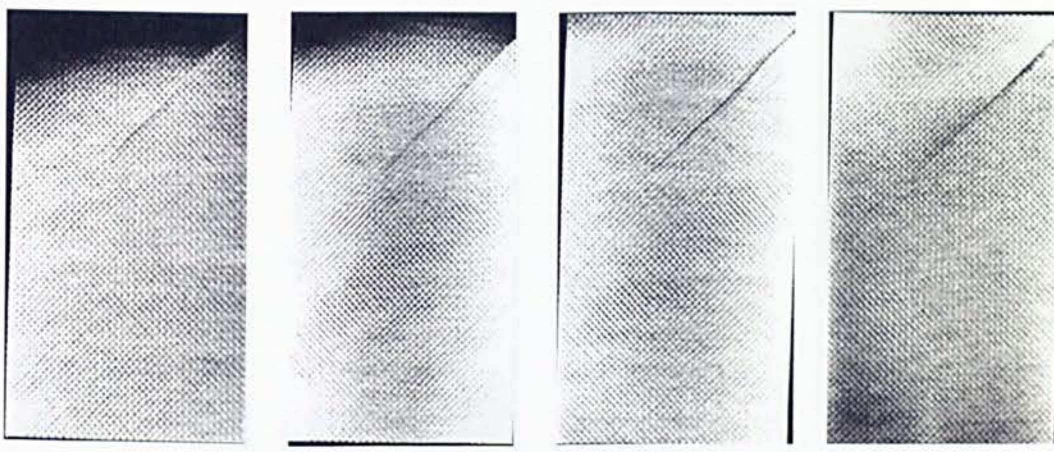

(b) D32b specimen

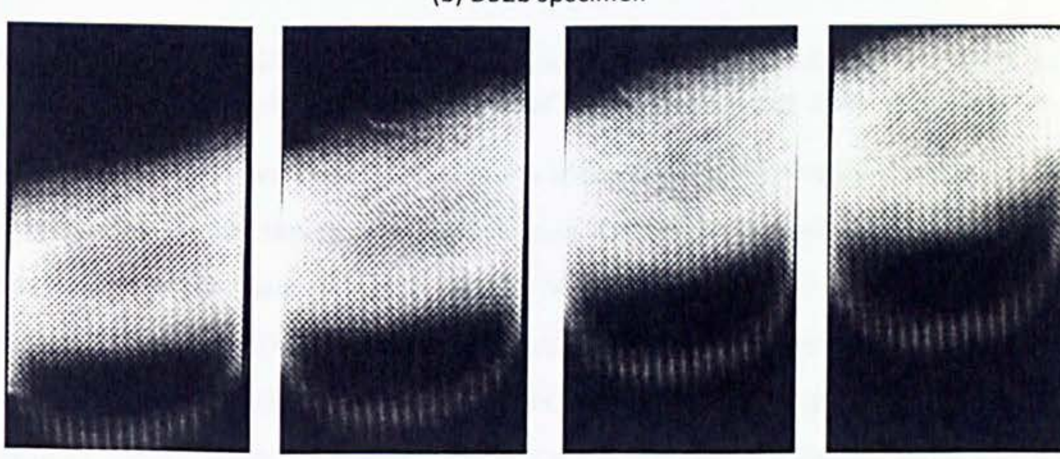

(c) D32c specimen

Fig. 3.58. Cross-sectional CT slices at various depth though the thickness of buckled GFRP plate with initial delamination diameter of 32 mm at the centre of the plate.

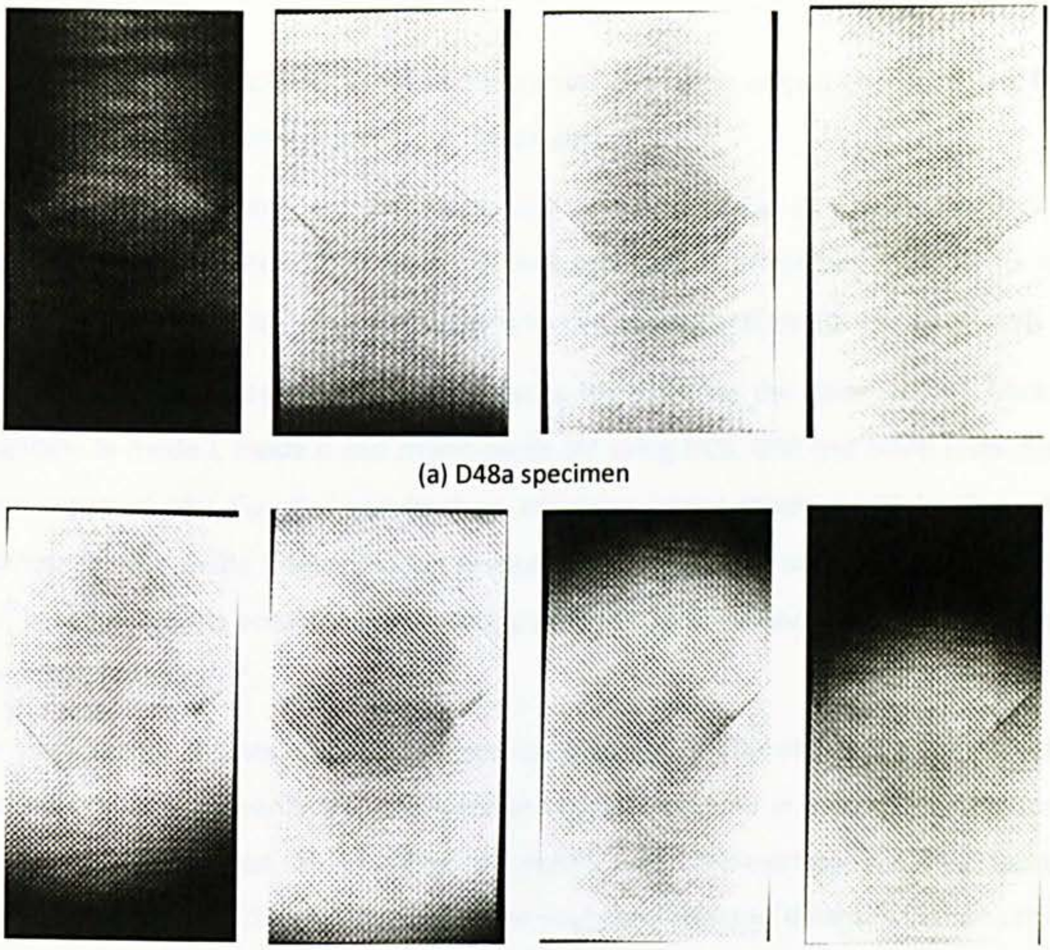

(a) D48a specimen

(b) D48b specimen

Fig. 3.59. Cross-sectional CT slices at various depths though the thickness of buckled GFRP plate with initial delamination diameter of 48 mm at the centre of the plate.

The results of crack front from CT scan are in accordance to the results observed in the IR thermography. Again the plates with 48 mm diameter pre-existing centrally located delamination patch have different pattern of crack propagation relative to the other plates. In those plates the delamination grows along the ±45° fibre direction whilst in the 16 mm delaminated plates the failure occurs near the loaded edge. The plates with 32 mm delaminated areas have mixed results, some fail near the loaded edge and some crack propagated along the fibre direction.

3.9. Conclusion

In this chapter various experimental studies carried out in this project are presented. Four series of test which were conducted for this project are:

The first series of tests were for mechanical characterisation of unidirectional GFRP composite materials. From this series of test mechanical properties such as Young's modulus, shear modulus, Poisson's ratio and tensile and shear strength were obtained.

The second series of tests were performed to characterise the delamination fracture toughness in mode I, mode II and mixed-mode I/II using DCB, ENF and MMB tests. From these series of test G_{IC}, G_{IIC} and fracture envelope under mixed mode loading were determined. The mode I delamination fracture toughness of an average of G_{IC}= 463±15 J/m^2 based on CBT is obtained. The average mode II delamination fracture toughness is about G_{IIC}=710±50 J/m^2.

The third series of tests were performed on buckling of the plates with preselected stacking sequence to verify the optimisation results discussed in Chapter 5. Also some tests were carried out on buckling of plates with pre-existing centrally located delamination patch at the plate mid-plane to study the effect of delamination on critical buckling load of the plate. The optimum critical buckling load was obtained for plate with $[(45/-45)_2]_s$ stacking sequence. However in the case of plates with pre-existing centrally located delamination patch with diameter less than 32 mm the critical buckling load has not changed. But in the case of D48 specimen with the diameter of delamination at 48 mm (at around 60% of plate width) there is significant reduction in the critical buckling load.

The fourth series of tests were performed on buckling of the plates with cut out (hole). The cut out will significant influence the value of critical buckling stress although small size (less or equal to 25% out of width), the critical buckling stress will be decrease.

Finally non-destructive tests were carried out on plates with pre-existing centrally located delamination patch to study the direction and the extent of delamination crack propagation and its effect on the critical buckling load. IR thermography and CT-Scan non-destructive testing have been used to study the delamination crack growth in the buckled plates. Both IR and CT-Scan images showed that in plates with pre-existing centrally located delamination patch with a diameter of 16 mm the plate failure occurs near the loading edge. In the case of plates with delamination patch of D=32mm some plate failed near the loading edge and in some plates crack propagated along the 45° fibre direction around delamination patch. However in the case of delamination patch with diameter of D=48mm, in all samples the delaminated area grows along the fibre direction around the delaminated area and no failure observed near the loading edge.

3.10. References

(n.d.). Retrieved 2014, from www.composites.northwestern.edu: http://www.composites.northwestern.edu/research/characterization/images/10.50.jpg

Ahanchian, N. (2008). *MSc Thesis: Effects of stacking sequence and cut-out size on buckling behaviour of composite plates.* London: Faculty of Engineering Kingston Uni.

Aslan, Z., & Sahin, M. (2009). Buckling behavior and compressive failure of composite laminates containing multiple large delaminations. *Composite Structures, 89*, 382-390.

ASTM Specification D2584. (2002). *Standard test method for ignition loss of cured reinforced resins.* Conshohocken, PA: ASTM International .

ASTM Specification D3039/D3039M. (2006). *Standard test method for tensile properties of polymer matrix composites.* Conshohocken, PA: ASTM International .

ASTM Specification D3518/3518M. (2007). *Standard test method for in-plane shear response of polymer matrix composite materials by tensile test of a +-45 laminate.* Conshohocken, PA: ASTM International.

ASTM Specification D5528. (2007). *Standard test method for mode I interlaminar fracture toughness of unidirectional fiber-reinforced polymer matrix composites.* Conshohocken, PA: ASTM International.

ASTM Specification D6671/6671M. (2006). *Standard test method for mixed mode I-mode II interlaminar fracture toughness of unidirectional fiber reinforced polymer matrix composites.* Conshohocken, PA: ASTM International.

ASTM Specification D7137/D7137M. (2005). *Standard test method for compressive residual strength properties of damaged polymer matrix composite plates.* Conshohocken, PA: ASTM International.

ASTM Specification D7264. (2007). *Standard test method for flexural properties of polymer matrix composite materials.* Conshohocken, PA: ASTM International.

ASTM WK22949. (2010). *New test method for determination of the mode II interlaminar fracture toughness of unidirectional fiber reinforced polymer matrix composites using the end-notched flexure (ENF) test.* Conshohocken, PA: ASTM International.

Blanco, N., Turon, A., & Costa, J. (2006). An exact solution for the determination of the mode mixture in the mixed-mode bending delamination test. *Comp Sci Tech, 66,* 1256-1258.

de Moura, M. F., & de Morais, A. B. (2008). Equivalent crack based analyses of ENF and ELS tests. *Engineering Fracture Mechanics, 75,* 2584–2596.

de Moura, M. F., Dourado, N., Morais, J. J., & Pereira, F. A. (2010). Numerical analysis of the MMB test for mixed-mode I/II wood fracture. *Fatigue Fract Engng Mater Struct, 34,* 149–158.

de Moura, M. F., Oliveira, J. M., Morais, J. J., & Dourado, N. (2011). Mixed-mode (I + II) fracture characterization of wood bonded joints. *Construction and Building Materials, 25,* 1956–1962.

Groover, M. P. (2007). *Fundamentals of Modern Manufacturing* (3 ed.). John Wiley & Sons, Inc.

Gurit. (n.d.). *Guide to composites.* Retrieved February 28, 2014, from www.gurit.com/files/document/guide-to-composites-v5pdf.pdf

Heibenstein, H. (2014). *IR thermography measurements: fibred plastic-first hints.* Germany.

Kim, H., & Hong, C. (1997). Buckling and postbuckling behavior of composite laminate with a delamination. *Composites Science and Technology, 57,* 557-564.

Mazumdar, S. (2002). *Composite manufacturing materials, product, and process engineering.* CRC Press LLC.

Parlapalli, M. S., Wenge, T., & Shu, D. (2005). Buckling analysis of tri-layer beams with enveloped delaminations. *Composites: Part B, 36,* 33-39.

Reeder, J. R. (2003). Refinements to the mixed-mode bending test for delamination toughness. *Journal Composite Technology Research, 25,* 191–195.

Reeder, J. R., & Crews, J. H. (1990). Mixed-Mode Bending Method for Delamination Testing. *AIAA Journal, 28,* 1270-1276.

Siemens. (2014). *Maximize Outcome. Minimize Dose SOMATOM Definition AS.* Retrieved from Siemens Global Website: //www.siemens.com

Simran, H. (2014). *'Buckling analysis of damaged and undamaged laminated composite GFRP plates'.* Supervisors: Dr Homayoun Hadavinia, Joko Sedyono, CEng Aerospace Engineering Final Year Individual Project, Kingston University, UK.

Sultan, R. A., Guirguis, S. W., Younes, M. M., & El-Soaly, E. E. (2013). Delamination detection by thermography. *International Journal of Engineering Research and Application (IJERA), 3*(1), 279-288.

Wang, J., & Qiao, P. (2004). Novel beam analysis of end notched flexure specimen for mode-II fracture. *Eng Fract Mech, 71,* 219-231.

Wang, Y., & Williams, J. G. (1992). Corrections for mode II fracture toughness specimens of composite materials. *Compos Sci Technol, 43*(3), 251-256.

Williams, J. G. (1989). The fracture mechanics of delamination tests. *J Strain Anal, 24*(4), 207-214.

Chapter 4

Theory of Optimisation

4.1. Introduction

In this chapter, a brief review of optimum design theories required for further analysis of optimum design of FRP composite structures under buckling load that will be discussed in Chapters 5 & 6 will be presented. Figure 4.1(a) shows a self-explanatory flowchart for a conventional design method and Figure 4.1(b) shows a similar flowchart for the optimum design method. Both methods are iterative, as indicated by a loop between blocks 6 and 3. In the block 0 for optimum design methodology, an objective function is defined that measures the merits of different designs but that in the conventional is not. In block 4 for the conventional design method checks to ensure that the performance criteria are met, whereas the optimum design method checks for satisfaction of all of the constraints for the problem formulated in block 0. The conventional design method updates the design based on the designer's experience and intuition and other information gathered from one or more trial designs, whereas the optimum design method uses optimisation concepts and procedures to update the current design (block 6) (Arora, 2012).

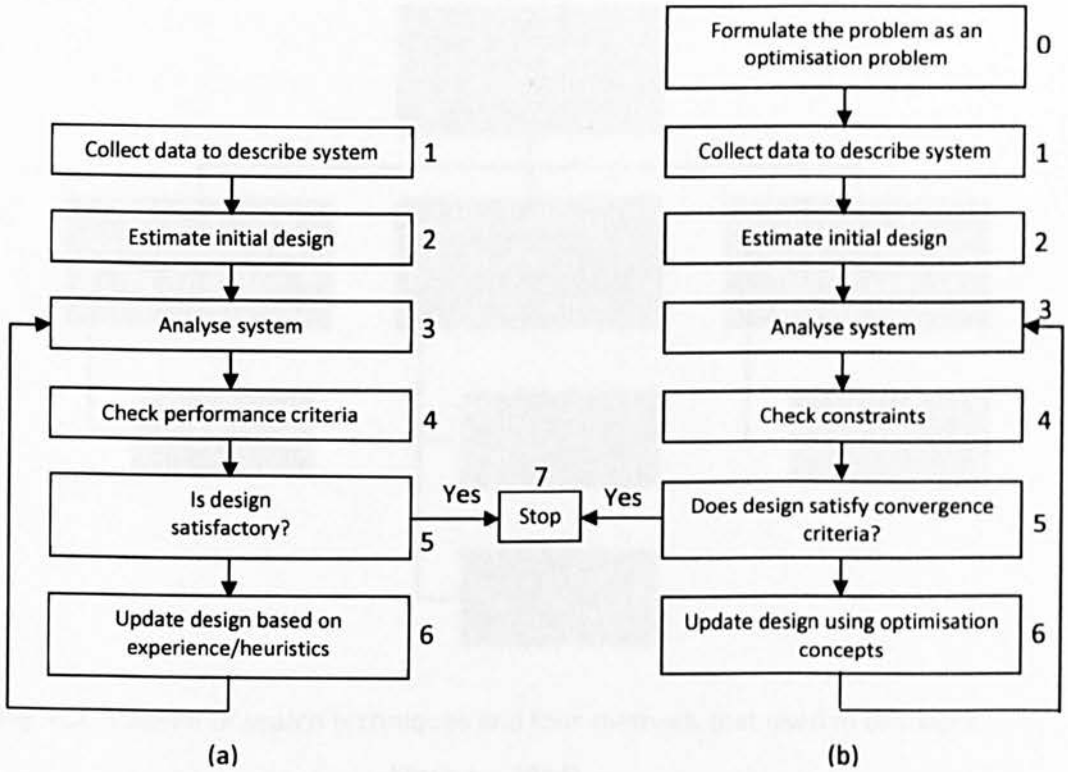

Fig. 4.1. Design method (a) conventional design method and (b) optimum design method (Arora, 2012).

Setoodeh *et al.* (2006) and Ghiasi *et al.* (2009) classified optimisation methods of stacking sequence of FRP composite materials into two classes as the following:

- Constant stiffness, in which the composite structure is assumed as a single entity with the same stacking sequence all over the domain.
- Variable stiffness, in which the structure consists of multiple entities with material distribution and fibre orientations might change over the structural domain.

The optimisation methods that used in this work are shown in Figure 4.2, i.e. enumeration search method (ESM), sequential quadratic programming (SQP), genetic algorithm (GA), and simulated annealing (SA). These methods are the representation of every search technique.

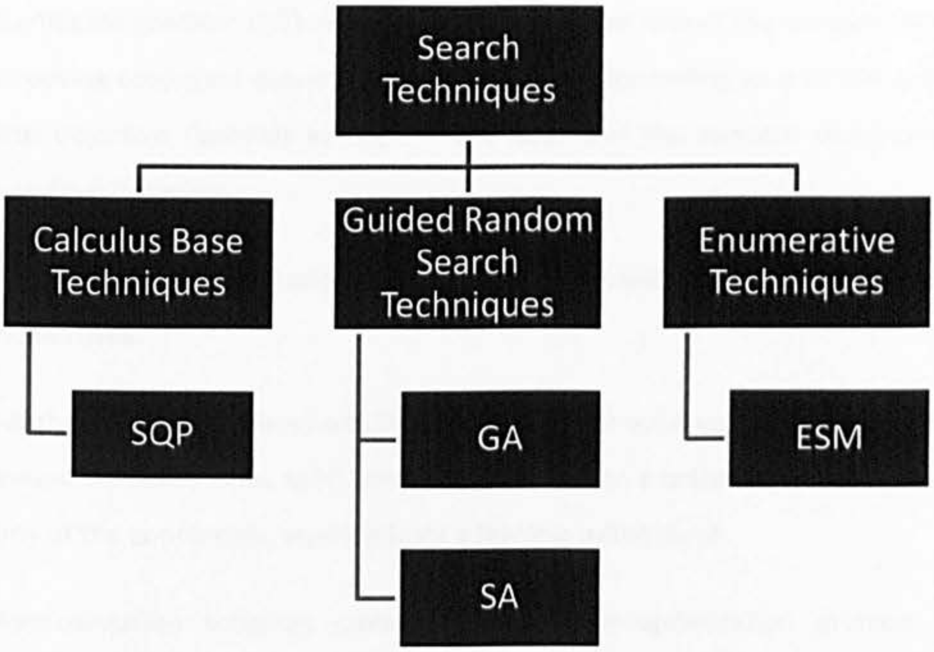

Fig. 4.2. Scheme of search techniques and four methods that used in this work (Zaritsky, 2014).

4.2. Constant Stiffness Type

For the case of constant stiffness type, the following four optimisation methods will be examined.

4.2.1. Gradient-based Methods

Gradient of the objective and constraint are utilized to find the direction and size of the step towards the optimum solution. The advantage of these methods is the faster convergence rate as opposed to that achieved by direct and heuristic methods, yet the solutions obtained with it are only local optima. The methods in this category are:

- Vanishing the function's first gradient is the simplest and the most common method by setting the first gradient of the objective function to zero.

- Steepest descent (SD) is a minimisation method that performs, at each step, a line-search in the opposite direction of the gradient of the objective function.

- Conjugate gradient (CG) improve the convergence rate of the steepest descent by choosing conjugate descent directions that are depending on both the gradient of the objective function at the current step and the descent directions in the previous iteration.

- Quasi-newton method allows determining the Hessian without using second-order derivatives.

- Method of feasible directions (MFD) is created to solve optimisation problem with inequality constraints. MFD tries to find a move to a better point without violating any of the constraints, starting from a feasible initial point.

- Approximation schemes replaces the primary optimisation problem with a sequence of explicit approximate sub-problems, each expressed by a first or second-order Taylor series expansion of the corresponding structural function (Schmit & Fleury, 1980).

4.2.2. Direct Search and Heuristic Methods

These methods do not need any gradient information; rather they require only the values of the objective function. These features are noteworthy advantage as in composite laminate design, derivative calculation are often costly to obtain. The optimum solution is approached systematically by these methods by using function values from the preceding steps. The methods in this category are:

- Partitioning methods is a line search strategy that can handle a single-variable optimisation problem.

- Enumeration search is one of the first attempts in optimum design of laminated composite materials, consisted of trying all possible combinations of design variables and simply selecting the best combination. Although cumbersome, this technique was used to find the lightest composite laminate during the 1970s (Waddoups, 1969) and (Verette, 1970).

- Simplex method uses the concept of a simplex, which is a set of (n+1) points in an n-dimensional design space. It might be a line segment in one dimension, or a triangle in two dimensions. This algorithm stars with an initial simplex, which is generally improved by moving its vertices toward better positions.
- In random and greedy search method random search evaluate a number of randomly selected points in the design space of a given optimisation problem and simply selects the best sampled point, while a track of previously sampled points may be kept by the program to avoid recycling. Greedy search evaluates a set of points around the current solution and moves one step in the direction of the best point, the last move is retained until no more improvement achieved, and then the whole procedure is repeated from the new point.
- Simulated annealing (SA) mimics the annealing process in metallurgy, globalizes the greedy search by permitting unfavourable solutions to be accepted with a probability related to a parameter called "temperature". It is initially assigned a higher value, which corresponds to more probability of accepting a bad move and is gradually reduced by a user-defined cooling schedule. Holding the best solution is recommended in order to preserve the good solution (Erdal & Sonmez, 2005). SA is the most common method after genetic algorithms (GA) for stacking sequence optimisation of laminated composite materials (Lombardi, Haftka, & Cinquini, 1992) (Sadagopan & Pitchumani, 1998) (Sargent, Ige, & Ball, 1995) (Bakis & Arvin, 2006).
- Genetic algorithm (GA) is an evolutionary optimisation technique using "survival of the fittest" to improve a population of solutions. If the population size is suitably large, GA is not at the risk of being stuck in a local optimum. Nevertheless, finding a global solution is not necessarily guaranteed to be successful unless an infinite number of iterations are performed. GA has been the most popular

method for optimising the stacking sequence of a laminated composite, despite the high computational cost (Venkataraman & Haftka, 1999).

- Tabu search (TS) is a local search optimisation method that starts from an initial point and progresses by changing the design variables, one at a time. In a short term memory, the potential solutions that have already been visited and marks them as "Tabu". This strategy prevents solution re-sampling. TS was implemented by Pai *et al.* (2003) for discrete optimisation of the stacking sequence of a composite laminate subjected to buckling.

- Scatter search (SS) is a technique that generates a reference set from a population of randomly selected solutions. Then, a subset of solutions is selected and enhanced by using an improvement procedure (e.g. a greedy search). The improved solutions are then used to update the reference set, and the process is sustained with a new subset.

- Particle swarm optimisation (PSO) is also a population-based, inspired by the flocking behaviour of birds. Each solution in the search space is called a "particle" and resembles a bird among others, which adjusts its position in the search space according to its own flying experience (best solution in its individual history) and the flying experience of the other particles (the best solution among all particles).

- Ant colony optimisation (ACO) is inspired by the behaviour of the ants and their ability in finding the shortest paths between their nest and the food source. Aymerich and Serra (2008) reported the application of this technique to the lay-up design of laminated panels for maximising the buckling load.

4.2.3. Specialised Algorithms

Some properties of composite laminates are used to simplify the problem of optimisation process for a particular application. Some of these methods are:

- Design with lamination parameters are integrated trigonometric functions through the thickness of a laminate, instead of lay-up variables. This has the big advantage of reducing the number of parameters required to express a laminate properties to maximum of 12, regardless of number of layers (Miki, 1982) (Tsai, 1992) (Gurdal, Haftka, & Hajela, 1999).

- Layerwise optimisation method optimises the overall performance of a composite laminate by sequentially optimising one or some of the layers within a laminate. This technique works with one layer (or a subset of layers) in the laminate and requires first the selection of the best initial laminate and then the addition of the layer that best improves the laminate performance, which is usually achieved by an enumeration search (Kere & Koskli, 2002) (Kere, Lyly, & Koski, 2003).

- Problem partitioning, composite lay-up design is governed by variables of different nature, which increase the complexity of the design problem. To simplify the design problem, one possible approach is to split the problem into some dependent sub-problems, each described with a small number of variables of similar nature. Two-part methods of problem partitioning are the first part finds the fibre direction that provides optimum property such as stiffness, displacement, natural frequency, etc., and the second part, optimises ply thicknesses for minimum weight (Soares, Franco, Mateus, & Herskovits, 1995) (Kim & Sin, 2001).

- Discrete material optimisation (DMO) can be equally applied to constant and variable stiffness design; the material stiffness is computed as a weighted sum of some candidate material (fibre orientations). Then, the discrete problem of choosing the best material (with the right orientation) is converted to a continuous formulation where the design variables are the weight functions on each candidate material. The goal for each ply is to drive the influence of all but one of these weight functions to zero.

- Fractal branch-and-bound (FBB) method is based on branch-and-bound method, whose computational cost is reduced using a response surface to approximate the objective function in terms of lamination parameters. This method performs an evaluation of the objective function to prune inefficient branches (laminates) by utilising the fractal patterns of feasible region of lamination parameters in symmetrical laminates.

- Knowledge-based methods (KBM) aims at bringing the expert's knowledge into the computer design process by performing a screening of the concepts ill-suited to the specific requirements and focusing quickly on the most viable and attractive alternatives.

4.2.4. Hybrid Methods

These methods combine two or more optimisation techniques described above to benefit from the strength of all constituent techniques.

4.3. Variable Stiffness Methods

For the case of variable stiffness scenario type (Setoodeh, Abdalla , & Gurdal, 2006) (Ghiasi, Pasini, & Lessard, 2009), the design of variable stiffness composite structures requires a particular formulation that spatially defines the arrangement of the constituent materials at each point of the structure. Part of the effort is dedicated to minimising the number of design variables in the problem formulation and to maintaining the continuity in the structure.

This type consisted gradient-based methods (methods working with the original problem), approximation methods, optimality criterion (strain energy, co-alignment of principal directions, other criteria), topology optimisation, direct search methods (deterministic methods, stochastic methods), multi-level optimisation (hierarchical sub structuring, non-hierarchical decomposition) and hybrid methods.

4.4. Optimisation Algorithms

Here are explanations of optimisation algorithm by Gantovnik (2005). For the successful solution of the problem, the choice of an optimisation strategy is very essential. There are many important parameters such as the type of design variables (continuous, discrete or mixed), the type of objective function (smooth or non-smooth, differentiable, etc.), constrained or unconstrained problem, shape of feasible design space, the number of design variables, the number of constraints, cost of each simulation, linear or nonlinear functions, availability of first and second-order derivatives, local and global optima, etc.

As described in Chapter 2 Gantovnik (2005) categorised optimization algorithms into two classes:

1. Deterministic methods

These methods use function and/or gradient information to construct mathematical approximation of the functions then find an optimum point employing hill-climbing methods. These methods work normally with continuous design variables and need a small number of function evaluations, but they may not find a global optimum point.

2. Nondeterministic methods

These methods work entirely using only function values and can work with discrete variables and (with infinite time) find a global optimum in the presence of several local optima. The most common methods in this class are random search, genetic algorithms (GAs), evolutionary programming (EP), evolution strategies (ES), simulated annealing (SA), and particle swarm optimization (PSO).

According to Conti *et al.* (1994) and Sadagopan & Pitchumani (1998) optimisation algorithms are divided into three categories:

1. Mathematical method. This method based on gradient of objective function nevertheless it deals with local optimum.
2. Enumerative method. Enumeration method attempts to get global optimum with every point of the objective function one point at a time, but sometime it require tedious computation.
3. Random method. This technique deals global optimum with random search.

4.5. Mathematical Optimisation

In general mathematical for optimisation from Gurdal *et. al* (1999) an optimization problem has an objective function which measures the goodness or efficiency of the design. The maximisation of the goodness is generally performed within some limits that constrain the choice of design. Such limits are called constraints. Finally an optimisation problem has design variables, which are the parameters that are changed during the design process. Design variables can be continuous or discrete depending on whether they can take values from a continuum or are limited to a number of discrete values. A special case of discrete variables are integer variables.

The commonly used notation for design variables, objective function, and constraints is as follows. We use a vector x with n components to describe the design variables. To allow for the case that some of the design variables may be discrete or limited otherwise, we use X to denote the domain of these design variables. For the objective function, we use the notation f(x) and for constraints, the notation g(x) for inequality constraints and h(x) for equality constraints. The standard form of the optimisation problem is written as

$$\begin{array}{lll} \text{minimise} & f(x) & x \in X \\ \text{such that} & h_i(x) = 0, & i = 1, \dots, n_e, \\ & g_j(x) \le 0, & j = 1, \dots, n_g, \\ & x^L \le x \le x^U, & \end{array} \tag{4.1}$$

where the elements of the vectors x^L and x^U are the lower and upper bounds on the values of the design variables. Note that in this standard form we minimise rather than maximise the objective function. To convert a maximisation problem into a minimisation problem, we just need to change the sign of the objective function. That is, instead of maximising f(x) we can minimise –f(x).

The set of design points in X that satisfy all the constraints is called the feasible domain. At a given point x, a constraint may be satisfied or violated. An inequality constraint for which the equality condition holds at a particular design point x is called an active constraint. All satisfied equality constraints are active, while inequality constraints can be active or may be satisfied with a margin, in which case they are called inactive.

In the context of optimisation, tailoring of the material properties is also associated with maximisation or minimisation of a performance criterion. The performance criterion may be the weight of the laminate, and the desirable response quantities, such as stiffness, become the constraints. Alternatively, a response quantity can be maximised or minimised subject to a constraint on weight. In either case, the variables typically used for design optimisation define the fibre orientation, number of plies, and stacking sequence of plies that make up the composite laminate.

According to Gantovnik (2005), the objective of optimisation is to determine the best or optimum point out of the number of possible combinations of parameters defining the problem mathematically. The optimum solution is either the maximum or minimum of an objective function $f(s)$. The independent variable s is named design variable. For mixed integer programming problems, the objective function depends on integer variables $y \in Z^{\ell}$, where ℓ is the number of integer design variables, and continuous variables $x \in \Re^{m}$, where m is the number of continuous design variables, i.e., $s=(y,x)$.

Consider the optimization problem with only continuous design variables, i.e., s = x. The design variables lie in the design space $\Re^{m}$. The design variables ought to satisfy a set of constraints that normally involve nonlinear functions of the design variables. The constraints split the design space into feasible F and infeasible U regions. The constraints consist equality constraints $h_k(x) = 0$, inequality constraints $g_j(x) \leq 0$, and upper and lower bounds for the vector of design variables x. The upper and lower bounds are inequality constraints of the form $a_i \leq x_i \leq b_i$ for each design variable xi.

Definition A (Optimization Problem). Let $f:\Re^{m} \rightarrow \Re, g:\Re^{m} \rightarrow \Re^{q}, h:\Re^{m} \rightarrow \Re^{p}$. The optimisation problem standard form is

$$\begin{aligned}
&\text{Minimise } f(x)\\
&\text{subject to}\\
&\qquad g_j(x) \le 0, \quad j \in \{1,\dots,q\},\\
&\qquad h_k(x) = 0, \quad k \in \{1,\dots,p\},\\
&\text{and}\\
&\qquad (x_i)_{\min} \le x_i \le (x_i)_{\max,} \quad i \in \{1,\dots,m\},
\end{aligned} \tag{4.2}$$

where *f(x)* is the objective function, $x=(x_1,x_2,\dots,x_m)\in\Re^m$ is the vector of design variables, $g_j(x) \le 0$ are inequality constraints, $h_k(x) = 0$ are equality constraints, $(x_i)_{min}$ and $(x_i)_{max}$ are lower and upper bounds on the *i*th design variable, *q* is the number of inequality constraints, *p* is the number of equality constraints, and *m* is the number of design variables.

An equality constraint can be substituted by two inequality constraints, and (4.2) can be represented as

$$\begin{aligned}
&\text{Minimise } f(x)\\
&\text{subject to}\\
&\qquad g_j(x) \le 0, \quad j \in \{1,\dots,q+2p\},\\
&\text{and}\\
&\qquad (x_i)_{\min} \le x_i \le (x_i)_{\max,} \quad i \in \{1,\dots,m\},
\end{aligned} \tag{4.3}$$

Finally, the optimization problem without equality constraints is considered in the form

$$\begin{aligned}
&\text{Minimise } f(x)\\
&\text{subject to}\\
&\qquad g_j(x) \le 0, \quad j \in \{1,\dots,q\},\\
&\text{and}\\
&\qquad (x_i)_{\min} \le x_i \le (x_i)_{\max,} \quad i \in \{1,\dots,m\},
\end{aligned} \tag{4.4}$$

The feasible region F is designated more closely in the following definition.

Definition B (Constraints). $F := \{x \in \Re^m \mid g_j(x) \le 0 \ \ \forall j \in \{1,\dots,q\}\}$ is entitled the feasible region of the problem (4.4). The functions $g_j : \Re^m \to \Re$ define the constraints, and at a point $x \in \Re^m$ a constraint g_j is called

$$\begin{array}{lll} \text{satisfied} & \Leftrightarrow & g_j(x) \leq 0, \\ \text{active} & \Leftrightarrow & g_j(x) = 0, \\ \text{inactive} & \Leftrightarrow & g_j(x) \langle 0, \text{ and} \\ \text{violated} & \Leftrightarrow & g_j(x) \rangle 0. \end{array} \tag{4.5}$$

The optimization problem is named unconstrained if $F = \Re^m$; otherwise, constrained.

In the dealing of optimisation problems it is significant to make a distinction between global and local minima. The following definitions are invoked.

Definition C (Global minimum). Given a function $f : F \subseteq \Re^m \rightarrow \Re, F \neq 0,$, for $x^* \in F$ the value $f^* := f(x^*) \rangle -\infty$ is named a global minimum if

$$\bullet \forall x \in F, \quad f(x^*) \leq f(x). \tag{4.6}$$

Then x^* is called a global minimum point, f is the objective function, and the set F is the feasible region. The problem of determining a global minimum point is called the global optimisation problem.

Definition D (Local minimum). For $\hat{x} \in F$ the value $\hat{f} := f(\hat{x})$ is named a local minimum and $\hat{x}$ is a local minimum point if •

$$\exists \varepsilon \in \Re, \ \ \varepsilon \rangle 0 \ : \ \forall x \in F, \|x - \hat{x}\| \langle \varepsilon \Rightarrow \hat{f} \leq f(x). \tag{4.7}$$

These definitions do not restrict generality of the optimization problem, since the identity

$$\max \ \{f(x) \mid x \in F\} = -\min \ \{-f(x) | x \in F\} \tag{4.8}$$

holds.

The required but not sufficient conditions for an optimum are the Karush-Kuhn-Tucker (KKT) conditions. A local optimum point of (4.4) has to satisfy the KKT conditions

Definition E (KKT conditions). KKT conditions are

$$
\begin{aligned}
&\frac{\partial f(x)}{\partial x_i}+\sum_{j=1}^{q}\lambda_j\frac{\partial g_j(x)}{\partial x_i}=0 \quad \text{at} \quad x=x^{*}, \quad \text{for } i=1,\dots,m; \\
&\lambda_j g_j(x)=0, \quad g_j(x)\le 0, \quad \text{for } j=1,\dots,q; \\
&\lambda_j\ge 0 \quad \text{for } j=1,\dots,q,
\end{aligned}
\tag{4.9}
$$

where q is the number of constraints.

The geometric explanation of these conditions means that the negative gradient vector of the objective function is inside a cone built by the positive gradient vectors of the active constraints.

It is assumed that all functions, objective function and constraint functions are nonlinear for most practical problems. Due to for many engineering problems the nonlinearities are small enough that is reasonable to approximate them with linear functions. Nevertheless, when the nonlinearities are not small enough, it has to deal directly with nonlinear programming models.

The types of programming (mathematical optimisations) problems can be classified as follows:

- linear programming problems (LP): in these problems both the objective function and constraints are linear and the variables are continuous;
- nonlinear programming problems (NLP): in these cases the objective function or the constraints can be either linear or nonlinear and the variables are continuous ;
- mixed-integer programming problems (MIP): in these problems the objective function and constraints are integer functions and continuous variables;
- integer programming problems (IP): in these problems there is no continuous variables involved;

- binary programming problems (BP): in these problems the variables have either a value of 0 or 1 (binary).

To solve NLP, number algorithms have been developed, each with its own advantages and disadvantages. It consist three basic categories of algorithms:

1) gradient algorithm, where gradient search procedure is modified in a way to keep the search path from penetrating any constraint boundaries;

2) sequential unconstrained algorithm, where the constraints are incorporated into a penalty or barrier function. The role of such penalty function is to impose a penalty for violating constraints or even to consider only feasible solutions;

3) sequential approximation algorithm includes linear approximation and quadratic approximation methods (sequential quadratic programming). It replaces a nonlinear objective function and nonlinear constraints by a sequence of linear or quadratic approximations.

4.6. Enumeration Search Method (ESM)

Enumeration search is one of nondeterministic optimisation algorithm methods. As explained above, it is one of the first attempts in optimum design of laminated composite materials, consisted of trying all possible combinations of design variables and simply selecting the best combination.

Enumeration search method included also selection chart techniques, which aim at visualising the impact of the variables throughout the whole design space. Park (1982) plotted the change of the optimum fibre angle for a particular class of laminates under all possible normalised loading conditions. Weaver (2002) reported selection charts as well, in which each class of laminates was displayed within an elliptical contour. These charts can be used to identify a small subset of potential laminates that might be investigated in more details.

This technique can be called Exhaustive Enumeration and categorised as discrete optimisation method (Venkataraman P. , 2009). This involves identifying solution to the mathematical model for all possible combinations of the discrete variables. The second method is the Branch and Bound method, which is based on partial enumeration where only part of the combinations, is explored. The remaining are snipped from consideration because they will not contain the solution. The last method is Dynamic Programming, which did not gain goodwill because it involved significantly large amount of computation than competitive methods. Sequential selections of the design variables are needed with it. These techniques are classified as heuristic methods. This encourages unique and personal implementations of the search for discrete optimisation that can be tailored for our class of problems. Event today discrete optimisation is very different, difficult, diverse, and continues to develop. Today, almost all types of communication, signals, and controls have moved to the digital format where information is coded, usually in binary form that is essentially discrete information. Dealing with this method will be essential for the engineer. These problems are largely combinatorial and are computationally more time intensive and expensive than continuous problem.

There have been only few books in the area of discrete, integer, or combinatorial programming (Venkataraman P. , 2009). Engineering optimisation, by contrast, mostly incorporates nonlinear problems. Reality, discrete design variables should be fundamental to engineering optimisation.

4.6.1. Standard Format Discrete Optimisation

According to Venkataraman (2009), there is no standard format for the discrete optimisation problem as it subsumes the format of the corresponding continuous relaxation problem. Although, the following format for mixed optimisation is used.

$$\text{Minimise } f(X,Y), \ [X]_{n_c};[Y]_{n_d} \qquad (4.10)$$

Subject to:

$$\begin{aligned} &h(X,Y)=[0]; \quad [h]_l \\ &g(X,Y)\le[0]; \quad [g]_m \\ &x_i^l \le x_i \le x_i^u; \quad i=1,2,3,...n_c \\ &\mathrm{y_i} \in Y_{d_i}; \quad [Y_{d_i}]_{p_i}; \quad i=1,2,3,...n_d \end{aligned} \tag{4.11}$$

X represents the set of n_c continuous variables. Yrepresents the set of n_d discrete variables. $f$is the objective function. h is the set of l equality constraints. g is the set of m inequality constraints. If n_d= 0 then it a continuous optimisation problem. If n_c= 0 then it is a discrete optimisation problem. It both is nonzero then it is a mixed problem.

4.6.2. Reduced Model

It is important in subsequent discussions as it is the continuous relaxation model solved after a set of discrete variable is set at some allowable discrete values. This removes those variables from the problem, as their values have been set. The mathematical model is then defined by the remaining discrete variables, as well as the original continuous variables. If Z is the remaining discrete variable then n_z needs to be solved from:

$$\text{Minimise}\ \tilde{f}(X,Z), \quad [X]_{n_c};[Z]_{n_z} \tag{4.12}$$

Subject to:

$$\begin{aligned} &\tilde{h}(X,Z)=[0]; \quad [h]_l \\ &\tilde{g}(X,Z)\le[0]; \quad [g]_m \\ &x_i^l \le x_i \le x_i^u; \quad i=1,2,3,...n_c \\ &\mathrm{y_i} \in Z_{d_i}; \quad [Z_{d_i}]_{z_i} \end{aligned} \tag{4.13}$$

To be noted that Z_{di} is not a new set. It reflects the remaining discrete variable and the appropriate Y_{di}. However, in an exhaustive enumeration $n_z$is zero, as all the discrete variables are set to some allowable value.

4.6.3. Enumeration Search Method (Exhaustive)

It evaluates an optimum solution for all combinations of the discrete variables; therefore it is the simplest of the discrete optimisation methods. The best solution is obtained by comparing the list of feasible solutions in the previous investigation. The total numbers of evaluations, n_e are described below.

$$n_e = \prod_{i=1}^{n_d} p_i \tag{4.14}$$

It represents an exponential growth in the calculations with the number of discrete variable.

4.7. Sequential Quadratic Programming (SQP)

Since 1970s, sequential quadratic programming has arguably become the most successful method for solving nonlinearly constrained optimisation problems (Boggs & Tolle, Sequential quadratic programming, 1996). SQP is not a single algorithm, but rather a conceptual method from which numerous specific algorithms have evolved. The problems arise in a variety of applications in science, engineering, industry, and management.

In the section some basic ideal of the SQP method will be described for solving nonlinearly constrained optimisation problem (Boggs, Sequential quadratic programming, 1995). The problem is, as usual,

$$\begin{aligned}
&\text{(P) Minimise } f(x) \\
&\text{subject to} \\
&\qquad g_j(x) \le 0, \\
&\qquad h_k(x) = 0,
\end{aligned} \tag{4.15}$$

where at least one of the constraints is nonlinear.

In order to stimulate SQP we have to use Newton's method for solving the KKT conditions for the problem (P). An alternative way to view the basic idea of SQP is to model (P) at a given approximate solution, say x_k, by a quadratic programming sub problem, and then use the solution to the sub problem to construct a better approximation x_{k+1}. This process is iterated to create a sequence of approximations that, it is hoped, will converge to a solution x^* of (P). It will be attempted to demonstrate that SQP methods can be viewed as the natural extension of Newton methods to constrained optimisation setting, as mentioned above.

In general SQP is not a feasible-point method, i.e., it iterates need not be feasible.

4.7.1. The Basic SQP Method

The Lagrangian function associated with problem (P) by

$$L(x,u,\upsilon) = f(x) + g(x)^T u + h(x)^T \upsilon \tag{4.16}$$

Let $G(x)$ denote the Jacobean of the function corresponding to active constraint (i.e., the rows of $G(x)$ are the (transposed) gradients of all $h_i(x)$'s and active $g_i(x)$'s) for any feasible point x. It will denoted by x^* any particular local solution. We assume that the following conditions hold for any such solution:

A1 The first order necessary conditions are satisfied, A2 $G(x^*)$ has full row rank, A3 Strict complementarity holds at x^*, A4 The Hessian of the Lagrangian function with respect to x is p.d. on the null space of $G(x^*)$.

At a current iteration x_k we seek to (locally) approximate the problem (P) by a quadratic sub problem, an optimisation problem with a quadratic objective function and linear constraints. We thus will construct the sub problem by linearizing the constraints of (P) around x_k:

$$\begin{aligned} \min_{d_x} \quad & (r_k)^T g_x + \frac{1}{2} d_x^T B_k d_x \\ \text{s.t.} \quad & \nabla g(x_k)^T d_x + g(x_k) \le 0, \\ & \nabla h(x_k)^T d_x + h(x_k) = 0 \end{aligned} \tag{4.17}$$

Where $d_x = x - x_k$. It remains to specify the vector and symmetric matrix to form the objective function. The most obvious choice would be the local quadratic approximation to f at x_k. However, the following A1-A4 implies that x^* is local minimiser of the problem $\min_x \{L(x,u^*,\upsilon^*) : g(x) \le 0,\ h(x) = 0\}$. Although the optimal multiplier vector is not known, an approximation (x_k, u_k, υ_k), the quadratic approximation in x for the Lagrangian is

$$L(x_k,u_k,\upsilon_k) + \nabla L((x_k,u_k,\upsilon_k)^T d_x + \frac{1}{2} d_x^T \nabla^2 L(x_k,u_k,\upsilon_k) d_x, \tag{4.18}$$

and we can construct the quadratic sub problem by letting B_k to be an approximation of $\nabla^2 L((x_k, u_k, \upsilon_k)$, and $r_k = \nabla L((x_k, u_k, \upsilon_k)$.

The solution d_x of QP can be used as a search direction for the next iterate x_{k+1}. We also need to update the estimates of the multipliers, which is done as follows: let (u^{QP}, υ^{QP}) be the vector of optimal multipliers for QP. Then we will define the corresponding search directions as $(d_u, d_\upsilon) = (u^{QP} - u_k, \upsilon^{QP} - \upsilon_k)$. We then choose a step-size α and define the next iterate to be $(x_{k+1}, u_{k+1}, \upsilon_{k+1}) = (x_k, u_k, \upsilon_k) + \alpha(d_x, d_u, d\upsilon)$.

4.7.2. SQP Algorithm

Initialisation: given (x_0, u_0, υ_0), B_0, and a merit function ϕ, set *k=0.*

1. Form and solve QP to obtain (d_x, d_u, d_υ).
2. Choose α so that $\phi(x_k + \alpha d_x) \langle \phi(x_k)$
3. Set $(x_{k+1}, u_{k+1}, \upsilon_{k+1}) = (x_k, u_k, \upsilon_k) + \alpha(d_x, d_u, d\upsilon)$.
4. Compute B_{k+1}.
5. Set $k \leftarrow k+1$, go to 1.

4.8. Genetic Algorithm (GA)

4.8.1. Evolutionary Optimisation Algorithms

Evolutionary computation includes several major branches, i.e., evolutionary strategies, evolutionary programming, genetic algorithms (GAs), and genetic programming. At the algorithmic level, they differ mainly in their representations of potential solutions and their operators used to modify the solutions. According Gantovnik (2005) evolution strategies were first proposed by Rechenberg (1964) and Schwefel (1968) as a numerical optimization technique. The original evolution strategy did not use populations. A population was introduced into evolution strategies later (Schwefel, 1981) (Schwefel, 1995). Evolutionary programming was first proposed by Fogel *et al.* in the mid 1960's as one way to solve artificial intelligence problems (1966a) (Fogel, Owens, & Walsh, 1966b). Since the late 1980's evolutionary programming has also been applied to various combinatorial and numerical optimization problems.

The current framework of GAs was first proposed by Holland (1975) and his student Jong (Jong, 1975) in 1975, and was finally popularized by another of his students, Goldberg (1989). It is worth noting that some of the ideas of genetic algorithms appeared as early as 1957 in the context of simulating genetic systems (Fraser, 1957). Genetic algorithms were first proposed as adaptive search algorithms, although they have mostly been used as a global optimization algorithm for combinatorial and numerical problems.

A special branch of genetic algorithms is genetic programming. Genetic programming can be regarded as an application of genetic algorithms to evolve tree- structured chromosomes. The term genetic programming was first used by Koza (1989) (1990).

All evolutionary algorithms have two prominent features that distinguish themselves from other search algorithms. First, they are all population based. Second, there is information exchange among individuals in a population. Such information exchange is the result of selection and recombination in evolutionary algorithms. A general framework for evolutionary algorithms can be summarized by Figure 4.2, where the search operators are also called genetic operators for genetic algorithms. Obviously Figure 4.3 specifies a whole class of algorithms, not any particular one. Different representations of individuals and different schemes for implementing fitness evaluation, selection, and search operators define different algorithms.

1. Set i = 0;
2. Generate the initial generation P(i) at random;
3. REPEAT
    a) Evaluate the fitness of each individual in P(i);
    b) Select parents from P(i) based on their fitness;
    c) Apply search operators to the parents and produce generation P(i + 1);
4. UNTIL the halting criterion is satisfied.

Fig. 4.3. A general framework of evolutionary algorithms.

4.8.2. Detail Genetic Algorithm

Here most of explanations details about genetic algorithm are described by Gantovnick (2005). Genetic algorithms (Holland, 1975) (Goldberg, 1989) (Michalewicz, 1996) emphasize genetic encoding of potential solutions into chromosomes and apply genetic operators to these chromosomes. A canonical genetic algorithm (also called simple or standard GA) (Goldberg, 1989) is the one that uses binary representation, one-point crossover and bit-flipping mutation. A canonical genetic algorithm can be implemented as shown in Figure 4.4.

The GA-based methods can deal with discrete and/or continuous design variables, and are computationally simple. They are not limited by restrictive assumption about the search space. The following GA operators can be adopted: reproduction, crossover, and mutation. GAs work with a coding of the design variable set, they search from a population of designs rather than working with a single design. GAs use function values, and do not need derivatives.

1. Generate the initial population P(0) at random and set i = 0;
2. REPEAT
   a) Evaluate the fitness of each individual in P(i);
   b) Select parents from P(i) based on their fitness as follows:
      Given the fitness of μ individuals as f1, f2, . . . , fμ. Then select individual i with probability

      $$p_i = \frac{f_i}{\sum_{j=1}^{\mu} f_j},$$

      This is called roulette wheel selection or fitness proportional selection.
   c) Apply crossover to selected parents;
   d) Apply mutation to crossed-over new individuals;
   e) Replace parents by the offspring to produce generation P(i + 1);
3. UNTIL the halting criterion is satisfied.

Fig. 4.4. A framework of canonical genetic algorithm.

In a GA the chromosomes contain all of the necessary information about the individuals they represent, which, in the present context, is a structural design. The GA randomly creates an initial population of individuals and then breeds new generations using some selection mechanism.

4.8.3. Representation

Encoding is the first operation in a GA. Each variable is represented using a bit-string. Each bit-string is then merged to form a chromosome that represents a design. From a mathematical point of view, we take this problem and encode the design variables as strings or vectors where each component is a symbol from an alphabet A. The elements of the string corresponds to genes, and the values those genes can take to alleles.

Consider binary representation of continuous design variables. In this case, it is necessary to divide the search interval into a number of intervals determined by a tolerance defined by the designer. Assume that chromosomes have fixed length ℓ. The vector $x \in \prod_{i=1}^{m}\left[(x_i)_{\min,}(x_i)_{\max}\right]$ transforms into the chromosome y = (y1, . . . , ym) $\in B^{\ell}$, where the chromosome is divided into m segments of equal length ℓ_0, such that $\ell = m \times \ell_0$, and each segment $y_i = (y_{i1}, \ldots, y_{i\ell 0}) \in B_{\ell 0}$, i = 1, . . . ,m encodes the corresponding design variable x_i. The decoding of a chromosome is two-step process including decoding the genes into the corresponding integer value between 0 and $2^{\ell 0} - 1$ and then mapping that integer to the real interval $[(x_i)_{min}, (x_i)_{max}]$. The decoding function Γ for the *i*th segment has the following form

$$\Gamma_i(y_{i1},\ldots\ldots,y_{i\ell_0}) = (x_i)_{\min} + \frac{(x_i)_{\max} - (x_i)_{\min}}{2^{\ell_0} - 1}\left(\sum_{k=1}^{\ell_0} y_{i(\ell_0+1-k)} 2^{k-1}\right) \tag{4.19}$$

In such representation only grid points are searched instead of the continuous space, and the solution of nonlinear programming problem is expected to be the grid point with the smallest value of objective function instead of the true global minimum point. The resolution Δ_i between two adjacent grid points with respect to dimension I is determined by the number l_0 of genes for encoding design variable x_i and the design variable range $[(x_i)_{min}, (x_i)_{max}]$ by

$$\Delta_i = \frac{(x_i)_{max} - (x_i)_{min}}{2^{l_0} - 1} \tag{4.20}$$

Therefore, grid density and accuracy of the results can be increased by increasing ℓ_0.

4.8.4. Selection Schemes

A selection scheme determines the probability of an individual being selected for producing offspring by crossover and mutation. In order to search for increasingly better individuals, fitter individuals should have higher probabilities of being selected while unfit individuals should be selected only with small probabilities. Different selection schemes have different methods of calculating selection probability. There are three major types of selection schemes, roulette wheel selection (also known as the fitness proportional selection), rank-based selection, and tournament selection.

Roulette Wheel Selection

Let $f_1, f_2, \ldots, f_\mu$ be fitness values of individuals 1, 2, ...,μ. Then the selection probability for individual i is

$$p_i = \frac{f_i}{\sum_{j=1}^{\mu} f_j} \tag{4.21}$$

Roulette wheel selection calculates the selection probability directly from individual's fitness values. This method may cause problems in some cases. For example, if an initial population contains one or two very fit but not the best individuals and the rest of the population are not good, then these fit individuals will quickly dominate the whole population (due to their very large selection probabilities) and prevent the population from exploring other potentially better individuals. On the other hand, if individuals in a population have very similar fitness values, it will be very difficult for the population to move towards a better one since selection probabilities for fit and unfit individuals are very similar.

Rank-Based Selection

Rank-based selection does not calculate selection probabilities from fitness values directly. It sorts all individuals according to their fitness values first and then computes selection probabilities according to their ranks rather than their fitness values. Hence rank-based selection can maintain a constant selection pressure in the evolutionary search and avoid some of the problems encountered by roulette wheel selection. There are many different rank-based selection schemes. Several are introduced below.

- Assume the best individual in a population ranks first. The probability of selecting individual I can be calculated as follows (Baker, 1985):

$$p_i = \frac{1}{\mu}\left(\eta_{\max} - (\eta_{\max} - \eta_{\min})\frac{i-1}{\mu-1}\right) \tag{4.22}$$

where μ is the population size, $\eta_{max} + \eta_{min} = 2$, η_{max} is the probability of the best individual, η_{min} is the probability for the worst individual. Intermediate individuals' ranks are decreased from η_{max} to η_{min} proportionally to their rank. Setting $\eta_{min} = 0$, the maximum selective pressure is obtained.

- A rank-based selection scheme with a stronger selection pressure is the following nonlinear ranking scheme (Yao, 1993) :

$$p_i = \frac{\mu+1-i}{\sum_{j=1}^{\mu} j} \tag{4.23}$$

- The exponential function has the following form (Michalewicz, 1996)

$$p_i = \frac{\eta(1-\eta)^{i-1}}{c} \tag{4.24}$$

where c is the normalization factor chosen so that the sum of the probabilities is unity. In this case a larger value of η implies stronger selection pressure.

Tournament Selection

Both roulette wheel selection and rank-based selection are based on the global information in the whole population. Tournament selection only needs part of the whole population to calculate an individual's selection probability. The idea of this selection consists in finding a better solution in the tournament. The population is divided into subgroups and the best individual from each group is chosen for the next generation. Subgroups may contain 2 or more individuals.

Elitist Selection

Elitist selection is also known as elitism and elitist strategy. It always copies the best individual to the next generation without any modification. More than one individual may be copied, i.e., the best, second best, etc., may be copied to the next generation without any modification. Elitism is usually used in addition to an accepted selection scheme.

4.8.5. Crossover Operators

The crossover operator is emphasized as the most important search operator of a GA. Crossover in a GA with crossover probability pc selects two parent individuals and recombines them to form two new individuals, i.e., two new designs.

Crossover for integer strings

Common crossover operators for integer strings include k-point crossover, $c'_{(pc,k)}$, $(k \geq 1)$ and uniform crossover, $c'_{(pc)}$.

• k-point crossover. This crossover can be applied to strings of any alphabet. Given two parents of length ℓ, k random numbers, $r_1, r_2, \ldots, r_k$, between 1 and $\ell - 1$ will be generated uniformly without repetition. Then an offspring is produced by taking segments (separated by $r_1, r_2, \ldots, r_k$) of parent strings alternately, i.e., the first segment from the first parent, the second from the second parent, the third from the first parent, and so on.

• uniform crossover. This crossover is also applicable to strings of any alphabet. An offspring is generated by taking each bit or character from the corresponding bit or character in one of the two parents. The parent that the bit or character is to be taken from is chosen uniformly at random.

Crossover for Real-valued Vectors

The blending method (McMahon, Watson, Soremekun, Gurdal, & Haftka, 1998) is used to combine parameter values from the two parents into new parameter values in the offspring in the case of real valued design variables. A single offspring parameter value, c, comes from a combination of the two corresponding parent parameter values, p1 and p2, as follows

$c_1 = \mu + \sigma r$,

$c_2 = \max(c_1, x_{min})$,

$c = \min(c_2, x_{max})$,

where

$$\mu = \frac{p_i + p_2}{2}, \qquad \sigma = \frac{|p_2 - p_1|}{2} \tag{4.25}$$

r is a normally distributed random number with mean zero and unit standard deviation.

4.8.6. Mutation Operators

Mutation operators, $m'_{\{pm\}}$, used for vectors of real values are usually based on certain probability distributions, such as uniform, Gaussian (normal), and Cauchy distributions. Mutation for integer strings is usually a bit-flipping operation. Mutation is needed because it allows new genetic patterns to be formed improving the search method. The mutation probability pm ∈ [0, 1] per bit is usually very small. The common setting is pm = 0.001.

Mutation for Integer Strings

- Bit-Flipping. Bit-flipping mutation simply flips a bit from 0 to 1 or from 1 to 0 with a certain probability. This probability is called the mutation probability or mutation rate. Bit-flipping mutation can be generalized to mutate strings of any alphabet. The generalized mutation works as follows: for each character in a string, replace it with another randomly chosen character (not the same as the one to be replaced) in the alphabet with certain mutation probability.

- Random Bit. This mutation does not flip a bit. It replaces a bit by 0 or 1 with equal probability, i.e., 0.5, respectively. The generalized version of this mutation works as follows: for each character in a string, replace it with a randomly chosen character (could be the same as the one to be replaced) in the alphabet with a certain mutation probability.

4.8.7. Constraint Handling

GA is suited for unconstrained optimization problems. The main problem in applying evolutionary algorithms to solving a constrained problem is how to deal with constraints because evolutionary operators used for manipulating chromosomes may yield infeasible solutions. Extensive overviews of the different constraint handling techniques available are given by (Michalewicz, 1996) and (Coello, 2002).

A penalty function strategy is based on the strategies developed for conventional optimization methods in which solutions that are out of the feasible domain are penalized using a penalty coefficient. In other words a constrained optimization problem is transformed to an unconstrained optimization problem.

In this Gantovnik's (2005) study the method implemented is based on the approach used by Powell and Skolnick (1993) and recently modified by Deb (2000). This method is called the method of superiority of feasible points. The fitness function $\phi(s)$ has the following form

$$\phi(\mathbf{s}) = \begin{cases} \mathbf{f}(\mathbf{s}), & \text{if s is feasible,} \\ \mathbf{f}_{\max} + \sum_{j=1}^{q} c_j(s), & \text{otherwise,} \end{cases} \tag{4.26}$$

where f_{max} is the function value of the worst known feasible solution, the function c_j measures the violation of the j-th constraint as follows

$$c_j(s) = \max\{0, g_j(s)\}, \quad 1 \leq j \leq q \tag{4.27}$$

There is no need for penalty coefficients here because the feasible solutions are always evaluated to be better than infeasible solutions, and infeasible solutions are compared purely based on their constraint violations. The constraints gj should be normalized.

It is possible to obtain several solutions that will have the same value of the objective function and will satisfy all the constraints. In this situation, the weighted average ranking method is used to obtain the best solution from a set of candidate solutions (Collette & Siarry, 2003). This method is frequently used in multi-objective optimisation, and it is based on the algorithm shown in Figure 2.3. The design with smallest rank can be selected as the best optimal solution.

4.8.8. Convergence Criteria

Three convergence criteria are used in this work. If just one of them is reached, then the optimization process terminates. These criteria are

1. s is a solution to compare;
2. A is a set of solutions, which have best objective function and satisfy all constraints g_j (A does not contain s);
3. j = 1;
4. REPEAT
   a) Compare s with A with respect to the g_j ;
   b) N_j=number of solutions from A better than s with respect
   c) to the g_j ;
   d) j=j+1;
5. UNTIL j > q
6. The rank assigned to s is $N = \sum_{j=1}^{q} N_j$,

Fig. 4.5. Weighted average ranking.

1. when the percentage difference between the average value of all the designs and the best design in a population reaches a very small specified value c1,

$$\frac{|f_a - f^*|}{|f_a|}\times 100 \leq c_1, \tag{4.28}$$

where f^* is the fittest design in a population, f_a is the average objective value in a generation defined by

$$f_a = \frac{1}{\mu}\sum_{j=1}^{\mu} f_j \tag{4.29}$$

and μ is the population size,

2. if the fittest design has not changed for 50 successive generations, or the difference of the fittest design of the current generation, f_c^* , and that of 50 generations before, f_b^* , is less than a small amount c_2, i.e.,

$$\frac{|f_c^* - f_b^*|}{|f_c^*|}\times 100 \leq c_2, \tag{4.30}$$

3. if the total number of generations is reached.

4.9. Simulated Annealing (SA)

Simulated annealing is a probabilistic method proposed in Kirkpatrick, Gelett and Vecchi (1983) and Cerny (Cerny, 1985) for finding the global minimum of a cost function (Bertsimas & Tsitsiklis, 1993). SA is the most common method after genetic algorithms for stacking sequence optimisation of laminated composite materials (Lombardi, Haftka, & Cinquini, 1992) (Sargent, Ige, & Ball, 1995) (Sadagopan & Pitchumani, 1998) (Bakis & Arvin, 2006).

The SA is a powerful optimisation method. It actually mimics the behaviour of this dynamical system to achieve the thermal equilibrium at a given temperature. The SA process consist of first "melting" the system being optimised at a high temperature, and then lowering the temperature by very slow stages until the system "freezes" and no further change occurs. The annealing must proceed long enough for the system to reach a steady state (Erdal & Sonmez, 2005). It has the distinguishing ability of escaping from the local minimum by a accepting or rejecting new solution candidates according to a probability function. The SA method only requires little computation resource. The flow chart of a basic SA method is described in Fig. 4.6. It can be showed by the following steps (Wang, Gao, & Ovaska):

1. Specify initial temperature T_0, and initialise the candidate.
2. Evaluate fitness E of the candidate.
3. Move the candidate randomly to a neighbouring solution.
4. Evaluate the fitness of new solutions E.
5. Accept the new solution, if $E \leq E$ or $E > E$ with accepting probability P.
6. Decrease temperature T. The SA search is terminated, if the temperature is close to zero.

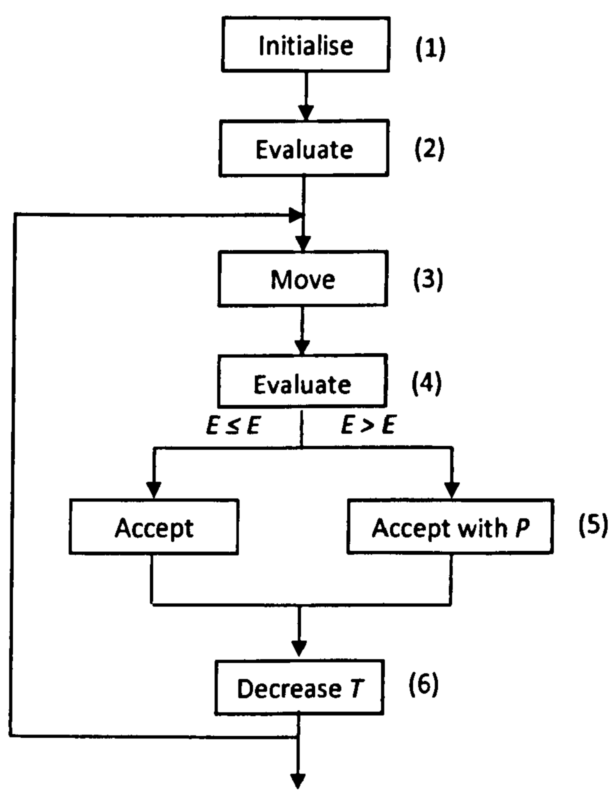

Fig. 4.6. Flow chart of basic SA method (Wang, Gao, & Ovaska).

As we can see that the SA algorithm simulates the procedure of gradually cooling a metal until the energy of the system archives the global minimum. Each configuration of the physical system and energy of the atoms correspond to the current solution to the optimisation problem and fitness of the objective function, respectively, and the temperature is used to control the whole optimisation procedure. At every generation, according to the Metropolis criterion (Wang, Gao, & Ovaska) (de Castro & von Zuben, 1999) the candidate is updated through the random perturbation, and the improvement of its fitness is calculated. If $E \leq E$, the moving change result in a lower or equivalent energy of the system, and the new solution is accepted.

Otherwise, the displacement is only accepted with a probability *P*:

$$P = e^{\frac{-(E'-E)}{T}}. \tag{4.31}$$

The temperature is updated by:

$$T(k+1) = \lambda T(k), \quad 0 < \lambda < 1, \tag{4.32}$$

where *k* is the number of generations. In fact, the cooling schedule can be adjusted by modifying parameter λ.

The SA is terminated when the final temperature is sufficiently low, which makes is reach the global optimal solution with a high probability. The probability-dependent acceptance policy for the new solutions helps the SA algorithm in the solution exploitation. The temperature plays an important role in the cooling procedure control. The initial temperature should be high enough to explore the whole solution space (Wang, Gao, & Ovaska) (Simopoulos, Kavatza, & Vournas, 2006).

4.10. Summary

In this chapter first of all different optimisation techniques applicable to FRP composite design were discussed. The fundamental mathematical optimisation methodologies that will be used in the remaining chapters are presented.

In order to assess the performance of every search technique, four optimisation methods, i.e. enumeration search (also called exhaustive method), sequential quadratic programming (SQP), genetic algorithm (GA) and simulated annealing (SA) methods have been selected for further works reported in Chapters 5 & 6. In these chapters, the performances of these methods were evaluated by solving some cases studies.

Enumeration is one of optimisation method that accurately finds the optimal solution although in some cases the solution is time consuming as it checks all of possible domain.

Sequential quadratic programming is a method of optimisation that demonstrates the natural extension of Newton methods to constrained optimisation setting for nonlinear objective function.

Genetic algorithm is searching for a global optimum solution and it mimics an evolution process. It is population based and there is information exchange among individuals in a population. Such information exchange is the result of selection and recombination in evolutionary algorithms.

The last optimisation method is simulated annealing (SA). Global optimisation adapt metal process of annealing to get the optimum solution.

4.11. References

Arora, J. S. (2012). *Introduction to optimum design* (3rd ed.). Waltham, USA: Academic Press.

Aymerich, F., & Serra, M. (2008). Optimization of laminate stacking sequence for maximum buckling load using the ant colony optimization (ACO) metaheuristic. *Compos A: Appl Sci Manuf, 39*(2), 262-272.

Bakis, C. E., & Arvin, A. C. (2006). Optimal design of press-fitted filament wound composite flywheel rotors. *Compos Struct, 72*(1), 47-57.

Bertsimas , D., & Tsitsiklis, J. (1993). Simulated Annealing. *Statistical Science, 8*, 10-15.

Boggs, P. T. (1995). Sequential quadratic programming. In M. A. Epelman, *IOE 511/Math 652: Continous optimisation methos, section 1.* Acta Numerica.

Boggs, P. T., & Tolle, J. W. (1996). Sequential quadratic programming. *Acta Numerica*, 1-52.

Cerny, V. (1985). A thermodynamic approach to the traveling salesman problem: An efficient simulation. *J. Optim. Theory Appl., 45*, 41-51.

Coello, C. A. (2002). Theoritical and numerical constraint-handling techniques used with evolutionay algorithms: a survey of the state of the art. *Comput. Methods Appl. Mech. Engrg, 191*, 1245-1287.

Collette, Y., & Siarry, P. (2003). *Multiobjective optimization.* Berlin Heidelberg: Springer.

Conti, M., Orcioni, S., & Turchetti, C. (1994). Parametric yield optimization of MOS VLSI circuit based on simulated annealing and its practical implementation. *IEEE Proceedings, Circuits, Devises and Systems, 141*, pp. 387-398.

de Castro, L. N., & von Zuben, F. J. (1999). *Artificial immune systems: Part I-Basic theory and applications, Technical Report RT-DCA 01/99.* Brazil: FEEC/UNICAMP.

Deb, K. (2000). An efficient constraint handling method for genetic algorithms. *Computer Methos in Applied Mechanics and Engineering, 186*, 311-338.

Erdal, O., & Sonmez, F. O. (2005). Optimum design of composite laminates for maximum buckling load capacity using simulated annealing. *Compos Struct, 71*(1), 45-52.

Fogel, L. J., Owens, A. J., & Walsh, M. J. (1966a). *Adaptation of evolutionary programming to the prediction of solar flares.* San Diego, CA: Report NASA-CR-417, General Dynamics-Convair.

Fogel, L. J., Owens, A. J., & Walsh, M. J. (1966b). *Artificial intellegence through simulated evolution.* New York: John Wiley & Sons.

Fraser, A. S. (1957). Simulation of genetic systems by automatic digital computers, I. Introduction. *Australian Journal of Biological Sciences, 10*, 484-491.

Gantovnik, V. B. (2005). *An improved genetic algorithm for the optimization of composite structures.* Virginia: Dissertation, Virginia Polytechnic Institute and State University.

Ghiasi, H., Pasini, D., & Lessard, L. (2009). Optimum stacking sequence design of composite materials Part I: Constant stiffness design. *Composite Structure, 90*, 1-11.

Goldberg, D. E. (1989). *Genetic algorithms in search, optimization, and machine learning.* Reading, MA: Addison-Wesley.

Gurdal, Z., Haftka, R. T., & Hajela, P. (1999). *Design and optimization of laminated composite materials.* Canada: A Wiley-Interscience Publication, John Wiley & Sons, Inc.

Holland, J. H. (1975). *Adaptation in natural and artificial systems.* Ann Arbor, MI: The University of Michigan Press.

Jong, K. A. (1975). *An analysis of the behavior of a class of genetic adaptive systems.* Ann Arbor, MI: Department of Computer and Communication Sciences.

Kere, P., & Koskli, J. (2002). Multicriterion optimization of composite laminates for maximum failure margins with an interactive descent algorithm. *Struct Multidisc Optim, 23*, 436-447.

Kere, P., Lyly, M., & Koski, J. (2003). Using multicriterion optimization for strrength design of composite laminates. *Compos Struct, 62*, 329-333.

Kim, T. U., & Sin, H. C. (2001). Optimal design of composite laminated plates with the discreteness in ply angles and uncertainty in material properties considered. *Comput Struct, 79*(29-30), 2501-2509.

Kirkpatrick, S., Gelett, C. D., & Vecchi, M. P. (1983). Optimization by simulated annealing. *Science, 220*(4598), 621-630.

Koza, J. R. (1989). Evolving programs using symbolic expressions. *Proc. of the 11th Int'l Joint Conf. on Artificial Intelligence* (pp. 768-774). San Mateo, CA: Morgan Kaufmann.

Koza, J. R. (1990). *Genetic algorithm: a paradigm for genetically breeding populations of computer programs to solve problems.* Stanford: Tech. Rep. STAN-CS-90-1314, Depart. of Computer Science, Stanford Uni.

Lombardi, M., Haftka, R. T., & Cinquini, C. (1992). Optimization of composite plates for buckling using simulated annealing. *AIAA/ASME/ASCE/AHS/ASC 33rd structures, structural dynamics and materials conference, Part 5*, (pp. 2552-2563). Dallas, Texas.

McMahon, M. T., Watson, L. T., Soremekun, G. A., Gurdal, Z., & Haftka, R. T. (1998). A Fortran 90 genetic algorithm modul for composite laminate structure design. *Engineering with Computers, 14*(3), 260-273.

Michalewicz, Z. (1996). *Genetic algorithms + data structures.* Berlin, Germany: Springer-Verlag.

Miki, M. (1982). Material design of composite laminates with required in-plane elastic properties In: Hayashi, T; Kawata, K; & Umekawa, S; editors. *ICCM-IV*, (pp. 1725-1731). Tokyo.

Pai, N., Kawa, A., & Weng, M. (2003). Optimization of laminate stacking seqeunce for failure load maximization using Tabu search. *Compos B: Eng, 34*(4), 405-413.

Park, W. J. (1982). An optimal design of simple symmetric laminates under the first py failure criterion. *J Compos Mater, 16*, 341-355.

Powell, D., & Skolnick, M. M. (1993). Using genetic algorithms in engineering design optimization with non-linear constraints. In S. Forrest (editor), *Proceedings of the Fifth International Conference on Genetic Algorithms* (pp. 424-430). San Mateo, CA: Morgan Kaufmann.

Rechenberg, I. (1964). Cybernatic solution path of an experimental problem. *The joint annual meeting of the WGLR & DGRR.* Berlin: Royal Aircraft Establishment, Library Translation 1122.

Sadagopan, D., & Pitchumani, R. (1998). Application of genetic algorithms to the optimal tailoring of composite materials. *Compos Sci Technol, 58*, 571-589.

Sargent, P. M., Ige, D. O., & Ball, R. N. (1995). Design of laminate composite layups using genetic algorithms. *Eng Comput, 11*(2), 59-69.

Schmit, L. A., & Fleury, C. (1980). Structural synthesis by combining approximation concepts and dual methods. *AIAAJ, 18*(10), 1252-1260.

Schwefel, H. P. (1968). *Experimentelle optimierung einer zweiphasenduse teil I.* Berlin: Report 35 for the project MHD-Strasrahlrohr, AEG Research Institure.

Schwefel, H. P. (1981). *Numerical optimization of computer models.* Chishester: John Wiley & Sons.

Schwefel, H. P. (1995). *Evolution and optimum seeking.* New York: John Wiley & Sons.

Setoodeh, S., Abdalla , M. M., & Gurdal, Z. (2006). Design of variable - stiffness laminates using lamination parameters. *Compos B: Eng, 37*, 301-309.

Simopoulos, D., Kavatza, S., & Vournas, C. (2006). Unit commitment by un enhanced simulated annealing algorithm. *IEEE Transactions on Power Systems, 21*(1), 68-76.

Soares, C. M., Franco, C. V., Mateus, H., & Herskovits, J. A. (1995). Optimization of laminated composite structures using a bilevel strategy. *Compos Struct*, 147-157.

Tsai, S. W. (1992). *Theory of composite design.* Dayton, OH: Think composite.

Venkataraman, P. (2009). *Applied optimization with MATLAB programming* (2nd ed.). Canada: John Wiley & Sons.

Venkataraman, S., & Haftka, R. T. (1999). Optimization of composite panels - a review. *14th Annual technical conference of the American society of composites.* Dayton, OH.

Verette, R. M. (1970). *Stiffness, strength and stability optimization of laminated composites.* Hawthorne, California: NOR-70-138, Northrop Aircraft Co.

Waddoups, M. E. (1969). *Structural airframe application of advanced composite materials - analytical methods.* Ohio: AFML-TR-69-101, vol. VI Air Force Materials Laboratory, Wright-Patterson Air Force Base.

Wang, X., Gao, X. Z., & Ovaska, S. J. (n.d.). A simulated annealing-based immune optimization method. *Anonim.*

Weaver, P. M. (2002). Designing composite structures: Lay-up selection, In: Proceedings of The Institution of Mechanical Engineers-part G. *J Aerospace Eng, 216*, 105-116.

Zaritsky, A. (2014). *Introduction to genetic algorithms.* Retrieved from www.cs.bgu.ac.il/~assafza

Chapter 5

Optimisation of Stacking Sequence of Laminated Composite Plates Subjected to Buckling using Enumeration Search Method

5.1. Introduction

Laminated fibre reinforced plastic (FRP) composite materials have many applications in thin-walled structures such as an airplane fuselage. In aerospace structural applications, a high strength to weight ratio are required. It is crucial when designing these types of structures against buckling under compressive loading to keep the weight of the structure to a minimum. Under compressive loading, structures are susceptible to buckling and as a result, the structure could fail in its functionality.

Enumeration search is one of the methods in optimum design of laminated composite materials that try all possible combinations of design variables and simply select the best combination. Although cumbersome, this technique was used to find the lightest composite laminate during the 1970s (Waddoups, 1969) (Verette, 1970). This technique will be applied in this chapter.

White & Weaver (2012) investigated shells structure in which both the bending moments and the changes in curvature have been suppressed under uniform pressure with variable-angle tow derived anisotropy. They used analytical enumeration search method (exhaustive method) with variation of angle from 0 to 90 degree around a quartercircumference. They found that if membrane hypothesis could be applied, a totally bend-free can be designed by attractive to material constitutive equation. Legland & Beaugrand (2013) used exhaustive method to determine formal definition of the geodesic diameter of natural fibre for characteristic of morphometric features and particle clustering. Park (1982) plotted the change of the optimum fibre angle for a particular class of laminates under all possible normalised loading conditions. Weaver (2002) reported selection charts as well, in which each class of laminates was displayed within an elliptical contour. These charts can be used to identify a small subset of potential laminates that might be investigated in more details.

Many more application of enumeration search exist in other field such as computer (Todman, Fu, Tsaoi, Mencer, & Luk) (Nievergelt, 2000) and electronic rewiring (Chang, Markov, & Bertacco, 2007).

5.2. Eigen Buckling for Laminated Plate

We consider a membrane prebuckled state. The differential equations governing the buckling from it are (Al Humdany & Hussein, 2012) (Sun, 2009) (Kamruzzaman, Naqvi, Umar , & Siddiqui, April 2005):

$$\begin{aligned}
&\delta N_{x,x} + \delta N_{xy,y} = 0 \\
&\delta N_{xy,x} + \delta N_{y,y} = 0 \\
&\delta M_{x,xx} + 2\delta M_{xy,xy} + \delta M_{y,yy} + N_x \delta w_{,xx} + 2N_{xy}\delta w_{,xy} + N_y \delta w_{,yy} = 0
\end{aligned} \tag{5.1}$$

where δN_x..............δM_x are variations of forces and moment respectively then the term $\delta w, \delta u$ and δv are variations in displacement. Since prebuckling deformations are assumed to be a membrane state (Sun, 2009), the boundary conditions for buckling problem are applied only to the buckling deformations. By substituting variations in external strains and curvature, the buckling differential equations can be expressed.

5.2.1 Finite Element Eigen Solution

In this study, from the FEA results the stresses and failure buckling modes will be obtained using ANSYS software. The linear buckling analysis in ANSYS finite elements software is performed in two steps. In the first step, a static analysis of the structure is performed to determine the prebuckling stress state in the structure. The second step the Eigen value problem given in the Eq. (5.2) is solved. This equation takes into consideration the prebuckling stress effect matrix [S] calculated in the first step.

$$([K] + \lambda_i[S])\{\psi_i\} = \{0\} \tag{5.2}$$

Where [K] is stiffness matrix, [S] is initial stress matrix, λ_i is the i^{th} eigen value (used to multiply the loads which generated [S] and $\{\psi_i\}$ is the i^{th} eigenvector of displacements. The 'Block Lanczos' method in ANSYS was used to extract the eigen values resulting from Eq. (5.2). The eigen values obtained from the buckling analysis are factors by which the initially applied unit force is multiplied. As a result, the critical buckling load is calculated according to equation (5.3) below.

$$P_{cr} = \lambda_{min} PA \tag{5.3}$$

Where λ_{min} is the minimum eigen value, A is the total area on which force is applied, P is the initially applied load. By applying a unit load (P =1) in Eq. (5.3) the critical buckling load will be as follow

$$P_{cr} = \lambda_{min} A \tag{5.4}$$

<u>**Case studies for verification of FEA**</u>

The first case study is an FEA eigen buckling analysis of a laminated FRP plate under uniaxial loading. Eigen buckling analysis predicts the theoretical critical buckling load of a structure that is idealised as elastic. The structural eigenvalues are computed from constraints and loading conditions. The critical buckling loads are then derived, each associated with a buckled mode shape that represents the shape of the structure under buckling. However, in a real structure, imperfections and geometric and nonlinear material behaviour hinder the structure from achieving this theoretical buckling strength, leading eigen buckling analysis to over-predict buckling load.

The effects of various parameters of the angle of plies, the aspect ratio of length of the plate to the width (a/b) and the ratio of the length to the laminate thickness (a/t) on the critical buckling load using FEA eigen buckling analysis for antisymmetric[1] for a ±45° laminate were studied. FEA is carried out using ANSYS software 14.0, the elements are 8-node SHELL281 (see Figure 5.1). SHELL281 is suitable for analysing thin to moderately thick shell structures. This element has eight nodes. It has six degrees of freedom at each node: translations in the x, y, and z-axes, and rotations about the x, y, and z-axes. By defining the same node number for nodes K, L, and O, a triangular-shaped element may be formed (www.sharcnet.ca).

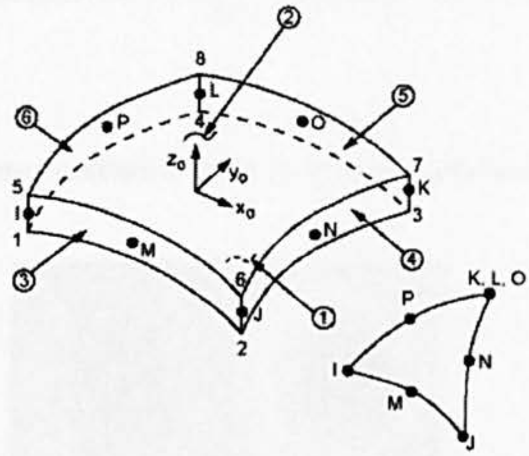

Fig. 5.1. SHELL281 geometry element structure (2011)

The boundary conditions of the laminated plate are SSSS (simply supported on all edges) and the material properties are $E_1 = 36\,\text{GPa}$, $E_2 = E_3 = 13\,\text{GPa}$, $\nu_{12} = \nu_{13} = 0.22$, $\nu_{23} = 0.25$, $G_{12} = G_{13} = 4.3\,\text{GPa}$, $G_{23} = 5.2\,\text{GPa}$. The length of plate, a is 150 mm, the width, b is 80 mm and the thickness of ply, t_{ply}, is 0.288 mm. The boundary conditions of SSSS the laminated plate is described in Figure 5.2. The first mode shape of the plate is shown in Figure 5.3.

The results of FEA eigen buckling for the first mode shape, N_{cr} versus ply angle, N_{cr} versus plate aspect ratio a/b and finally N_{cr} versus length to thickness aspect ratio are respectively presented in Figure 5.3-5.5. The results shown in Figures 5.4-5.5 are in accordance with the results published by Al-Humdany and Hussein (2012) and

[1] In antisymmetric laminate, all plies above the mid-plane have the opposite (negative) angle as the ply in the equivalent position below the mid-plane.

(Kamruzzaman, Naqvi, Umar , & Siddiqui, April 2005). Hence, the validity of the FEA method used for determining of critical buckling load is verified.

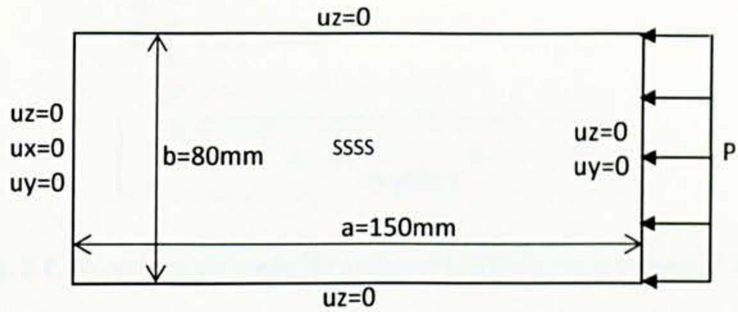

Fig. 5.2. Boundary conditions of SSSS for the representative laminated plate

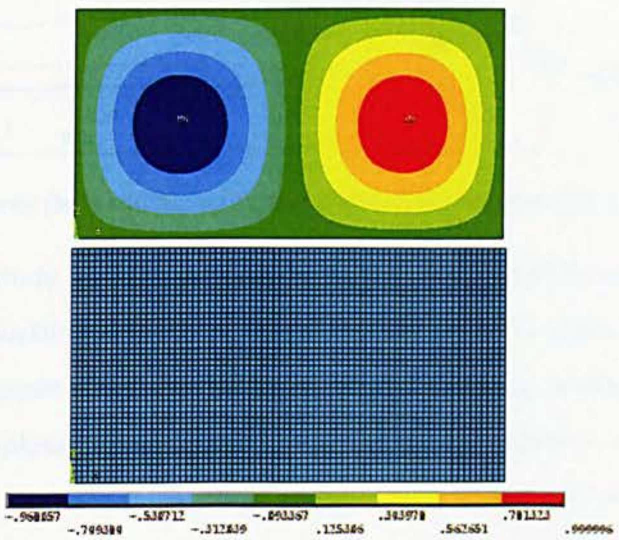

Fig. 5.3. The first mode shape of ±45 antisymmetric laminated plate with number of layers are 10, $m = 2, n = 1$, top view (left) and side view (right). The contour indicates ratio of w/w_{max}.

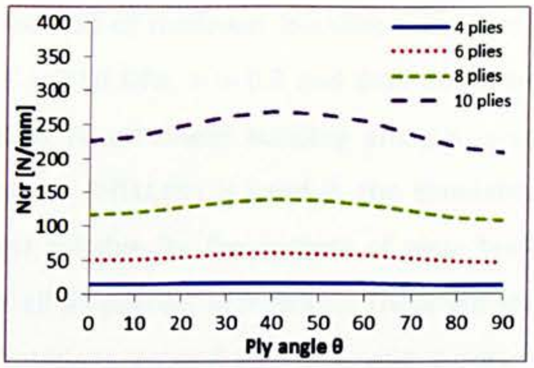

Fig. 5.4. N_{cr} **versus ply angle for antisymmetric stacking sequence ±45°.**

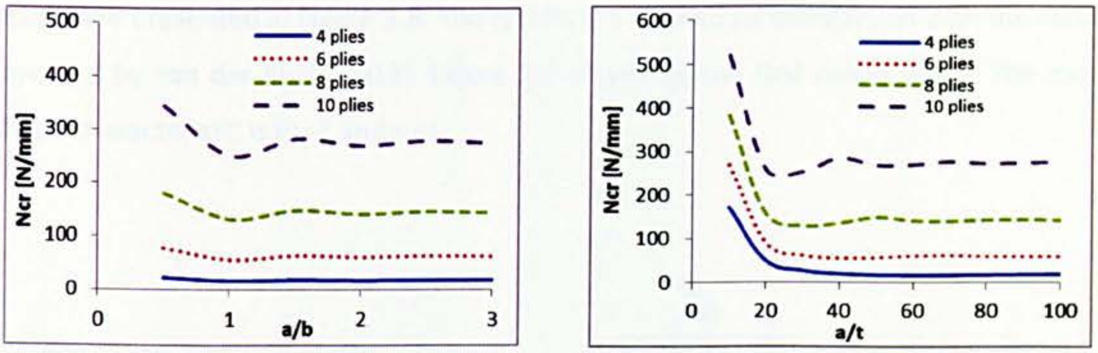

Fig. 5.5. N_{cr}-a/b **curve (left) and** N_{cr}-a/t **curve (right) for antisymmetric ±45° stacking sequence.**

The second case study for FEA verification is nonlinear buckling analysis of an isotropic plate. Nonlinear buckling analysis provides greater accuracy than elastic eigen buckling analysis. Load is applied incrementally until a small change in load level causes a large change in out-of-plane displacement. This condition indicates that a structure has become unstable. Nonlinear buckling analysis is a static method that accounts for material and geometric nonlinearities, load perturbations, geometric imperfections, and gaps. For initiating the buckling either a small destabilising load or an initial perturbation is necessary to initiate the solution of a desired buckling mode. In this case study initially an eigen buckling analysis has been solved and then all nodes of the plate has been updated with first mode-shape by a magnitude of $e=b/200$ (hence in this case e=5mm) before nonlinear analysis performed. This value of e has been found by nonlinear FE analysis as shown in Figure 5.8 as recommended by Eurocode (NEN-EN 1993-1-5 (en), 2006).

For verification of the method of nonlinear buckling behaviour, an isotropic plate with material properties of $E = 210$ GPa, $\nu = 0.3$ and SSSS boundary condition as shown in Figure 5.7 was studied. A FE nonlinear buckling analysis is carried out using ANSYS software. The shell element SHELL181 is used in the simulation (see Figure 5.6). This element type is the most suitable for the analysis of plate buckling. It has four nodes, each nodes is capable of all six degrees of freedom. These are six displacements, three in x, y, and z-axes, and rotations around the x, y, and z-axes. The nonlinear buckling behaviour of the plate was obtained by plotting load versus out-of-plane displacement. The sensitivity of the analysis to the perturbation magnitude e is investigated and the results are presented in Figure 5.8. The results are verified by comparison with the results reported by van der Burg (2011). Figure 5.9 illustrates the first mode shape. The mode shape characteristic is m=2 and n=1.

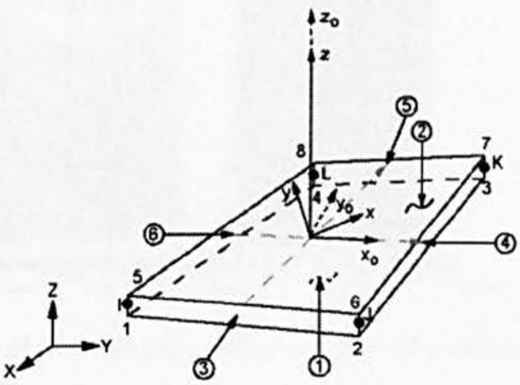

Fig. 5.6. SHELL181 geometri element structure (www.sharcnet.ca)

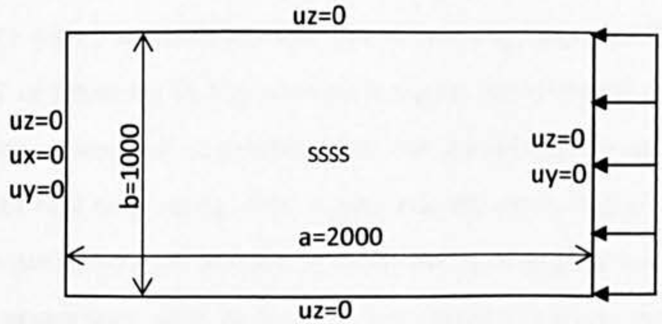

Fig. 5.7. Boundary condition of unstiffened plate field with the thickness 20mm.

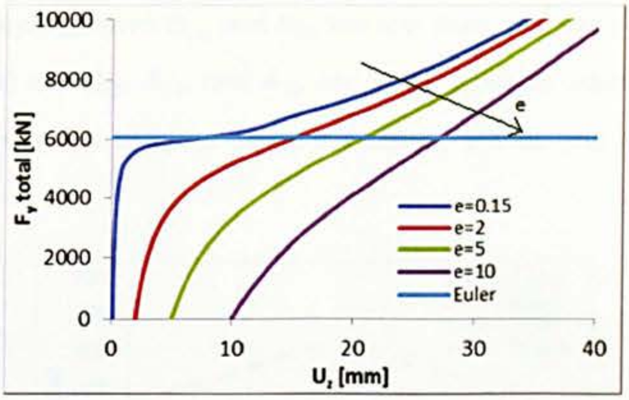

Fig. 5.8. Effect of initial perturbation magnitude on nonlinear elastic plate buckling behaviour for an isotropic plate.

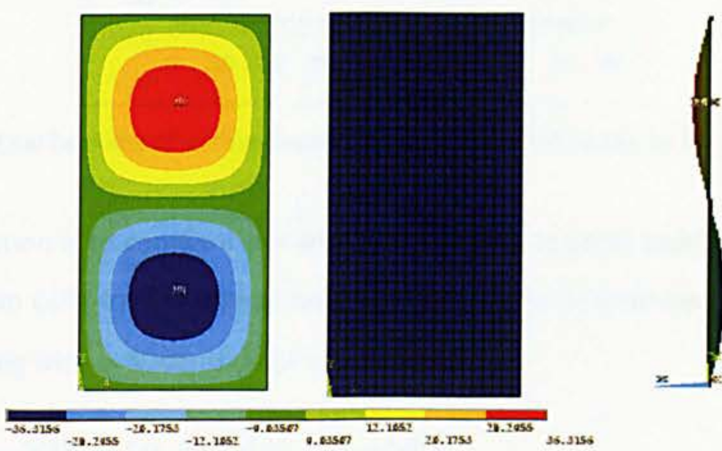

Fig. 5.9. First mode shape of isotropic plate with $e = 5$ mm. The contour indicates out of plane displacement value.

Case studies for verification of analytical solution CLPT

In order to validate with the above antisymmetric stacking sequence critical buckling load, an analytical CLPT of Equation (2.11) was carried out. The material properties, boundary condition, and dimension are according to those presented in the above FEA eigen buckling analysis of first case study. The results are shown in Figure 5.10. In addition, the first mode shape parameter of number of half wave, *m* equals two and *n* equals one therefore it is in agreement with Figure 5.3. The results indicate those critical buckling loads are the similar with Figure 5.4. They are in accordance with the results published by Al-Humdany and Hussein (2012) and (Kamruzzaman, Naqvi, Umar , & Siddiqui, April 2005). It is also in accordance with the statement of Kassapoglou (2010) that if the bending-twisting coupling terms D_{16} and D_{26} are less than 15% than the next larger term (such as in this case) and B_{ij}, A_{16}, and A_{26} are to be assumed equal to zero, it can use that von Karman equation in order to give accurate trends and reasonable buckling predictions.

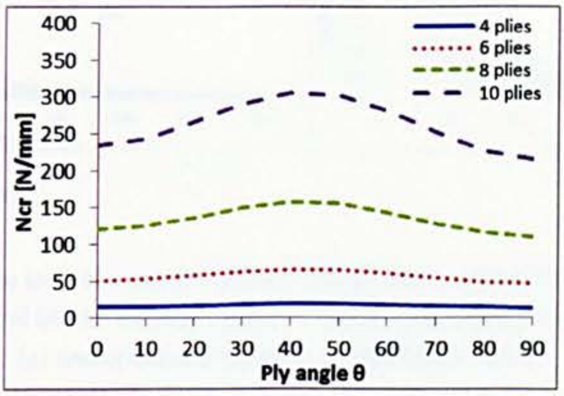

Fig. 5.10. Critical buckling of antisymmetric stacking sequence based on Equation (2.11).

The final verification is to compare the analytical solution to other published results. The analytical solution CLPT for the critical buckling load N_c for a laminated plate subjected to a biaxial loading with $k=N_y/N_x$ and $N_x=-N_c$ is equal to:

$$N_c = \frac{\pi^2\left[D_{11}m^4 + 2(D_{12}+2D_{66})m^2n^2R^2 + D_{22}n^4R^4\right]}{a^2(m^2+kn^2R^2)} \tag{5.5}$$

where N_x and N_y are the axial compressive loads in the x and the y direction, respectively. The critical buckling load with the materials properties reported in Chapter 3 are compared to the published results for a square plate with quasi-isotropic layup $[\pm45_2/0_2/90_2]_s$ with material properties E_1=137.9GPa, E_2=11.7GPa, ν_{12}=0.31, G_{12}=4.82GPa and t_{ply}=0.1524mm (Kassapoglou, 2010). The problem is to determine the critical buckling load N_C for several values of k whilst the boundary condition is SSSS. The results are shown in Figure 5.11. The trends of the results are in accordance with the published results by Kassapoglou (2010).

In summary eigen buckling, nonlinear buckling, and analytical methodology have been verified. These solution strategies will be employed in the various buckling optimisation methods in the remaining part of this chapter.

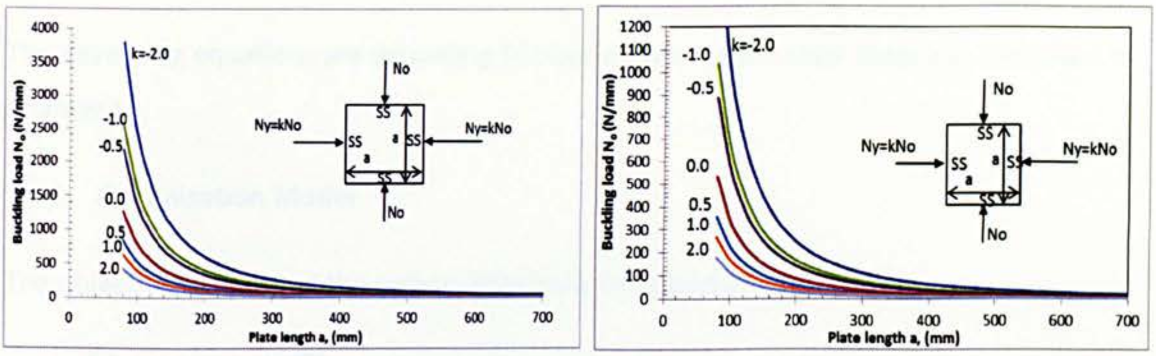

(a) (b)

Fig. 5.11. Critical buckling load of a square quasi-isotropic plate with SSSS boundary condition as a function of plane size and biaxial loading ratio $k = N_y/N_x$ (materials properties from Chapter 3): (a) analytical and (b) after Kassapoglou (2010).

5.3. Optimisation Problem Formulation

A CSCS boundary condition of glass fibre composite plate with the dimensions of 150mm long, 80mm wide and the buckling target load equals to 200 N/mm is to be designed. The properties of material are the same as described in Chapter 3 and the aim is to determine the lightest laminates. In case 1, a symmetric and balanced laminate for design of a non-crimp fabric is sought that consist of the following options:

- Option (0) = [0/0]
- Option (1) = [90/90]
- Option (2) = [0/90]
- Option (3) = [90/0]
- Option (4) = [45/-45]

In case 2, the optimisation is to find the lightest symmetric laminate made from unidirectional lamina. The unidirectional (UD) fibre orientation options are 0, 90, 45, and -45 layers.

5.4. Solution

The governing equations are according to classical lamination plate theory as explained in Chapter2.

5.4.1. Optimisation Model

The objective function of the optimisation may be stated as

$$\min \sum \text{weight} = \min \sum \text{number of plies} \tag{5.6}$$

Subject to

$$\frac{N_c}{N_t} \geq 1 \tag{5.7}$$

where N_c is critical buckling load and N_t is the target compressive load.

In this thesis, one out of four optimisation methods, enumeration search (ESM) is applied. It consisted of all possible combinations of design variables and finally simply selecting the best combination.

In order to arrange all possible combinations, a new combination programming code in MATLAB has been developed. The developed combination programming generates all possible stacking sequences for laminates. Details of ESM programming is described in the flow chart shown in Figure 5.12.

5.5. Validation

Buckling tests have been done for some of validation between modelling and experiment (see Chapter 3).

5.5.1. Result and Discussion

The result of optimisation and FEA eigen buckling are illustrated in Table 5.1-5.7, and Figure 5.13 - 5.21. The Eigen solution used element of shell 281.

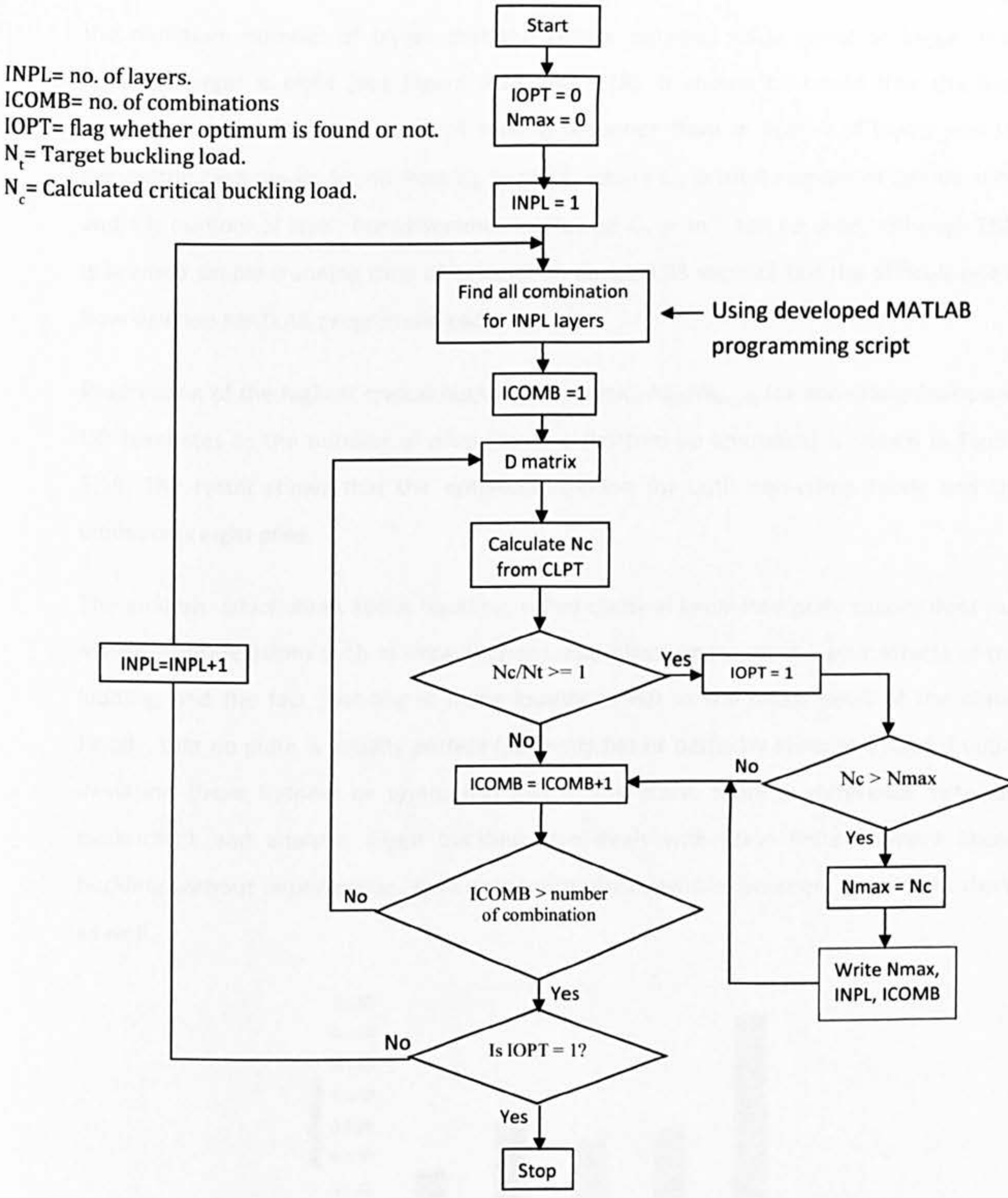

Fig. 5.12. Flow chart of developed ESM optimisation programming.

The ESM optimisation is used to determine the stacking sequence, fibre orientation for the minimum number of layers. All possible answers are shown in Table 5.1- 5.7, although the minimum number of layers that the critical buckling value equal or bigger than buckling target is eight (see Figure 5.14 and 5.18). It should be noted that the total number of possible combination of staking sequence from *m* option of layers and for symmetric case can be found from $C_n = m^{n/2}$ where C_n is total number of combination and *n* is number of layer. For unsymmetrical lay-up $C_n = m^n$ can be used. Although ESM is seemed simple (running time of calculation about 0.08 second) but the difficult one is how develop MATLAB programme code.

Progression of the highest critical buckling load ratio, N_{crit}/N_{target} for non-crimp fabric and UD laminates as the number of plies increase (bottom-up approach) is shown in Figure 5.19. The result shows that the optimum solution for both non-crimp fabric and UD laminate is eight plies.

The analysis, which deals about buckling, called classical laminated plate theory does not involve considerations such as imperfections, non-elastic material, dynamic effects of the loading, and the fact that the in plane loading is not in the initial point of the plate. Finally, that no plate is initially perfect (perfectly flat or perfectly symmetry) and if initial deviation (from flatness or symmetry) exists. Therefore, there is difference between experiment and analytic. Eigen buckling also deals with ideal finite element about buckling without imperfection. Hence, the differences with experiment results are there as well.

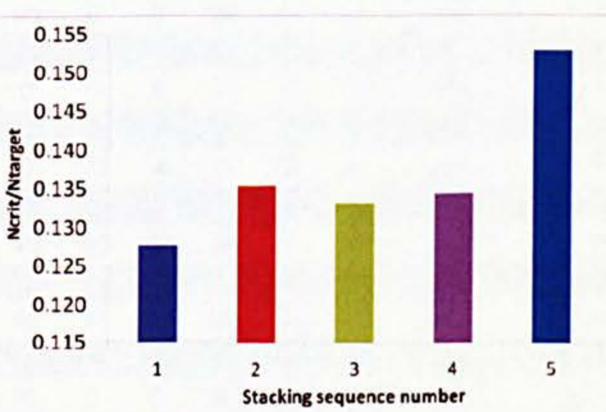

Fig. 5.13. Ratio of N_{crit}/N_{target} for all possible stacking sequence with 4 layers according to Table 5.1. Set buckling target load is 200 N/mm. All failed.

Table 5.1. Critical buckling load for all possible stacking sequence made from 4 layers for a non-crimp balanced and symmetric fabric. Set buckling target load is 200 N/mm. All failed.

Stacking sequence number	Layer 1	Layer 2	Layer 3	Layer 4	Ncrit [N/mm]	Ncrit/Ntarget
1	0	0	0	0	25.6	0.128
2	90	90	90	90	27.1	0.135
3	0	90	90	0	26.6	0.133
4	90	0	0	90	26.9	0.134
5	45	-45	-45	45	30.6	0.153

Table 5.2. Critical buckling for all possible stacking sequence of 8 layers for a balanced and symmetric non-crimp fabric. All stacking sequences pass the set target and the optimum solution is B4. Set buckling target load is 200 N/mm. All passed.

Stacking sequence number	L 1	L 2	L 3	L 4	L 5	L 6	L 7	L 8	Ncrit [N/mm]	Ncrit/Ntarget	Specimen
1	0	0	0	0	0	0	0	0	204	1.0225	
2	0	0	90	90	90	90	0	0	213	1.0653	B3
3	0	0	0	90	90	0	0	0	206	1.0278	
4	0	0	90	0	0	90	0	0	212	1.0600	
5	0	0	45	-45	-45	45	0	0	212	1.0611	
6	90	90	0	0	0	0	90	90	215	1.0753	
7	90	90	90	90	90	90	90	90	217	1.0835	
8	90	90	0	90	90	0	90	90	215	1.0763	
9	90	90	90	0	0	90	90	90	216	1.0825	
10	90	90	45	-45	-45	45	90	90	220	1.1010	
11	0	90	0	0	0	0	90	0	207	1.0373	B1
12	0	90	90	90	90	90	90	0	209	1.0455	
13	0	90	0	90	90	0	90	0	208	1.0383	
14	0	90	90	0	0	90	90	0	209	1.0445	
15	0	90	45	-45	-45	45	90	0	213	1.0629	
16	90	0	0	0	0	0	0	90	211	1.0558	
17	90	0	90	90	90	90	0	90	213	1.0640	
18	90	0	0	90	90	0	0	90	211	1.0568	
19	90	0	90	0	0	90	0	90	213	1.0630	
20	90	0	45	-45	-45	45	0	90	216	1.0814	B2
21	45	-45	0	0	0	0	-45	45	239	1.1975	
22	45	-45	90	90	90	90	-45	45	241	1.2057	
23	45	-45	0	90	90	0	-45	45	240	1.1985	
24	45	-45	90	0	0	90	-45	45	241	1.2046	
25	45	-45	45	-45	-45	45	-45	45	245	1.2231	B4

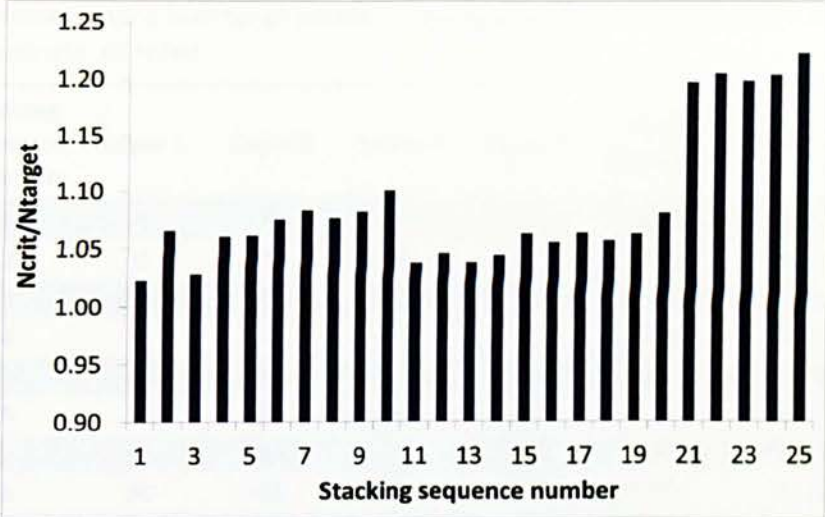

Fig. 5.14. Ratio of N_{crit}/N_{target} for all possible stacking sequence of 8 layers for a balanced and symmetric non-crimp fabric according to Table 5.3. The highest critical buckling load is stacking sequence number 25. Set buckling target load is 200 N/mm. All passed.

Table 5.3. Critical buckling load for all possible stacking sequence of 2 layers of symmetric UD laminate. Set buckling target load is 200 N/mm. All failed.

Stacking sequence number	Layer 1	Layer 2	Ncrit [N/mm]	Ncrit/Ntarget
1	0	0	3.20	0.016
2	90	90	3.39	0.017
3	45	45	3.82	0.019
4	-45	-45	3.82	0.019

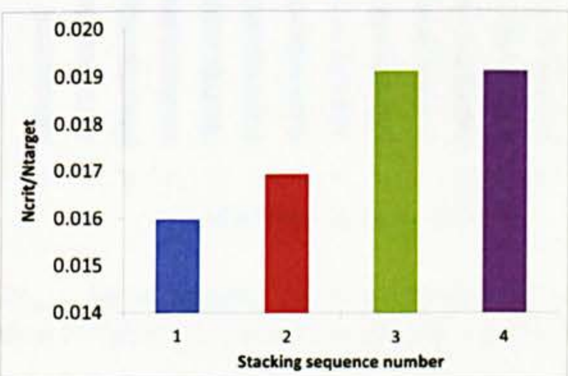

Fig. 5.15. Ratio of N_{crit}/N_{target} for all acceptable stacking sequence of symmetric UD with 2 layers according to Table 5.4. Set buckling target load is 200 N/mm. All failed.

Table 5.4. Critical buckling load for all possible stacking sequence of 4 layers of symmetric UD laminate. All failed.

Stacking sequence number	Layer 1	Layer 2	Layer 3	Layer 4	Ncrit [N/mm]	Ncrit/Ntarget
1	0	0	0	0	25.56	0.128
2	0	90	90	0	26.63	0.133
3	0	45	45	0	26.53	0.133
4	0	-45	-45	0	26.53	0.133
5	90	0	0	90	26.88	0.134
6	90	90	90	90	27.09	0.135
7	90	45	45	90	27.52	0.138
8	90	-45	-45	90	27.52	0.138
9	45	0	0	45	29.94	0.150
10	45	90	90	45	30.14	0.151
11	45	45	45	45	30.58	0.153
12	45	-45	-45	45	30.58	0.153
13	-45	0	0	-45	29.94	0.150
14	-45	90	90	-45	30.14	0.151
15	-45	45	45	-45	30.58	0.153
16	-45	-45	-45	-45	30.58	0.153

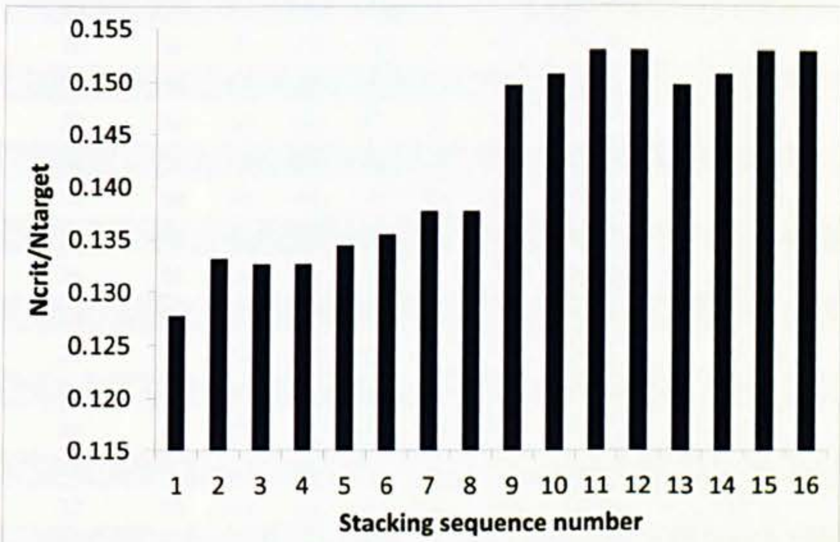

Fig. 5.16. Ratio of N_{crit}/N_{target} for all possible stacking sequence of symmetric UD with 4 layers according to Table 5.5. Set buckling target load is 200 N/mm. All failed.

Table 5.5. Critical buckling for all possible stacking sequence of 6 layers of symmetric UD laminate. Set buckling target load is 200 N/mm. All failed.

Stacking sequence number	L 1	L 2	L 3	L 4	L 5	L 6	Ncrit [N/mm]	Ncrit/Ntarget
1	0	0	0	0	0	0	86.27	0.431
2	0	0	90	90	0	0	87.34	0.437
3	0	0	45	45	0	0	87.24	0.436
4	0	0	-45	-45	0	0	87.24	0.436
5	0	90	0	0	90	0	93.77	0.469
6	0	90	90	90	90	0	87.52	0.438
7	0	90	45	45	90	0	87.95	0.440
8	0	90	-45	-45	90	0	87.95	0.440
9	0	45	0	0	45	0	93.03	0.465
10	0	45	90	90	45	0	94.10	0.470
11	0	45	45	45	45	0	93.99	0.470
12	0	45	-45	-45	45	0	93.99	0.470
13	0	-45	0	0	-45	0	93.03	0.465
14	0	-45	90	90	-45	0	94.10	0.470
15	0	-45	45	45	-45	0	93.99	0.470
16	0	-45	-45	-45	-45	0	93.99	0.470
17	90	0	0	0	0	90	89.78	0.449
18	90	0	90	90	0	90	89.98	0.450
19	90	0	45	45	0	90	90.42	0.452
20	90	0	-45	-45	0	90	90.42	0.452
21	90	90	0	0	90	90	91.22	0.456
22	90	90	90	90	90	90	91.42	0.457
23	90	90	45	45	90	90	91.86	0.459
24	90	90	-45	-45	90	90	91.86	0.459
25	90	45	0	0	45	90	94.27	0.471
26	90	45	90	90	45	90	94.48	0.472
27	90	45	45	45	45	90	94.91	0.475
28	90	45	-45	-45	45	90	94.91	0.475
29	90	-45	0	0	-45	90	94.27	0.471
30	90	-45	90	90	-45	90	94.48	0.472
31	90	-45	45	45	-45	90	94.91	0.475
32	90	-45	-45	-45	-45	90	94.91	0.475
33	45	0	0	0	0	45	98.07	0.490
34	45	0	90	90	0	45	98.27	0.491
35	45	0	45	45	0	45	98.71	0.494
36	45	0	-45	-45	0	45	98.71	0.494
37	45	90	0	0	90	45	99.51	0.498
38	45	90	90	90	90	45	99.71	0.499
39	45	90	45	45	90	45	100.15	0.501
40	45	90	-45	-45	90	45	100.15	0.501

41	45	45	0	0	45	45	102.56	0.513
42	45	45	90	90	45	45	102.76	0.514
43	45	45	45	45	45	45	103.20	0.516
44	45	45	-45	-45	45	45	103.20	0.516
45	45	-45	0	0	-45	45	102.56	0.513
46	45	-45	90	90	-45	45	102.76	0.514
47	45	-45	45	45	-45	45	103.20	0.516
48	45	-45	-45	-45	-45	45	103.20	0.516
49	-45	0	0	0	0	-45	98.07	0.490
50	-45	0	90	90	0	-45	98.27	0.491
51	-45	0	45	45	0	-45	98.71	0.494
52	-45	0	-45	-45	0	-45	98.71	0.494
53	-45	90	0	0	90	-45	99.51	0.498
54	-45	90	90	90	90	-45	99.71	0.499
55	-45	90	45	45	90	-45	100.15	0.501
56	-45	90	-45	-45	90	-45	100.15	0.501
57	-45	45	0	0	45	-45	102.56	0.513
58	-45	45	90	90	45	-45	102.76	0.514
59	-45	45	45	45	45	-45	103.20	0.516
60	-45	45	-45	-45	45	-45	103.20	0.516
61	-45	-45	0	0	-45	-45	102.56	0.513
62	-45	-45	90	90	-45	-45	102.76	0.514
63	-45	-45	45	45	-45	-45	103.20	0.516
64	-45	-45	-45	-45	-45	-45	103.20	0.516

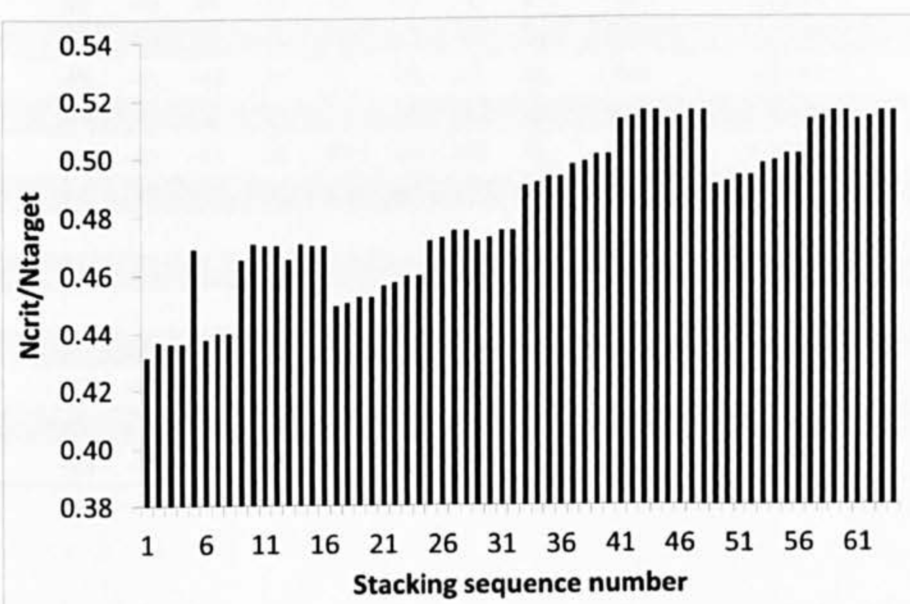

Fig. 5.17. Ratio of N_{crit}/N_{target} for all stacking sequence of symmetric UD with 6 layers according to Table 5.6. Set buckling target load is 200 N/mm. All failed.

Table 5.6. Critical buckling load for all possible stacking sequence of 8 layers of symmetric UD laminate. All passed.

Stacking sequence number	L 1	L 2	L 3	L 4	L 5	L 6	L7	L8	Ncrit [N/mm]	Ncrit/Ntarget	Specimen
1	0	0	0	0	0	0	0	0	204	1.0225	
2	0	0	0	90	90	0	0	0	206	1.0278	
3	0	0	0	45	45	0	0	0	205	1.0273	
4	0	0	0	-45	-45	0	0	0	205	1.0273	
5	0	0	90	0	0	90	0	0	212	1.0600	
6	0	0	90	90	90	90	0	0	213	1.0653	B3
•											
•											
•											
17	0	90	0	0	0	0	90	0	207	1.0373	B1
•											
•											
•											
76	90	0	45	-45	-45	45	0	90	216	1.0814	B2
•											
•											
•											
185	45	-45	45	0	0	45	-45	45	244	1.2199	
186	45	-45	45	90	90	45	-45	45	244	1.2209	
187	45	-45	45	45	45	45	-45	45	245	1.2231	
188	45	-45	45	-45	-45	45	-45	45	245	1.2231	B4
189	45	-45	-45	0	0	-45	-45	45	244	1.2199	
190	45	-45	-45	90	90	-45	-45	45	244	1.2209	
191	45	-45	-45	45	45	-45	-45	45	245	1.2231	
192	45	-45	-45	-45	-45	-45	-45	45	245	1.2231	
•											
•											
•											
253	-45	-45	-45	0	0	-45	-45	-45	244	1.2199	
254	-45	-45	-45	90	90	-45	-45	-45	244	1.2209	
255	-45	-45	-45	45	45	-45	-45	-45	245	1.2231	
256	-45	-45	-45	-45	-45	-45	-45	-45	245	1.2231	

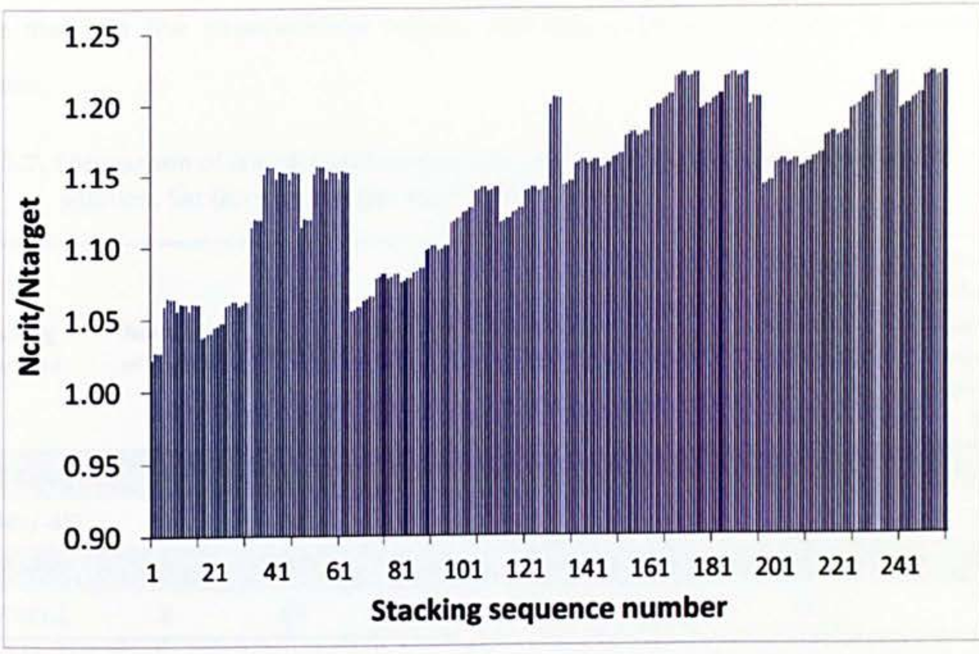

Fig. 5.18. Ratio of N_{crit}/N_{target} for all possible stacking sequence of symmetric UD with 8 layers according to Table 5.7. Set buckling target load is 200 N/mm. All passed.

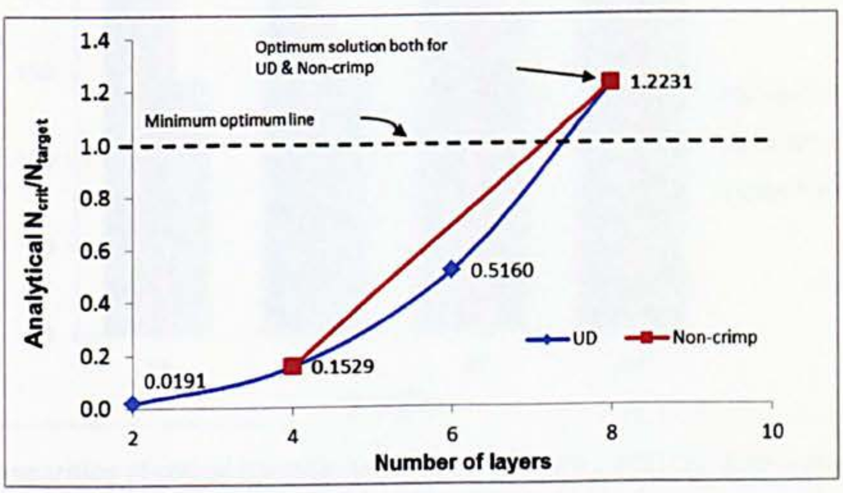

Fig. 5.19. Progression of the highest critical buckling load for laminates made from Non-crimp fabric or UD plies as the number of plies increased. Set buckling target load is 200 N/mm.

Nevertheless, the results of buckling test that described in Table 5.7 and Figure 5.20 for validation, the difference average between modelling and experiment result is relatively small especially specimen number B4, -3.2% between Eigen and experiment. In addition, the mode shape of B4 specimen from FE analysis is shown in Figure 5.21. The FEA mode shape matches the experimental results and this indicates that the FE modelling is accurate.

Table 5.7. Comparison of critical buckling load from experiment, CLPT, and finite element eigen solution. Set buckling target load is 200 N/mm.

Stacking sequence	Number of layers	Specimen	Analytic N_{crit}	Experiment N_{crit}	FE Eigen N_{crit}	Percent difference between analytic & experiment N_{crit}	Percent difference between FE Eigen & experiment N_{crit}
$[0/90/0/0]_s$	**8**	**B1**	**207**	**173**	**208**	**-16.4**	**-16.8**
$[90/0/45/-45]_s$	8	B2	216	153	188	-29.2	-18.6
$[0/0/90/90]_s$	**8**	**B3**	**213**	**185**	**202**	**-13.1**	**-8.4**
$[(45/-45)_2]_s$	8	B4	245	213	220	-13.1	-3.2

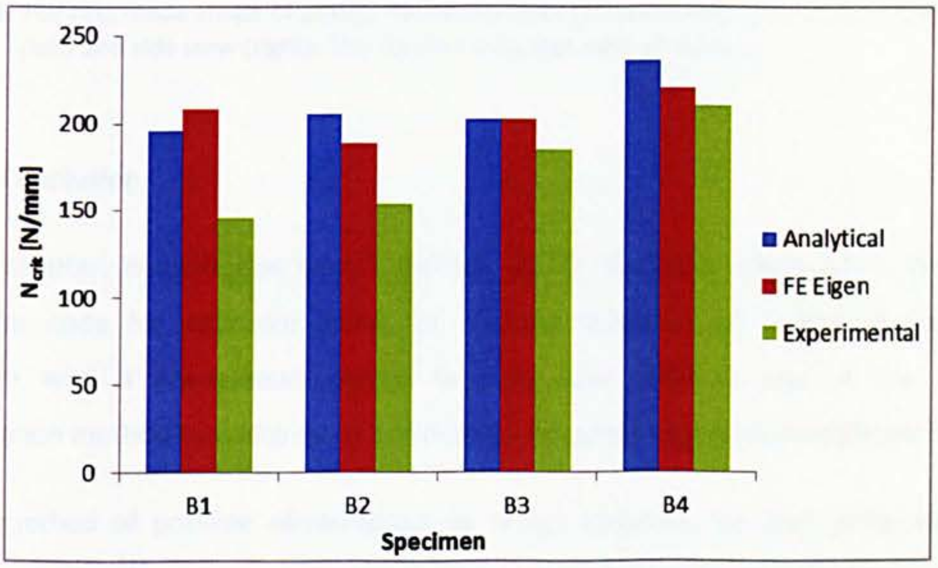

Fig. 5.20. Comparision of critical buckling load from experiment, CLPT, and finite element eigen solution. Set buckling target load is 200 N/mm.

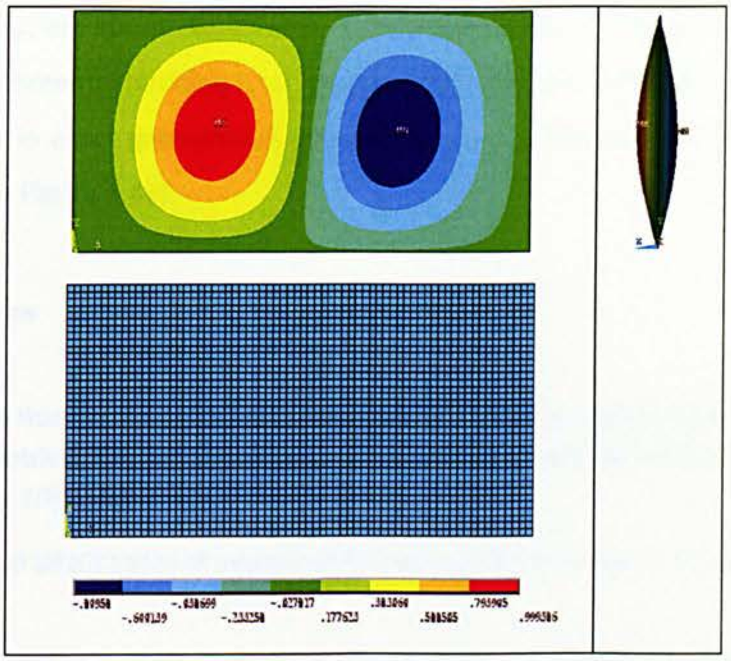

Fig. 5.21. The first mode shape of $[\pm45_2]_s$ laminated plate (B4 specimen); $m = 2, n = 1$, top view (left) and side view (right). The contour indicates ratio of w/w_{max}.

5.6. Conclusion

In this chapter, enumeration search method (ESM) has been employed to develop a computer code for optimum design of stacking sequence of laminated composite structure with a pre-selected critical buckling load. ESM is one of the discrete optimisation method by which many optimisation engineering problem might be solved.

In this method all possible combinations of design variables, i.e. fibre orientation and number of plies, from bottom-up approach was examined and the best combination of plies angle and number of layers was found. The optimum lay-up resulted in the minimum weight and satisfied the target critical buckling load. The ESM optimisation code was written for MATLAB and using CLPT for calculation of critical buckling load. The optimum number of layers for non-crimp fabric and unidirectional plies for the 200 N/mm target critical buckling load is found to be eight layers. Experimental specimens have been made from optimum (B4 specimen) and non-optimum (B1-B3 specimens) stacking sequences and the test results compared with the ESM results and FE analysis. The percentage of difference between analytical solution and FEA eigen solution with experimental critical buckling load, N_{cr}, are about -13.1% and -3.2%, respectively. It should be noted there are variation in experimental buckling load results as the selection of buckling is quite difficult and consistency in exact geometrical dimensions and microstructures of specimens are not possible (see Figure 3.46).

5.7. References

Al Humdany, A., & Hussein, E. Q. (2012). Theoretical and numerical analysis for buckling of antisymmetric simply supported laminated plates under uniaxial loads. *Journal of Kerbala University, 10*(4), 149-160.

ANSYS Release 14.0 UP20111024 UL registered ISO 9001:2000 Companies. (2011). ANSYS Help System.

Chang, K., Markov, I. L., & Bertacco, V. (2007). Postplacement rewiring by exhaustive search for functional symmetries. *ACM Trans. Des. Autom. Electron. Syst., 32*, 1-21.

Kamruzzaman, M., Naqvi, S. Q., Umar , A., & Siddiqui, N. A. (April 2005). *Buckling behavior of rectangular antisymmetric laminated plates.* India.

Kassapoglou, C. (2010). *Design and analysis of composite structures with applications to aerospace structures.* West Sussex: John Wiley & Sons, Ltd.

Legland, D., & Beaugrand, J. (2013). Automated clustering of lignocellulosic fibres based on morphometric features and using clustering of variables. *Industrial Crops and Products, 45*, 253-261.

NEN-EN 1993-1-5 (en). (2006). *Eurocode 3: Ontwerp en berekening van staalconstructies-Deel 1-5: Constructieve Plaatvelden.* Delft.

Nievergelt, J. (2000). Exhaustive search, combinatorial optimization and enumeration: exploring the potensial of raw computing power. In V. Hlavac, K. G. Jeffery, & J. Wiedermann, *SOFSEM 2000, LNCS 1963* (pp. 18-35). Berlin Heidelberg: Springer-Verlag.

Park, W. J. (1982). An optimal design of simple symmetric laminates under the first py failure criterion. *J Compos Mater, 16*, 341-355.

Sun, L. (2009). *Analytical strip method to antisymmetric laminated plates.* Kentucky: Doctoral dissertation University of Kentucky.

Todman, T., Fu, H., Tsaoi, B., Mencer, O., & Luk, W. (n.d.). Smart enumeration: a systematic spproach to exhaustive search.

van der Burg, M. J. (2011). *Master Thesis: Plate buckling in design codes the difference between NEN 6771 and NEN-EN 1993-1-5.* Delft: Delft University of Technology The Netherlands Fac. of Civil Eng. and Geosciences.

Verette, R. M. (1970). *Stiffness, strength and stability optimization of laminated composites.* Hawthorne, California: NOR-70-138, Northrop Aircraft Co.

Waddoups, M. E. (1969). *Structural airframe application of advanced composite materials - analytical methods.* Ohio: AFML-TR-69-101, vol. VI Air Force Materials Laboratory, Wright-Patterson Air Force Base.

Weaver, P. M. (2002). Designing composite structures: Lay-up selection, In: Proceedings of The Institution of Mechanical Engineers-part G. *J Aerospace Eng, 216*, 105-116.

White, S., & Weaver, P. M. (2012). Bend-free shells under uniform pressure with variable-angle tow derived anisotrophy. *Composite Structure*, 3207-3214.

www.sharcnet.ca. (n.d.). *SHELL181*. Retrieved June 12th, 2014, from www.sharcnet.ca: https://www.sharcnet.ca/Software/Fluent14/help/ans_elem/Hlp_E_SHELL181.html

www.sharcnet.ca. (n.d.). *SHELL281*. Retrieved June 12th, 2014, from www.sharcnet.ca: https://www.sharcnet.ca/Software/Fluent14/help/ans_elem/Hlp_E_SHELL281.html

Chapter 6

Shape Optimisation of Laminated Composite Plates with Stringers Subjected to Buckling using SQP, GA, and SA Methods

6.1. Introduction

Classical fields of composite materials applications are in aerospace engineering. Since many structural elements in such fields are of a rather thin-walled nature, the assessment of their buckling behaviour is a major aspect of analysis and design. Thin-walled composite structure are supported by stiffening elements (stringers), the application of which generally is very beneficial to their stability behaviour which leads to a significant increase in the resultant buckling loads. One very common type of stringer is the so-called blade stringer (Mittelstedt, 2007).

The wing of an aircraft is an example of a structure subjected to buckling load. The wing produces lift because of unequal pressures on its top and bottom surfaces (Arunkumar, Lohith, & Ganesha, 2012). This creates a shear force and a bending moment, both of which will be maximum at the point where the wing is attached to the fuselage wing root. The structure at this point should be very strong to resist the loads and bending moments, and simultaneously the wing needs to be stiff to reduce its deflection. This requirement results in a thick section at this point. However, the wing needs to have the maximum stiffness with minimum weight. When a wing bends, it deflects with respect to its neutral axis and tensile stress and compressive stress generated. Wing can be considered as a beam with the top surface undergoing compression and the bottom surface undergoing tension. As the top skin is subjected to compressive loads, it has to be designed to withstand both compression and buckling load. Usually ribs and stringers are used to stiffen panels to increase the buckling strength along with other functions like providing stability to the structure, structural integrity and maintaining aerodynamic shape.

Mallela and Upadhyay (2006) discussed the buckling behaviour of simply supported blade-stringer-stiffened composite panels under in-plane shear and performed detailed parameter studies using the finite element method. Möcker and Reimerdes (2006) investigated the buckling and postbuckling characteristic of curved stiffened composite panels by using the finite strip method. Petrisic *et al.* (2006) considered simply supported square plates with strengthening or weakening bands under in-plane normal and shear loads and reported extensive parametric studies, which were performed using the finite element method. Buermann *et al.* (2006) introduced an efficient semi-analytical model for the analysis of the local postbuckling behaviour of isotropic cylindrical panels stiffened by stringers and frames. Therein, the description of the buckling shapes of the plate and the stiffeners was done by using a Fourier approximation. Zimmermann *et al.* (2006) conducted buckling and postbuckling experiments and computations on axially compressed stiffened CFRP curved panels. Linde *et al.* (2006) described a numerical model for the parametric modelling and numerical simulation of test shells and presented result for welded and fibre metal laminate panels.

6.2. Finite Element Analysis of Plate with Stringer

In this section, the finite element analysis of composite plate buckling with stringers will be verified using ANSYS software as in the optimisation process, which will be discussed in the subsequent sections in this chapter, MATLAB will communicate with ANSYS to find the critical buckling load at every iteration.

The case study is buckling analysis of a uniaxially loaded blade-stringer-stiffened composite plate with periodic boundary conditions reported by Mittelstedt (2007). Mittelstedt developed closed form solution for critical buckling load of a blade-stringer stiffened plate under uniaxial compression. The approach depends on functional formulations for the buckling shapes of the plate as well as for the stringers accounting for periodicity properties resulting from the given structural situation of Buermann *et al.* (2006).

The methodology leads to an explicit closed-form analytical novel expression for the buckling load of a clamped stringer. The results by the closed-form solution for the buckling of the stiffened panel are compared with a full series expansion solution and to the finite element calculations. One very common type of stringer is blade stringer that actually is a plate perpendicularly attached to the composite plate. Figure 6.1 shows a typical arrangement of this class, where a composite plate stiffened by several blade stingers. The plate has the length a, the plate width between two stringers is denoted as b (as stringer pitch), the stringer height is h and it is subjected to some in-plane normal loading. Under compressive load, there are several possibilities that the plate will buckle. In addition, there are several possibilities for local buckling modes as shown in Figure 6.2 that are likely to occur. In all three cases, it is if stringers are of a sufficient bending stiffness such that they remain immovable in the state of the onset of buckling. In many applications, it can be assumed that a mixed buckling mode is likely to occur as can be seen in Figure 6.2(a). In such cases buckling of the plate in combination with simultaneous buckling of the blade stringers will occur. For the case of very stiff stringers, the stringers reinforce the plate in such a way that the buckling shape corresponds to a clamped plate as can be seen in Figure 6.2(b). Lastly, for cases of sufficiently strong plates only the stringer will buckle and the plate remains immovable as shown in Figure 6.2(c).

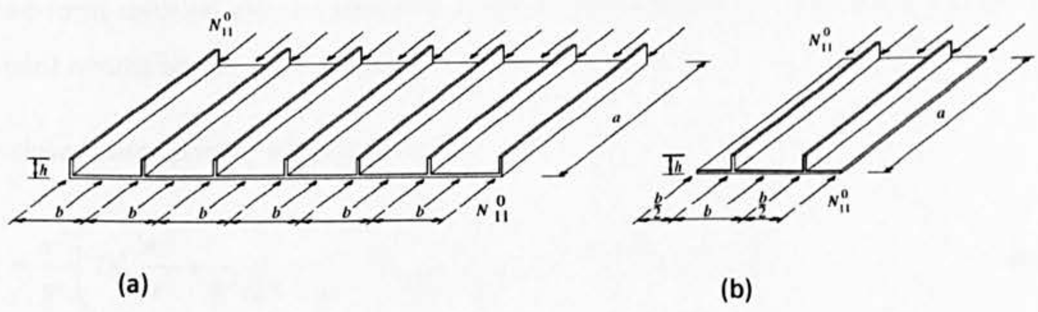

Fig. 6.1. Composite plate stiffened with (a) blade stringer and (b) representative unit cell for local buckling analysis (Mittelstedt, 2007).

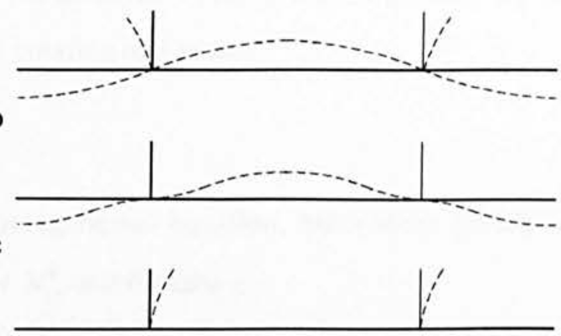

Fig. 6.2. Basic local buckling modes, (a) combined plate and stringer buckling, (b) plate buckling in the case of stiff stringers (case I), (c) stringer buckling in the case of stiff plate (case II) (Mittelstedt, 2007).

As Figure 6.2a reveals the resultant buckling shapes exhibit periodicity and as a result it is possible to reduce the analysis of a complex structural situation of a composite plate with multiple stringers as shown in Figure 6.1a to the analysis of a representative unit cell (RUC) in Figure 6.1b without loss of generality (Mittelstedt, 2007). In this case, the sides of RUC have periodic boundary conditions and the stringers are immovable at intersection to the plate. In addition, the plate and stringer material properties as well as the loading conditions do not vary.

Mittelstedt (2007) derived a closed-form solution, Eqs. (6.1)-(6.3), for the critical buckling loads of blade-stringer stiffened orthotropic composite plates under uniaxial compression. The approach considers an explicit functional formulation for the buckling shapes both for the plate and the stringer accounting for periodicity resulting from the given structural situation and as such follows Buermann *et al.* (2006). The results from the closed-form solution are compared to a full series expansion on one hand and to finite element results on the other hand.

The closed-form governing equation is:

$$N_{11}^{0}=\frac{\pi^{2}}{\psi}\left(D_{11}^{S}\frac{m^{2}}{a^{2}}+\frac{1}{h^{2}(3\pi-8)}\left(D_{22}^{S}\frac{\pi a^{2}}{16h^{2}m^{2}}+D_{12}^{S}\frac{\pi-4}{2}+D_{66}^{S}\pi\right)\right) \tag{6.1}$$

which estimates the buckling load N_{11}^{0} of a rigidly clamped stringer and as such describes the above-mentioned limit case II, where the plate is simply supported at the loaded edges along x_1=0 and x_1=a as shown in Fig. 6.11a. Differentiating Eq. (6.1) with respect to m yields the number of buckling half-waves:

$$m = \frac{a}{2h}\sqrt[4]{\frac{D_{22}^{S}}{D_{11}^{S}}\left(\frac{\pi}{3\pi - 8}\right)} \quad (6.2)$$

From the governing homogeneous equation, Mittelstedt (2007) obtained the following polynomial equation for N_{11}^{0} and for case I:

$$B_4(N_{11}^0)^4 + B_3(N_{11}^0)^3 + B_2(N_{11}^0)^2 + B_1 N_{11}^0 + B_0 = 0 \quad (6.3)$$

where the coefficients B_0 to B_4 are functions of the bending stiffness of the plate and the stringer. The solution of Eq. (6.3) with respect to N_{11}^{0} gives the critical buckling load for case I.

The FE analysis is verified by simulating a representative unit cell of a stiffened composite plate under uniform compressive load as shown in Figure 6.3, where the plate length is $a = 450$ mm and the stringer distance is $b = 150$ mm (Mittelstedt, 2007). The orthotropic material properties are E_{11}=138GPa, E_{22}=10GPa, G_{12}=5GPa and ν_{12}=0.27, ν_{23}=0.4 with a ply thickness of t=0.125mm. The stacking sequence is $[(0°/90°)_2]_s$ for the plate and $[(0°/90°)_3]_s$ for the stringer, while the load factor is $\psi = 1$. The stringers and the plate were loaded similarly. The stiffened composite plate is simply supported along the loaded edges, while the plate is bonded to the stringers along their common surface. As the plate is very wide, only one unit cell is chosen as a representative unit (Figure 6.3) and periodic boundary condition are applied along the unloaded edges (Figure 6.4). For the aforementioned problem, the critical buckling load was estimated through an FE eigenvalue buckling analysis using ANSYS version 14.0 and utilizing 8-node SHELL281 layered elements (see Chapter 5 for more details about SHELL281 element).

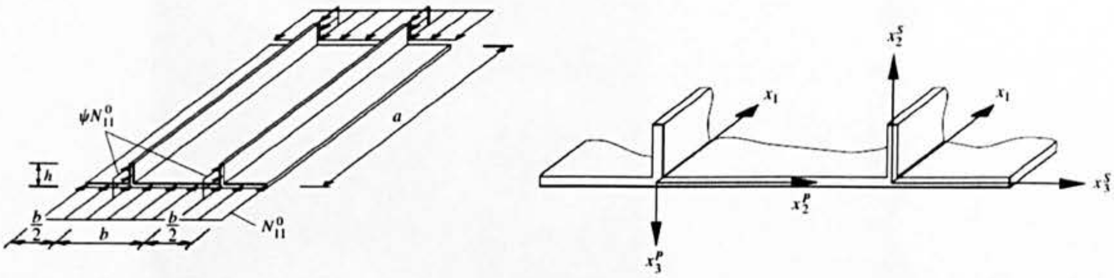

Fig. 6.3. Load and local coordinate system (Mittelstedt, 2007)

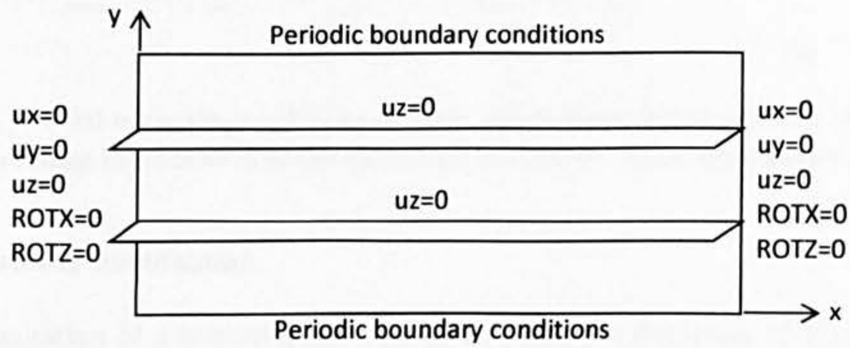

Fig. 6.4. Boundary conditions.

The theoretically anticipated first mode shape of the plate (Mittelstedt, 2007) is shown in Figure 6.2a, where a combined plate and stringer buckling occurs. The corresponding mode shape from the current work is shown in Figure 6.5. From visual inspection, it is clear that the two aforementioned mode shapes are in accordance.

The FEA results from the current work were verified against Mittelstedt (2007), as shown in Table 6.1. Mittelstedt (2007) used both a closed-form solution and FEA. It is evident that the difference between critical buckling load from analytical solution and FEA Mitterlstedt (2007) with the current FEA is -1.4% and 1.4%, respectively.

Table 6.1. Critical buckling load N_x of the examined laminated plate with stringers.

N_x from closed form (Mittelstedt, 2007) (N/mm)	N_x from FEM (Mittelstedt, 2007) (N/mm)	N_x from FEM (current work) (N/mm)
7.04	7.24	7.14

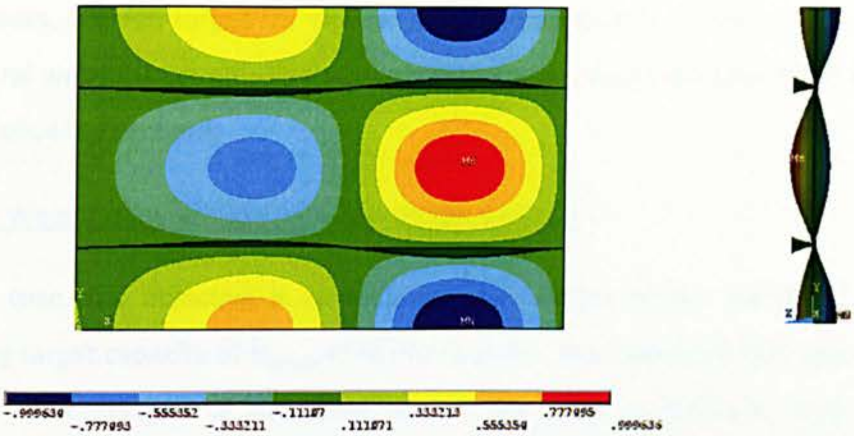

(a) (b)

Fig. 6.5. The first mode shape of laminated plate with stringer: (a) top view and (b) side view, showing the combined plate and stringer buckling (compare with Figure 6.2a).

6.3. Buckling Optimisation

The configuration of a laminate, i.e. fibre orientation, ply thickness, stacking sequence, reinforcement geometry, volume fraction of reinforcement, can be tailored to reduce its weight without compromising its performance, or even improve the performance without increasing its weight. This can be achieved through a process of design optimisation. Optimisation provides the engineers with a tool for finding the best design among countless number of acceptable designs (Erdal & Sonmez, 2005).

In this study, three optimisation methods are used in optimising a laminated plate with stringers. These are Sequential Quadratic Programming (SQP), Genetic Algorithms (GA) and Simulated Annealing (SA) methods.

Problem Statement

The optimisation problem considered in this study is a FRP laminated plate composite with stringers, where both the plate and the stringers are of the same material while the stacking sequence is $[(0/90)_2]_s$ for the plate and $[(0/90)_3]_s$ for the stringer. Two different optimisation cases were examined, the former having one design variable, which is related to the stringer height, and the latter having two design variables, which are related to the stringer height and the distance between the stringers, respectively. In both cases, a given target for the critical buckling load is defined, while the minimum structural weight is sought. The aforementioned two cases are presented in more details in the following sections.

Case 1: Weight minimization with one design variable

In this case, the objective is to minimise the weight of the examined structure if a buckling target capacity of N_{target}=7 N/mm is given. The examined RUC plate is considered to have two stringers of the same height. The ratio $x_1 = h/a$ is used as the design variable, where a is the plate length and h is the stringer height. The plate is made from n_p=8 layers $[(0/90)_2]_s$ and the stringers is made from n_s=12 layers $[(0/90)_3]_s$ from the same material. Thus, the optimisation problem is to find the minimum volume V of the structure defined by:

$$V = 2\left(n_p\left(\frac{b}{a}\right) + n_s\left(\frac{h}{a}\right)\right)a^2 t_{ply} \tag{6.4}$$

$$V = 2\left(n_p\left(\frac{b}{a}\right) + n_s(x_1)\right)a^2 t_{ply} \tag{6.5}$$

where b is the distance between the stringers. The ply thickness, t_{ply}, the plate length a and the ratio of b/a, are set equal to 0.125mm, 450mm and 0.33, respectively. Substituting these values into Eq. (6.5) and introducing the design variable $x_1 = h/a$ yields:

$$V = 133650 + 607500 x_1 \tag{6.6}$$

The target critical buckling load N_{target} is introduced as a non-linear normalized constraint related to the critical buckling load N_{crit} of the examined structure:

$$\left(\frac{N_{target}}{N_{critical}}\right) - 1 \le 0 \tag{6.7}$$

Furthermore, the domain of the design variable is chosen to be $0.03 \le x_1 \le 0.12$.

Case 2: Weight minimization with two design variables

This is a variation of Case 1, the only difference being that the ratio $x_2 = b/a$ is also used as a design variable, where $2b$ is the plate width. Again, a buckling target capacity of N_{target} = 7 N/mm is used. For Case 2, the objective function described in Eq. (6.5) takes the following form:

$$V = 405000x_2 + 607500x_1 \tag{6.8}$$

Furthermore, the domain of the design variables is chosen to be $0.03 \leq x_1 \leq 0.12$ and $0.2 \leq x_2 \leq 0.49$, respectively.

Solution of the optimization problem

The optimization problems described by Eqs. (6.6) and (6.8) may be interpreted as a search in three-dimensional space for a point corresponding to the minimum value of the objective function such that it lies within the region bounded by the subspaces representing the constraint functions. Iterative techniques are widely used for solving such optimization problems in which a series of directed design changes (moves) take place between successive points in the design space. The new design vector $\underline{X}_{i+1}$ is obtained from the old one $\underline{X}_i$ as follows:

$$\underline{X}_{i+1} = \underline{X}_i + \alpha \underline{S}_i \tag{6.9}$$

such that

$$F(X_{i+1}) < F(X_i) \tag{6.10}$$

where $F(X_i)$ is the value of the objective function for the design vector $\underline{X}_i$, $\underline{S}_i$ defines the direction of the move and the scalar quantity α gives the step length such that $\underline{X}_{i+1}$ does not violate the imposed constraints, let them be $G_j(x)$.

For solving the optimisation problems mentioned in Case 1 and Case 2, an in-house code was developed using MATLAB platform for technical programming. MATLAB has an optimization toolbox which is a powerful tool including many routines for different types of optimization concerning both unconstrained and constrained minimization algorithms

(Vekataraman, 2009). One routine is called "fmincon" and implements the method of Sequential Quadratic Programming in finding the constrained minimum of an objective function of several variables starting at an initial design. The search direction $\underline{S}_j$ must satisfy the two conditions $\underline{S}_j.\underline{\nabla}F < 0$ and $\underline{S}_j.\underline{\nabla}G_j < 0$, where $\underline{\nabla}F$ and $\underline{\nabla}G_j$ are the gradient vectors of the objective and constraint functions, respectively. For checking the constrained minima, the Karush-Kuhn-Tucker test (Vanderplaats, 1999) is applied to the design point $\underline{X}_D$, which lies on one or more set of active constraints. The Karush-Kuhn-Tucker equations are necessary conditions for a constrained optimization problem and their solution forms the basis to the method of feasible directions.

The optimization code was developed using MATLAB R2011a. However, the part of the eigenvalue buckling analysis was carried out using ANSYS version 14.0. Therefore, a communication between MATLAB and ANSYS was established (Figure 6.6) such that ANSYS was used as an external solver to obtain the critical buckling load.

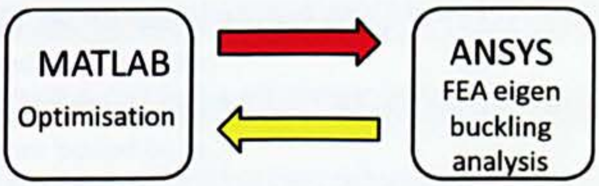

Fig. 6.6. Schematic communication between MATLAB and ANSYS

6.3.1. SQP Optimisation Procedure

For both Cases, the initial design vector was formed using randomly selected values from the corresponding design variable domains. The convergence tolerance was set equal to 10^{-6}, both for the constraints and for the objective function except for Case 2 tolerance constraint is default setting. Furthermore, the maximum number of function evaluations was set equal to 1000, while the maximum iteration number was set equal to 200 (see Table 6.2 and 6.3).

The iteration histories for Case 1 and Case 2 from the application of the SQP method are shown in Figures 6.7 and 6.12, respectively.

Table 6.2. Parameters used in SQP method in Case 1 (other parameters are default values)

Parameter	Value
Constraint tolerance	1e-6
Function tolerance	1e-6
Maximum function evaluation	1000
Maximum iteration	200
Lower bound	0.03
Upper bound	0.2
x_0	random
Algorithm	active-set

Table 6.3. Parameters used in SQP method in Case 2 (other parameters are default values)

Parameter	Value
Constraint tolerance	1e-6
Function tolerance	1e-6
Maximum function evaluation	1000
Maximum iteration	200
Lower bound (x_1, x_2)	0.03, 0.2
Upper bound (x_1, x_2)	0.12, 0.49
x_0	random
Algorithm	interior-point

6.3.2. GA Optimisation Procedure

Genetic Algorithm (GA) optimisation method has gained much attention because of their simplicity, ease of implementation and ability to handling non-convex problems, e.g. the orientation of the material as design variable that lead to a non-convex problem, and integer design variables type problems such as stacking sequence of laminates. However, for large-scale problems GA generally requires a significant larger number of function evaluations to achieve convergence, which is much higher than the gradient based optimisation methods.

With the GA method, both constrained and unconstrained optimisation problems can be solved. GA is based on natural selection, the process that drives biological evolution. At each step, the GA selects individuals at random from the current population to be parents and uses them to produce the children for the next generation. Over successive generations, the population 'evolves' towards an optimal solution.

The convergence tolerance for the constraints and the objective function was set equal to 10^{-3} and 10^{-6} for Case 1 and Case 2, respectively. The population size selected was 10 (see Table 6.4 and 6.5).

The iteration histories for Case 1 and Case 2 from the application of the GA are described in Figures 6.8 and 6.13, respectively.

Table 6.4. Parameters used in GA method in Case 1 (other parameters are default values)

Parameter	Value
Constraint tolerance	1e-3
Function tolerance	1e-3
Population size	10
Lower bound	0.03
Upper bound	0.12

Table 6.5. Parameters used in GA method in Case 2 (other parameters are default values)

Parameter	Value
Constraint tolerance	1e-6
Function tolerance	1e-6
Population size	10
Lower bound (x_1, x_2)	0.03, 0.2
Upper bound (x_1, x_2)	0.12, 0.49

6.3.3. SA Optimisation Procedure

Simulated Annealing (SA) is a method for solving unconstrained and bound-constrained optimisation problems. It is based on the annealing procedure met in metallurgy, thus one of its controlling parameters is related to 'temperature'. The distance of the new point from the current point, or the extent of the search, is based on a probability distribution with a scale proportional to the aforementioned temperature. The algorithm accepts all new points that lower the objective, but also, with a certain probability, points that raise the objective. By accepting points that raise the objective, the algorithm avoids being trapped in local minima, and is able to explore globally for solutions that are more feasible. An annealing schedule is selected to decrease the temperature as the algorithm proceeds. As the temperature decreases, the algorithm reduces the extent of its search to converge to a minimum.

In the present work, SA as implemented in the MATLAB Optimization Toolbox, was also utilized. The options for convergence tolerance as well as the range of the design variable domains were shown in Table 6.6 and 6.7.

The iteration histories from the application of SA are shown in Figures 6.9 and 6.14, for Case 1 and Case 2, respectively.

Table 6.6. Parameters used in SA method in Case 1 (other parameters are default values)

Parameter	Value
Function tolerance	1e-3
Lower bound	0.034
Upper bound	0.12
x_0	random

Table 6.7. Parameters used in SA method in Case 2 (other parameters are default values)

Parameter	Value
Function tolerance	1e-6
Lower bound (x_1, x_2)	0.03, 0.2
Upper bound (x_1, x_2)	0.12, 0.49
x_0	random

6.3.4 Results of Optimisation

Case 1 Results

The three methods gave similar minimum volume at about 153,000mm^3, although the duration for iteration is quite different. The shortest iteration time is for SA and the longest one is for GA (see Figures 6.7-6.9).

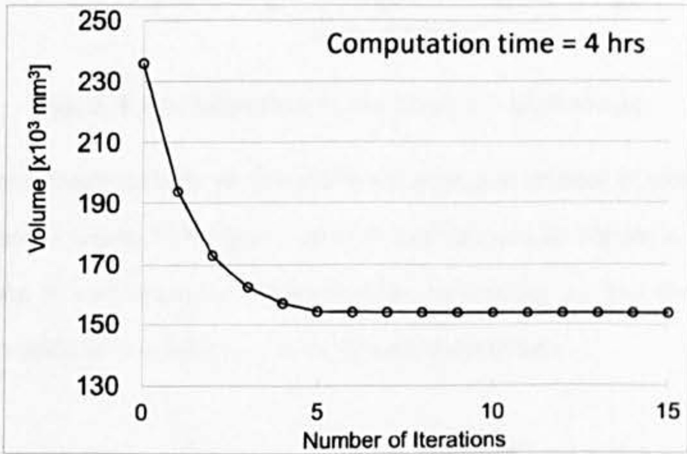

Fig. 6.7. Iteration history for Case 1 – SQP method.

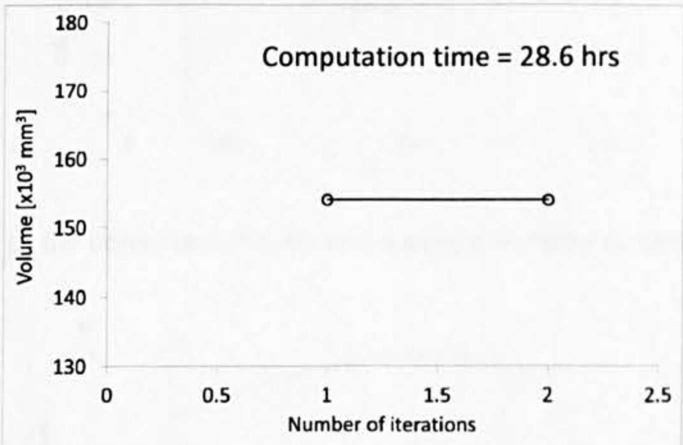

Fig. 6.8. Iteration history for Case 1 – GA method.

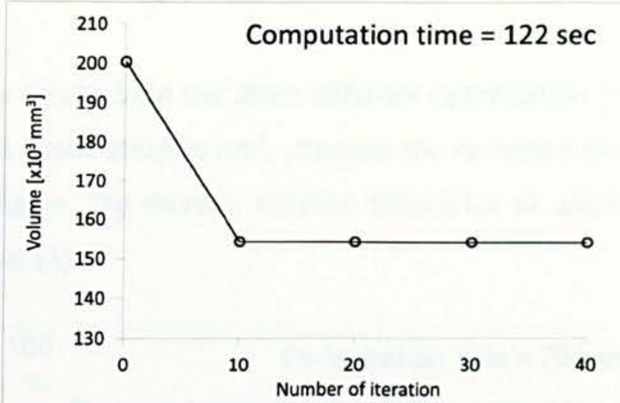

Fig. 6.9. Iteration history for Case 1 – SA method.

The parametric sensitivity studies of the plate volume and critical buckling load to design variable x_1 for Case 1 using FEA eigen solution are shown in Figure 6.10 and 6.11. The weight of the plate is continuously increasing by increasing x_1 but the critical buckling load reaches to an optimum around $x_1 = 0.16$ and then drop.

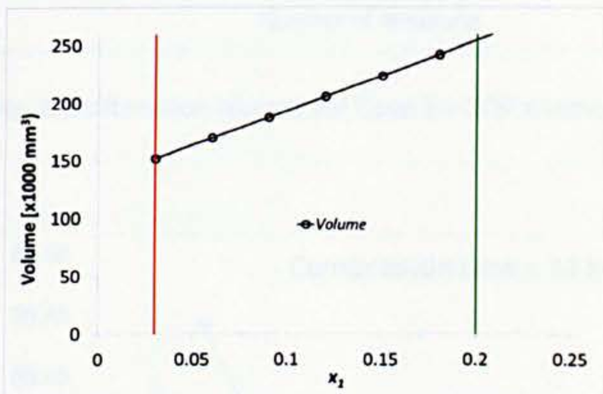

Fig. 6.10. Plot of the objective function vs the design variable x_1, lb=0.03, ub=0.2.

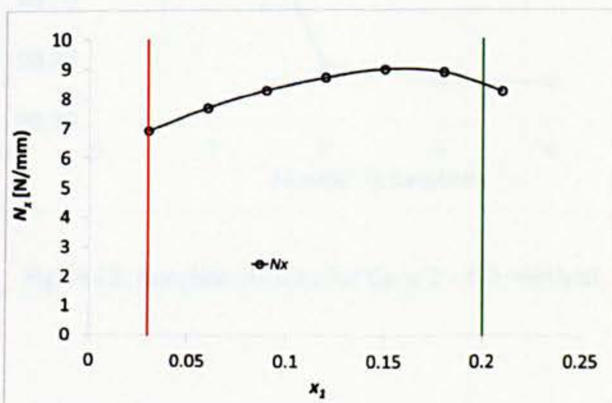

Fig. 6.11. Plot of the critical buckling load N_x vs the design variable x_1, lb=0.03, ub=0.2.

Case 2 Results

In this case also the results from the three different optimisation methods found similar minimum volume at about 100,000mm^3, although the iterations time are quite different as shown on each figure. The shortest iteration time is for SA and the longest one is for GA (see Figure 6.12-6.14).

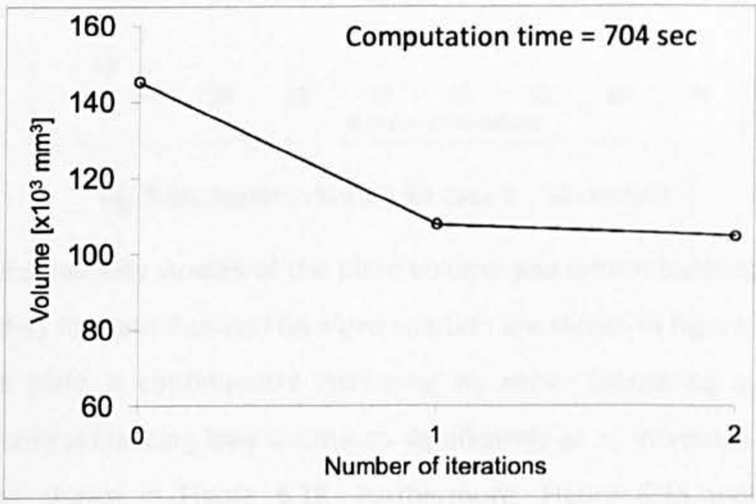

Fig. 6.12. Iteration history for Case 2 – SQP method.

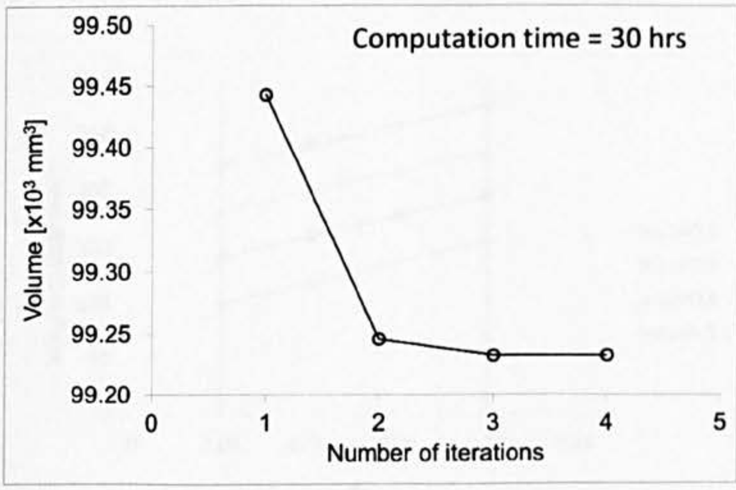

Fig. 6.13. Iteration history for Case 2 – GA method.

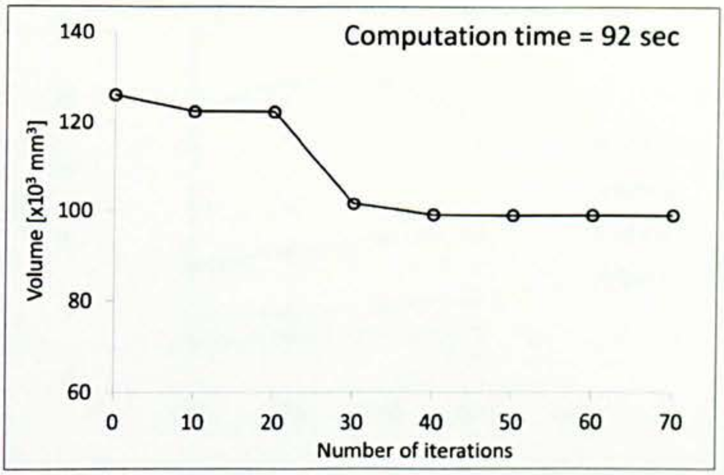

Fig. 6.14. Iteration history for Case 2 – SA method.

The parametric sensitivity studies of the plate volume and critical buckling load to design variable x_1 and x_2 for Case 2 using FEA eigen solution are shown in Figure 6.15 - 6.17. The volume of the plate is continuously increasing by either increasing x_1 or x_2 values. However, the critical buckling load decreases significantly as x_2 increases for any specific value of x_1 as shown in Figure 6.18. Furthermore, Figure 6.15 indicates that the correlation between the design variable x_1 and the objective function is linear whilst, as shown in Figure 6.18, the correlation between the design variable x_2 and the critical buckling load N_x is nonlinear (parabolic).

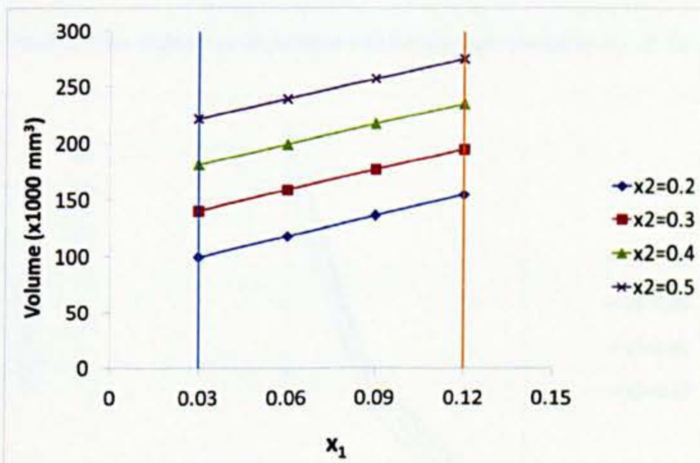

Fig. 6.15. Plot of the objective function vs the design variable x_1, lb=0.03, ub=0.2.

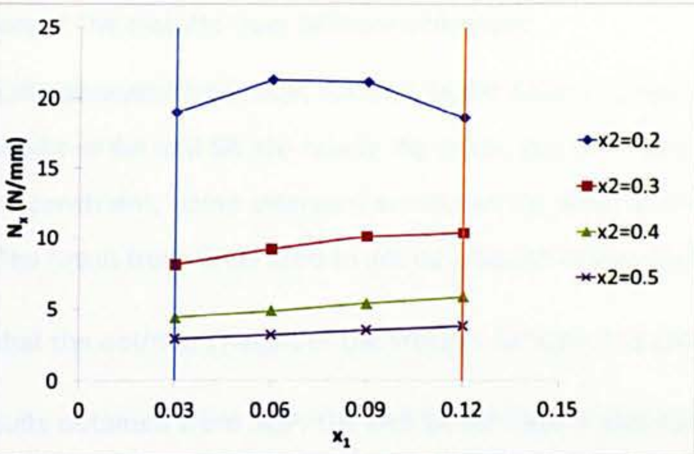

Fig. 6.16. Plot of the critical buckling load N_x vs the design variable x_1, lb=0.03, ub=0.2.

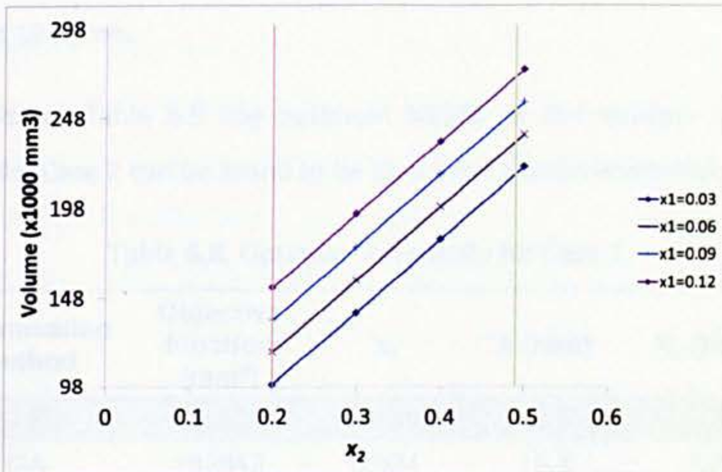

Fig. 6.17. Plot of the objective function vs the design variable x_2, lb=0.2, ub=0.49.

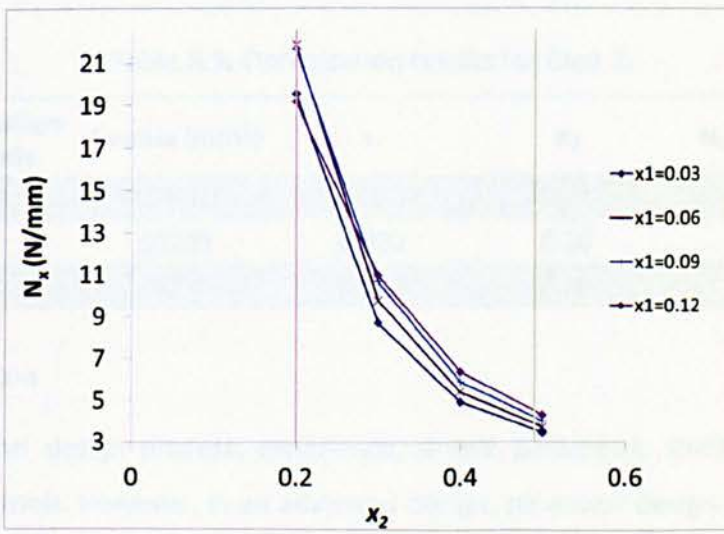

Fig. 6.18. Plot of the critical buckling load N_x vs the design variable x_2, lb=0.2, ub=0.49.

6.4. Comparison of The Results from Different Methods

The optimum results obtained from SQP, GA and SA for Case 1 summarised in Table 6.8 shows that the results of GA and SA are nearly the same, but different to SQP. Although, SA does not need constraint, some intervention should be done in order to obtain the optimum result. The result from GA is used to get new bound region for SA.

Table 6.8 shows that the optimum height of the stringer for Case 1 is about h=15.3mm.

The optimum results obtained from SQP, GA and SA for Case 2 summarised in Table 6.9 shows that the results from all three methods are almost the same and for all cases, the lower bounds for both x_1 and x_2 have been reached. For Case 2 the maximum buckling load obtained is 19 N/mm.

From the results of Table 6.9 the optimum height of the stringer and the distance between them for Case 2 can be found to be about h=13.5mm and b=90mm, respectively.

Table 6.8. Optimisation results for Case 1.

Optimisation method	Objective function (mm³)	x_1	h (mm)	N_x (N/mm)
SQP	151875	0.030	13.5	6.920
GA	152843	0.034	15.3	7.020
SA	154305	0.034	15.3	7.020

Table 6.9. Optimisation results for Case 2.

Optimisation methods	f value (mm³)	x_1	x_2	N_x (N/mm)
SQP	104661	0.030	0.21	16.6
GA	99231	0.030	0.20	19
SA	99225	0.030	0.20	19

6.5. Conclusion

In the traditional design process, experience, simple parametric studies, analysis and testing are the tools. However, in an advanced design, structural design optimisation is a very powerful tool and the results obtained can be far from intuitive imagination and display a superior performance relative to traditional design method. Nevertheless, from this method a design may appear superior against a given criterion, but its performance might be insufficient when evaluated against other may be equally important criterion.

In this chapter, the optimisation analysis was focused in improving the design by minimising the weight of the structure while it withstands a set target buckling load.

Before applying the shape optimisation methodology to a specific design, verification of various elements in the optimisation process has been done. Eigen solution of finite element of a stiffened plate structure was verified with the analytical and FEA results from the literature.

Sequential Quadratic Programming (SQP), Genetic Algorithms (GA) and Simulated Annealing (SA) optimisation methods in MATLAB optimisation programme have been used together with ANSYS finite element methods to optimise the weight of a blade stiffened laminated composite plate subjected to buckling and to be able to carry a minimum set target critical load. Two cases were studied. In Case 1 only one design variable, the height of the stringer, was considered. In Case 2, two design variables, the height of the stringer and distance between the stringers were selected. The optimum weight of the plate for the set target buckling load for each case was found.

The optimum weight of the plate for the set target buckling load was found to be for a plate with stringer height of around h=15.3mm from all three optimisation methods in Case 1. The optimum height of the stringer and the distance between them for Case 2 is about h=13.5mm and b=90mm, respectively.

The sensitivity analyses of the plate weight to design variables were conducted and the effect of the design variables on the critical buckling load was investigated.

In summary, it is demonstrated in this chapter that by employing shape optimisation in the design of composite structure, a higher safety factor could be achieved without any additional materials. It is only necessary to find the optimum shape for the geometry through optimisation process. This chapter complement the material optimisation problem for optimum stacking sequence of laminated FRP discussed in Chapter 5.

6.6. References

Arunkumar, K. N., Lohith, N., & Ganesha, B. B. (2012). Effect of ribs and stringer spacings on the weight of aircraft structure for aluminium material. *Journal of Applied Sciences, 12*(10), 1006-1012.

Buermann, P., Rolfes, R., Tessmer, J., & Schagerl, M. (2006). A semi-analytical model for local post-buckling analysis of stringer and frame-stiffened cylindrical panels. *Thin-Walled Structures, 44*, 102-114.

Erdal, O., & Sonmez, F. O. (2005). Optimum design of composite laminates for maximum buckling load capacity using simulated annealing. *Compos Struct, 71*(1), 45-52.

Linde, P., Schulz, A., & Rust, W. (2006). Influence of modelling and solution methods on the FE-simulation of the post-buckling behaviour of stiffened aircraft fuselage panels. *Compos Struct, 73*, 229-236.

Mallela, U. K., & Upadhyay, A. (2006). Buckling of laminated composite stiffened panels subjected to in-plane shear: a parametric study. *Thin-Walled Structures, 44*, 354-361.

MATLAB. (2014). Help - http://www.mathworks.co.uk/help/matlab/. MATLAB. Retrieved March 28th, 2014

Mittelstedt, C. (2007). Closed-form analysis of the buckling loads of uniaxially loaded blade-stringer-stiffened composite plates considering periodic boundary conditions. *Thin-Walled Structure, 45*, 371-382.

Mocker, T., & Reimerdes, H. G. (2006). Postbuckling simulation of curved stiffened composite panels by the use of strip elements. *Compos Struct, 73*, 237-243.

Petrisic, J., Kosel, F., & Bremec, B. (2006). Buckling of plates with strengthenings. *Thin Walled Structures, 44*, 334-343.

Vanderplaats, G. N. (1999). *Numerical optimization techniques for engineering design with applications.* New York: McGraw Hill.

Vekataraman, P. (2009). *Applied optimization with MATLAB programming, 2nd Edition.* New York: Wiley.

Zimmermann, R., Klein, H., & Kling, A. (2006). Buckling and postbuckling of stringer stiffened fibre composite curved panels-tests and computation. *Compos Struct, 73*, 150-161.

Chapter 7

Conclusion and Further Work

In this chapter a summary of the work carried out in this research and highlights of the main contributions are presented. The outcome of the results will be elaborated in accordance to the objectives set out in Chapter 1. At the end a number of suggestions for further development on buckling analysis of composite structures for the future work will be proposed.

7.1. Conclusions

In the traditional engineering design, experience, simple parametric studies, analysis and testing are commonly used tools. However, in an advanced engineering design, optimisation is employed which is a very powerful tool for the fittest design. The result outcome of the optimisation can be far from intuitive imagination, and potentially it has a superior performance relative to the traditional design outcome. Nevertheless, the design obtained from the optimisation may appear superior against a given criterion, but its performance might be insufficient when evaluated against another equally important criterion. So in using optimisation for structural engineering this point should be considered.

In this thesis the optimisation analysis was explored for improving the structural design of laminated structures under compressive load. The aim was to minimise the weight of the structure while maximising the compressive carrying load capacity or withstanding a set target buckling load.

Many issues arise when a laminated FRP composite plate subjected to compressive load and ultimately fail under buckling. Issues such as understanding FRP composite materials, post-buckling behaviour of the structure, delamination and detection of the crack front need attention. Hence, works carried out on all these areas as summaries below.

In Chapter 1, the importance of FRP composite materials in engineering structural applications and specifically their use in the aerospace industry where the weight of the structure is a sensitive parameter has been investigated. In addition, the fundamental governing equations of classical laminated plate theory (CLPT) for analysis of laminates were discussed and the governing equation of buckling of laminated plates presented. Literature review of important past works related to buckling of laminated FRP, delamination buckling, and non-destructive testing caused by buckling load are investigated.

In Chapter 2 various experimental studies carried out to study the delamination and buckling of FRP composite materials. Four series of tests that were conducted in this chapter are:

In the first series of tests mechanical properties of unidirectional GFRP composite materials has been identified. From this series of tests mechanical properties such as Young's modulus, shear modulus, Poisson's ratio and tensile and shear strength were determined.

The second series of tests were performed to characterise the delamination fracture toughness in mode I, mode II and mixed-mode I/II using DCB, ENF and MMB tests. From these series of test G_{IC}, G_{IIC} and fracture envelope under mixed mode loading were determined. The average mode I delamination fracture toughness based on CBT is G_{IC}= 460±15 J/m^2 and the average mode II delamination fracture toughness is about G_{IIC}=710±50 J/m^2.

The third series of tests were performed on buckling of the plates with optimum and non-optimum stacking sequence to verify the optimisation results. The effect of damage on buckling load was studied by tests on buckling of plates with pre-existing centrally located delamination patch at the plate mid-plane and on plate with a hole at the centre of the plate to investigate the effect of cut-out and damage on buckling load. The effect of stiffening of plate on the critical buckling load tests were carried out on the blade stiffened plate.

The plate with $[\pm45_2]_s$ stacking sequence showed the optimum critical buckling load. However, in the case of plates with pre-existing centrally located delamination patch with diameter less than 32 mm, the critical buckling load has not changed. But when the delamination patch diameter reached to 48 mm (at around 60% of plate width), there was significant reduction in the critical buckling load. In the case for plate with cut-out a noticeable reduction on the critical buckling load was observed when the diameter of the hole, D, was more than 25% of the plate width.

Finally, non-destructive tests (NDT) were carried out on plates with pre-existing centrally located delamination patch to study the direction and the extent of delamination crack propagation. For this objective IR thermography and CT-Scan tests have been used to study the delamination crack growth in the buckled plates. Both IR and CT-Scan images showed that in plates with pre-existing centrally located delamination patch with a diameter of D=16 mm the plate failure occurs near the loading edge. In the case of plates with delamination patch of D=32mm some plate failed near the loading edge and in some plates crack propagated along the ±45° fibre direction around delamination patch. However, in the case of delamination patch with diameter of D=48mm, in all samples the delaminated area grows along the fibre direction around the delaminated area and no failure observed near the loading edge. These results are in accordance with other published works.

In Chapter 5, initially verification of various tools used in the optimisation process has been done. Finite element eigen solution has been used to study the effect of fibre orientation, geometry and material properties on critical buckling load of a GFRP plate and the results were verified with the published results. In addition, non-linear buckling analysis was studied and the effect of imperfection on the critical buckling load and post-buckling were studied.

Next enumeration search method (ESM) has been used for optimum design of stacking sequence of laminated composite structure for maximum critical buckling load. ESM is one of the discrete optimisation method by which many optimisation engineering problem might be solved. In this method all possible combinations of design variables (i.e. orientation and number of plies) from bottom-up approach has been used to find the best combination of plies angle and number of layers which make the minimum weight for maximum critical buckling load. The ESM optimisation code was written for MATLAB using CLPT. For the selected target buckling load, the optimum number of layers (weave or pair of unidirectional layers) is found. Experimental specimens have been made from optimum (B4 specimen) and non-optimum (B1, B2 and B3 specimens) stacking sequences and the buckling test loads are compared with the ESM results and FE simulations. The percentage of difference between analytical solution and FEA eigen solution with experimental critical buckling load, N_{cr}, are about -13.1% and -3.2%, respectively.

In Chapter 6 optimisation is used to design structures under compressive load for minimum weight with a predefined stacking sequence but with geometry parameters as design variables. Initially finite element eigen solution of complex blade-stiffened structure was verified with the analytical and FEA results from literature.

When dealing with non-convex design space the Genetic Algorithm (GA) optimisation method is preferred method. GA's has gained much attention because of their simplicity, ease of implementation and ability for handling non-convex problems, e.g. the orientation of the fibres as design variable which lead to a non-convex problem, and integer design variables type problems such as stacking sequence of laminates. However, for large scale problems GA generally requires a significant larger number of function evaluations to achieve convergence which is much higher than the gradient based optimisation methods.

For shape optimisation of blade-stiffened plate, Sequential Quadratic Programming (SQP), Genetic Algorithms (GA) and Simulated Annealing (SA) optimisation methods in MATLAB optimisation programme have been used together with ANSYS finite element methods to optimise the weight of a blade-stiffened composite plate subjected to a set target critical buckling load. Two cases were studied. In Case 1 only one design variable, the height of the stringer, was considered. In Case 2, two design variables, the height of the stringer and distance between the stringers were selected. The optimum weight of the plate for the set target buckling load for each case was found.

We need to keep in mind structural instability caused by buckling can lead to sudden failure of structures and buckling usually depends on the stiffness of a structure rather than on the material strength. Therefore, the buckling analysis of structure at the design stage is very important for safety, especially with regard to thin-walled laminated FRP composite structures that are applied in many structures where the weight is an important factor and optimisation methods can be used to efficiently design the optimum structure enabling to save in cost and weight of structures.

7.2. Further Work

The outcomes of this work are promising and therefore it would be beneficial to continue further work in this area. Because of outcomes of this thesis, the following recommendations for a number of areas in which further research may be undertaken in buckling and optimisation of laminated FRP composite structures are suggested:

7.2.1. Stacking Sequence Optimisation of Laminated Structures under General Loading

The optimisation cases studied in this thesis were plate buckling subjected to uniaxial compressive loading. Further case studies for finding stacking sequences for minimum weight of engineering structures made from FRP composites under general loading using ESM is recommended. This study will complement the work presented in this thesis.

7.2.2. Shape Optimisation of Stiffened Plates With/Without Cut-outs

The application of SQP, GA and SM shape optimisation can be extended to shape complex laminated FRP composite structures with multi design variables.

Cut-out naturally exist in may laminated structures and the effects of these features on the buckling performance require further studies. The effect of various cut-out forms and their position to result in an optimum design is of great interest.

7.2.3. Use of Cohesive Zone Model for Analysis of Delaminated Plates Buckling

A cohesive zone model (CZM) for the prediction of delamination growth and post-buckling behaviour of composite plates with embedded delamination subjected to buckling is recommended. The delamination fracture toughness in mode I and mode II required in the CZM model reported in Chapter 3 will be used. A further extension of this work will be the combined buckling and crack growth in composite plates containing multiple numbers of delaminations.